Effect of Ions and Admixtures on the Growth of Synthetic Calcium Silicate Hydrate (C-S-H)

THÈSE N^O 9007 (2018)

ÉCOLE POLYTECHNIQUE FÉDÉRALE DE LAUSANNE

POUR L'OBTENTION DU GRADE DE DOCTEUR ÈS SCIENCES

PAR

Jirawan SIRAMANONT

acceptée sur proposition du jury:

Prof. P. Muralt, président du jury
Prof. P. Bowen, directeur de thèse
Dr S. A. Bernal López, rapporteuse
Prof. P. Suraneni, rapporteur
Prof. V. Tileli, rapporteuse

EPFL

ÉCOLE POLYTECHNIQUE
FÉDÉRALE DE LAUSANNE

Suisse
2018

Acknowledgements

Kiattisak (P'Kiat), Natechanok (Erng), Teerawat (Bank) and Boodsarin (Noom) for all the fun times we shared and making me feel at home.

Finally, I would like to express the special thanks to my lovely friends and beloved family. I would like to give my special thanks Supatchaya (Toon), Supunsa (Sa) and Suthatip (Pooh) for supporting and visiting me in Lausanne. Special thanks to my husband, Nithiwatthn (Kee) who endured this long process with me always offering his support and love. Special thanks also to my parents for unconditional love, supporting precious opportunity in all kinds of my learning and education. They encouraged me to accomplish my goals.

Lausanne, 27th September 2018

Jirawan Siramanont

Abstract

This thesis investigates the effect of different parameters such as Fe^{3+}, D-gluconate and heterogeneous particles on the nucleation and growth of synthetic C-S-H by using the dropwise precipitation method. Firstly, the effect of Fe^{3+} on the synthetic C-S-H system was investigated. This was achieved by controlling pH and also Fe^{3+} ion concentration. The experiments at pH≥11.0 of initial solutions containing Fe leads to the pre-precipitation of an amorphous Fe phase (ferrihydrite) which is then transformed to the more stable crystalline Fe phase of siliceous hydrogarnet ($C_3FS_{0.84}H_{4.32}$). This condition is closely related to the phase formation pathway in real systems where the formation of ferrihydrite precludes the formation of the more thermodynamically stable iron containing siliceous hydrogarnet ($C_3FS_{0.84}H_{4.32}$) is also observed. To investigate the possible inclusion of Fe into the C-S-H structure, the experimental conditions were designed to avoid the pre-precipitation of ferrihydrite. This was achieved by controlling ionic speciation of the solution containing Fe with controlled pH (2.5). Magnetic resonance data strongly supported that the Fe^{3+} is incorporated into the C-S-H structure.

Secondly, this thesis investigates the effect of D-gluconate on the nucleation and growth of synthetic C-S-H. One effect of D-gluconate on synthetic C-S-H was a surface interaction which led to the formation of bi-pyramidal cage-like structures from the assembly of the precipitated C-S-H nanofoils. Characterization confirmed the adsorption of D-gluconate on the C-S-H surface but no changes in the underlying C-S-H structure could be discerned. From calorimetry data, D-gluconate not only interacts with newly precipitated C-S-H surfaces but also strongly on the dissolving solids in Portland cement e.g. alite, retarding hydration significantly. The complexation between calcium and D-gluconate in solution showed that increasing D-gluconate concentration gave more complexation with calcium and modified the kinetics of nucleation and growth. When collecting kinetics data to look at influences of D-gluconate on nucleation and growth mixed C-S-H morphologies nanoglobules, nanfoils and nanofibrils were observed. For a quantitative analysis by the population balance method recently developed in our lab such a mixed morphology cannot be analyzed. The experimental conditions for the collection of kinetics data for uniform morphology of precipitated synthetic C-S-H were found by controlling pH and D-gluconate concentrations. This new and unique kinetics data will in the near future be evaluated by using population balance modeling in

order to discern the quantitative effect of nucleation and growth of precipitated synthetic C-S-H formation in the presence of D-gluconate.

Finally, to approach more real system conditions, heterogeneous particles (e.g. quartz and calcite) were introduced in the synthetic C-S-H system. Quartz and calcite were able to act as heterogeneous substrates for the nucleation and growth of precipitated synthetic C-S-H. The elemental maps confirmed uniformly distributed Ca, Si and O in nanofoils at the heterogeneous surfaces corresponding to the C-S-H composition. Without calcium ions in the silicate solution, calcite partially dissolved to give Ca^{2+} and CO_3^{2-} ions which then formed C-S-H on its surface. Kinetics data shows different growth of C-S-H formation and will be evaluated in the future by using population balance modeling for further quantitative details.

Overall, these results gave us a better understanding of these different parameters of Fe^{3+}, D-gluconate and heterogeneous particles from a basic well controlled precipitation system compared to a more complicated real cement system. This will help us approach conditions in Portland cements especially to better understand the roles of heterogeneous particles introduced via SCMs, their effect on cement hydration in early age strength development and durability that is affected by the C-S-H formation.

Keywords

Résumé

Cette thèse étudie l'effet de différents paramètres tels que le Fe^{3+}, le D-gluconate et les parti-
cules hétérogènes sur la nucléation et la croissance du C-S-H synthétique en utilisant la méthode de
précipitation goutte à goutte. Tout d'abord, l'effet du Fe^{3+} sur le système synthétique C-S-H a été
étudié. Ceci a été réalisé en contrôlant le pH et également la concentration en ions Fe^{3+}. Les expéri-
ences à pH≥11,0 des solutions initiales contenant du Fe conduisent à la pré-précipitation d'une
phase Fe amorphe (ferrihydrite) qui est ensuite transformée en la phase Fe cristalline plus stable de
l'hydrogarnet siliceux ($C_3FS_{0.84}H_{4.32}$). Cette condition est étroitement liée à la voie de formation de
la phase dans les systèmes réels où la formation de ferrihydrite empêche la formation de l'hy-
drogarnet siliceux contenant du fer, plus stable sur le plan thermodynamique ($C_3FS_{0.84}H_{4.32}$). Pour
étudier l'inclusion possible de Fe dans la structure C-S-H, les conditions expérimentales ont été
conçues pour éviter la pré-précipitation de la ferrihydrite. Ceci a été réalisé en contrôlant la spécia-
tion ionique de la solution contenant du Fe à pH contrôlé (2,5). Les données de résonance mag-
nétique ont fortement soutenu que le Fe^{3+} est incorporé dans la structure C-S-H.

Deuxièmement, cette thèse étudie l'effet du D-gluconate sur la nucléation et la croissance du C-S-H
synthétique. Un effet du D-gluconate sur le C-S-H synthétique était une interaction de surface qui
conduisait à la formation de structures en forme de cage bi-pyramidales à partir de l'assemblage des
nanofils de C-S-H précipités. La caractérisation a confirmé l'adsorption du D-gluconate sur la sur-
face C-S-H, mais aucun changement dans la structure C-S-H sous-jacente n'a pu être observé.
D'après l'analyse calorimétrique, le D-gluconate n'interagit pas seulement avec la surface de C-S-H
nouvellement précipitée, mais aussi fortement avec le solide dissolvant dans le ciment Portland, par
ex. alite, retardant considérablement l'hydratation. La complexation entre le calcium et le D-
gluconate en solution a montré que l'augmentation de la concentration en D-gluconate complexifiait
davantage le calcium et modifiait la cinétique de nucléation et de croissance. Lors de la collecte de
données cinétiques pour examiner les influences du D-gluconate sur la nucléation et la croissance,
des morphologies mixtes C-S-H, des nanoglobules, des nanofils et des nanofibrilles ont été obser-
vés. Pour une analyse quantitative par la méthode du bilan de population récemment développée
dans notre laboratoire, une telle morphologie mixte ne peut être analysée. Les conditions expéri-
mentales pour les données cinétiques de morphologie uniforme du C-S-H synthétique précipité ont

été trouvées en contrôlant les concentrations de pH et de D-gluconate. Ces nouvelles données cinétiques uniques seront évaluées prochainement en utilisant une modélisation de l'équilibre de la population afin de discerner l'effet quantitatif de la nucléation et de la croissance de la formation synthétique précipitée de C-S-H en présence de D-gluconate.

Enfin, pour approcher des conditions de système plus réelles, des particules hétérogènes (par exemple quartz et calcite) ont été introduites dans le système synthétique C-S-H. Le quartz et la calcite pouvaient agir comme substrats hétérogènes pour la nucléation et la croissance du C-S-H synthétique précipité. Les cartes élémentaires ont confirmé la répartition uniforme des Ca, Si et O des nanofils sur les surfaces hétérogènes correspondant à la composition en C-S-H. Sans ions calcium dans la solution de silicate, la calcite se dissout partiellement pour donner des ions Ca^{2+} et CO_3^{2-} qui forment alors le C-S-H à sa surface. Les données cinétiques montrent une croissance différente de la formation de C-S-H et seront évaluées à l'avenir en utilisant la modélisation de l'équilibre de la population pour d'autres détails quantitatifs.

Dans l'ensemble, tous ces résultats nous ont permis de mieux comprendre ces différents paramètres des particules de Fe^{3+}, D-gluconate et hétérogènes provenant d'un système de précipitation de base bien contrôlé par rapport à un système de ciment réel plus complexe. Cela nous aidera à aborder les conditions dans les ciments Portland en particulier pour mieux comprendre le rôle des particules hétérogènes introduites via les MCS, leur effet sur l'hydratation du ciment dans le développement précoce de la force et la durabilité de la formation C-S-H.

Mots-clés

Silicate de calcium hydraté, Fe^{3+}, D-gluconate, substrat hétérogène, quartz, calcite, C-S-H synthétique, nucléation et croissance, agrégation, précipitation goutte à goutte, SCMs, additifs, durabilité.

Contents

List of Figures

List of Tables

Chapter 1   Introduction

1.1   Cementitious materials

Concrete is extensively used in the construction industry for buildings, bridges, dams, tunnels, and roads. It is traditionally made by mixing cement, water, and aggregate. Concrete production has a significant carbon footprint due to the huge quantities used and this is expected to double in the next 30 years [1,2]. The main contribution to CO_2 release is by the chemical process of cement production called calcination, which produces cement clinker by heating a mixture of limestone, clay or other materials of similar bulk composition and sufficient reactivity. A small amount of gypsum also added to cement production in order to control the rate of hardening of the cement [3,4]. The calcination occurs when the limestone (mostly made up of $CaCO_3$) is heated, then $CaCO_3$ breaks down into calcium oxide (CaO) and CO_2. Figure 1.1 shows a schematic of the chemical process of cement production. To reduce CO_2 emissions, clinker substitution, replacing clinker by supplementary cementitious materials (SCMs) is a promising strategy [5–11]. SCMs such as slag, fly ash, clay, silica fume, and limestone are already in use for clinker replacement in the recent years. However, the level of SCMs replacement is limited because of their lower reactivity, which reduces strength at early ages [8,9].
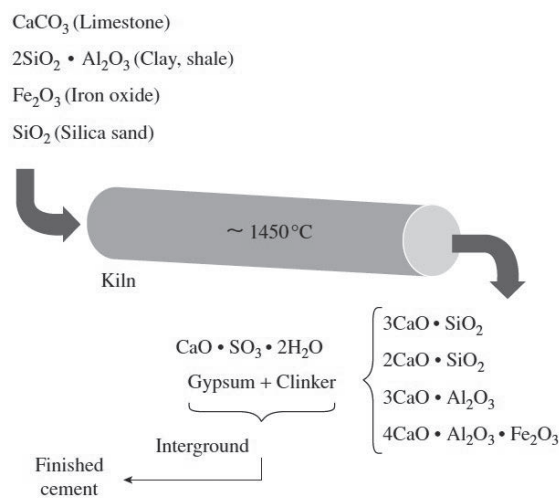
Figure 1.1 Schematic representation of the chemical process of cement production [4].

Chemical admixtures are widely used in the manufacture of cement to modify the hydration or processing properties. For example, retarding cement hydration, or decreasing amount of water needed in order to obtain a given degree of workability [3]. The effect of the admixtures on the hydration of cement is a key topic in modern cement technology as we try and reduce the clinker content by SCMs replacement often more admixtures are needed. A lack of knowledge regarding the interaction of the admixtures with cement used in modern concrete has lead recently to the study of a selection of molecules in the Nanocem [10] research network. Recent publications by Nalet and Nonat [11–14], they have generated fundamental knowledge of some organic molecules with different functional groups identified as being important in admixtures and on their effect of cement hydration. However, the effect could not be explained simply by either their capacity to complex calcium in solution or their affinity to adsorb onto calcium silicate hydrate (C-S-H).

Calcium silicate hydrate (C-S-H) is the major hydration product and the main binding phase in Portland cement. The C-S-H precipitates together with other hydrated phases from the ions produced in the pore solution by the dissolution of anhydrous phases. However, C-S-H is a poorly crystalline non-stoichiometric material, which is difficult to characterize and describe at an atomistic level. Additionally, minor elements in pore solution may come from either impure C_3S [15] in Portland cement or the replacement of environmentally friendly materials such as clay, slag, fly ash or limestone [16,17]. The minor elements can have an impact on cement hydration and the nucleation and growth of C-S-H. For example, zinc increases the rate of reaction at the first day of hydration [15] and can be incorporated into C-S-H with Ca/Si 0.66 by up to 6%wt [18]. Moreover, Ghorbel and Samet [19] studied the effect of iron in white cement. The iron enhanced pozzolanic activity of kaolin which increases compressive strength and its located in both the C-S-H and ettringite structures.

In Portland cement system, there are numerous phases and it is a complex mixture. Therefore, synthesis of C-S-H is an attractive tool to prepare homogeneous C-S-H which allows us to understand mechanisms of each individual parameter on nucleation and growth of C-S-H. In recent work from Kumar et al. [20] a method has been developed to produce synthetic C-S-H at high Ca/Si ratios from 1.0 to 2.0 without the presence of any second phases, namely portlandite ($Ca(OH)_2$). The reason has been shown to be due to a kinetics limitation of portlandite formation due to the very high supersaturations and good mixing conditions used in these precipitation experiments [21].

The C-S-H gel formation and densification affects mechanical properties such as strength, shrinkage of Portland cement and concrete [22–24]. Modification of nucleation and growth rate of C-S-H changes the degree of hydration and also the resulting microstructure which can modify the mechanical properties in concrete. To better understand the effects of ions and admixtures on the

mechanisms of C-S-H formation, there are fundamental questions that need to be addressed, for example, does the adsorption of ions or molecules influence the nucleation and growth of precipitated synthetic C-S-H. Answering these questions will provide fundamental knowledge that is a key factor in understanding early age strength often compromised when using SCMs to reduce CO_2 emissions.

1.2   Motivation and objectives

The overall objective of this thesis is to provide fundamental insights into the effects of pore solution ions (usually coming from fillers or SCMs or impurities from raw materials) and small organic molecules representative of organic admixtures often used in cements (e.g. superplasticizers). This is done by introducing foreign ions or small organic molecules into the synthetic C-S-H precipitation process. To approach real systems, heterogeneous particles (e.g. quartz and calcite) will be introduced in the synthetic C-S-H system. This will help in the overall understanding from a basic system to a more complex system to finally approach conditions in Portland cements. Sometimes heterogeneous surfaces get introduced with raw materials or SCMs that may not fully participate by dissolution of the solid but may affect hydration by providing reaction surfaces or other reactive ions by partial dissolution. Two of the most commonly occurring surfaces of quartz and calcite are studied in this thesis work.

The synthetic C-S-H has been prepared using a dropwise precipitation method, which produces homogeneous products, uniform in chemistry down to the 3nm level [20]. Furthermore, kinetics data will allow us to follow the nucleation and growth of precipitated synthetic C-S-H. Conductivity, pH and Ca^{2+} will be monitored in a controlled temperature and atmosphere reactor. The products will be analyzed using ex situ techniques such as TGA, TEM, SEM, STEM-EDX, NMR, FTIR and XRD. Also, thermodynamic modelling using the software GEMS [25–27] will be used to try and understand the expected phase assembly of the final products when the thermodynamic data for the ions and molecules to be investigated are available.

The expected outcome of the thesis is to contribute to the understanding of why early age strength is often compromised when in the presence of organic based admixtures often used for workability of the concrete. It can help formulate the better admixture compositions realistic to cement types. The results will also shed some light on the understanding the modified hydration conditions necessarily produced while using supplementary cementitious materials (SCMs). SCMs replacement of clinker phase can help reduce CO_2 emissions. The heterogeneous surface effect on hydration helps us un-

derstand the roles of inert impurities in strength and durability of cementitious systems resulting from the C-S-H formations.

1.3 Organization of the thesis

The thesis is composed of eight chapters. An overview of cementitious materials and general literature review, which is relate to this work, has been presented in Chapter 1 and Chapter 2. Synthetic precipitated C-S-H and charactretization have been explained in Chapter 3. Specific details will be given in the introduction section of each individual chapter. Chapters 4-6 have been written in a format as a paper to be eventually submitted to journals.

The thesis is organized as follows:

- *Chapter 1* Introduction – This chapter introduces context and topic of the thesis, which gives an overview of cementitious materials and chemical admixtures.

- *Chapter 2* General literature survey and theoretical background – This chapter summarizes the important points of view in cementitious materials which relates to C-S-H.

- *Chapter 3* Materials and methods – This chapter explains how to prepare synthetic precipitated C-S-H using the dropwise method and the experimental approach used for the general characterization methods such as TGA, XRD, ICP, TEM and STEM-EDX.

- *Chapter 4* Investigation of Iron (Fe^{3+} ions) on precipitated synthetic calcium silicate hydrate (C-S-H) –This chapter presents effect of Fe^{3+} ions on synthetic C-S-H. The aim of this work is to better understand the mechanisms of ions on the growth of precipitated C-S-H. *To be submitted to an international journal.*

- *Chapter 5* Effect of D-gluconate on nucleation and growth of synthetic C-S-H - This chapter investigates the influence of complexation between D-gluconate and calcium ions on the nucleation and growth of precipitated C-S-H. Kinetics data and morphology of precipitated C-S-H are obtained and discussed.

  5.1 Effect of D-gluconate on nucleation and growth of synthetic Calcium Silicate Hydrate (C-S-H), *12th ICSP 2018, ACI Proceedings, accepted.*

5.2 Effect of D-gluconate on morphology of synthetic C-S-H and kinetics analysis. ***To be submitted to an international journal.***

5.3 Kinetics analysis of single morphology of synthetic C-S-H in the presence of D-gluconate.

- ***Chapter 6***   Effect of heterogeneous substrates on synthetic C-S-H precipitation- This chapter presents observation of the heterogeneous substrates of quartz and calcite on the nucleation and growth of synthetic C-S-H. The goal of this work is to approach real system by introducing heterogeneous substrates in the synthetic precipitated C-S-H system. ***To be submitted to an international journal.***

- ***Chapter 7***   Summary of the thesis – This chapter summarizes the work on synthetic C-S-H and further avenues to be explored as a result of the findings in this thesis.

- ***Chapter 8*** – Appendix

8.1 Preliminary results of complexation between calcium and D-gluconate by GEMS calculation.

8.2 Initial observations: Effect of the presence of divalent ions (Ba^{2+}, Mg^{2+}, Zn^{2+}) on the morphology of precipitating calcium silicate hydrate.

Chapter 2   General literature survey and theoretical background

In this chapter, an overview of state of the art knowledge about cement hydration, minor elements, chemical admixtures and filler effect is summarized. The first part presents the kinetics of cement hydration and the major phases which contribute to C-S-H formation. The second part explains about C-S-H composition, structure and morphology. Then, the effect of using chemical admixtures such as Polycarboxylate ether (PCE) and gluconate are reviewed. There is some retardation of cement hydration from PCE which is unintentional effect. Finally, the filler effect on cement hydration is shown by using supplementary cementitious materials (SCMs).

2.1   Cement hydration

Cement is a complex mixture of numerous compounds. The major compounds found in cement are tricalcium silicate (C_3S), dicalcium silicate (C_2S), tricalcium aluminate (C_3A), tetracalcium aluminoferrite (C_4AF). When cement is mixed with water, cement grains starts to dissolve in the aqueous solution. Various anhydrous phases can react with water forming various hydration products. Calcium silicate hydrate (C-S-H) is the major hydration product and the main binding phase in Portland cement. C-S-H and portlandite ($Ca(OH)_2$) precipitate from the ions produced in the pore solution by the dissolution of anhydrous calcium silicate phases (C_3S and C_2S) [3,6]. In the presence of gypsum, ettringite and monosulphoaluminate precipitate from hydration of C_3A and C_4AF. A schematic of the hydration reactions of cement are shown in the following shorthand equations [28].

$$(C_3S, C_2S) \ + \ water \ \longrightarrow \ C\text{-}S\text{-}H \ + \ portlandite$$

$$(C_3A, C_4AF) + calcium \ sulphate + water \ \longrightarrow \ ettringite \ + \ monosulphoaluminate$$
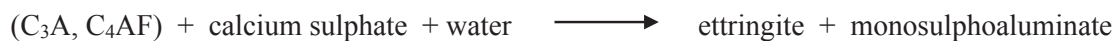
Cement hydration is a highly exothermic reaction which is typically monitored by isothermal calorimetry. The hydration curve is usually divided into 5 stages (Fig.2.1) [3,6,28,29]. The main reactions of hydration occur within the first 24 hours. The first period (stage I) is generally referred to as

the initial dissolution period in which the rate of reaction rapidly slow. The reaction period in stage II is called induction period. The reaction rate of this stage is low without the presence of retarding admixtures. At the end of the induction period, calcium silicate hydrate (C-S-H) and portlandite, which is a crystalline form of hydrated lime, start to grow rapidly. The main heat evolution peak is the so-called "acceleration period" (approx. 3-24 hrs) which corresponds to stage III which then slows down or "decelerates" in stage IV [30]. C_3S and C_3A continue their hydration during stage III and IV. The hydration of C_2S and C_4AF mostly occur in stage V.
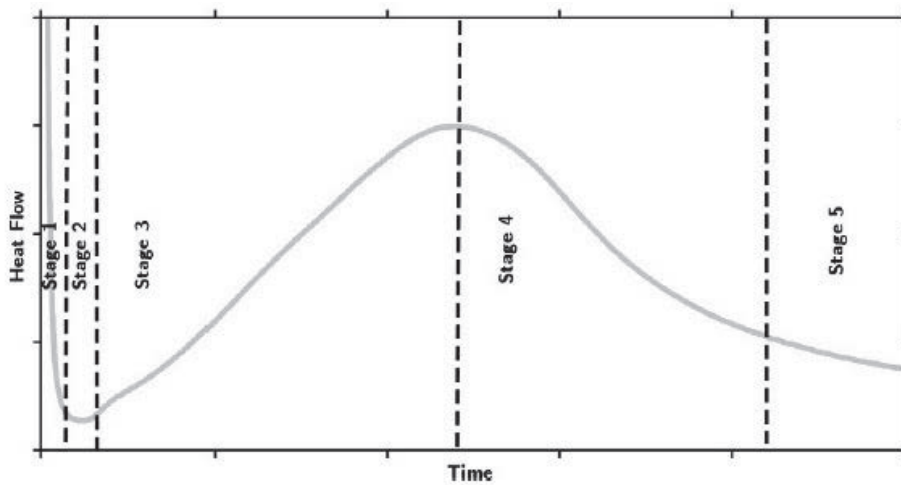
Figure 2.1 Schematic representation of the heat release of cement hydration [6].

2.2   Calcium silicate hydrate (C-S-H)

Calcium silicate hydrate (C-S-H) is the major hydration product and has variable stoichiometry and has poor crystallinity. Scanning electron microscope (SEM) image shows needle-like morphology of C-S-H which grows outward from the cement grain (Fig.2.2) during the early stage of hydration. The composition of C-S-H is characterized by the molar ratio between calcium and silicon which varies from 1.2-2.1. Generally, the typical Ca/Si ratio of C-S-H in hydrated cement is approx. Ca/Si ~1.5-2. This variation depends on the activity of ions in the local pore solution. Structure of C-S-H is composed of Ca-O sheets which are bordered with dreierketten chains of silica (Fig.2.3). Such a dreierketten structure is similar to the structure observed in some naturally occurring minerals such as tobermorite [31]. The silica arrangement in C-S-H is parallel linear rows of dimers of silica tetrahedral more or less bridged by a third tetrahedron. The interlayer space of C-S-H contains water molecules, hydroxyl groups and some calcium ions.
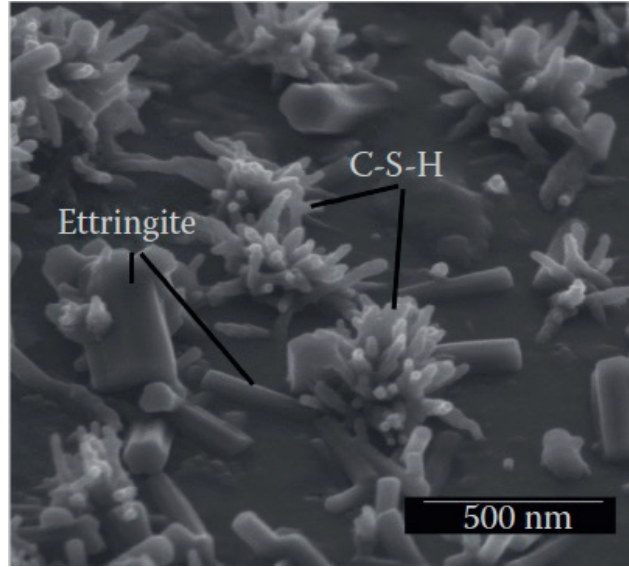
Figure 2.2 SEM image of cement grain after 4 hours of cement hydration [32].

However, since C-S-H is poorly crystalline and non-stoichiometric material, it is difficult to characterize and describe at an atomistic level by classic techniques such as X-ray diffraction [33]. For this reason, many researches have studied synthetic C-S-H to understand formation mechanisms and its structure. ^{29}Si Nuclear magnetic resonance (NMR) [34] has been the most relevant method to study Si arrangement in C-S-H [20,31,35–37]. This technique can distinguish between Si monomers (Q^0) and Si connected to a number X of bridging oxygens of other silicate species (Q^X). ^{29}Si-enriched C_3S has been synthesized and the evolution of C-S-H has been monitored [38]. By reducing the specific surface area of the C_3S, the degree of hydration decreases. The information of the proximities between various ^{29}Si species in C-S-H structure has been shown by using 2D NMR.
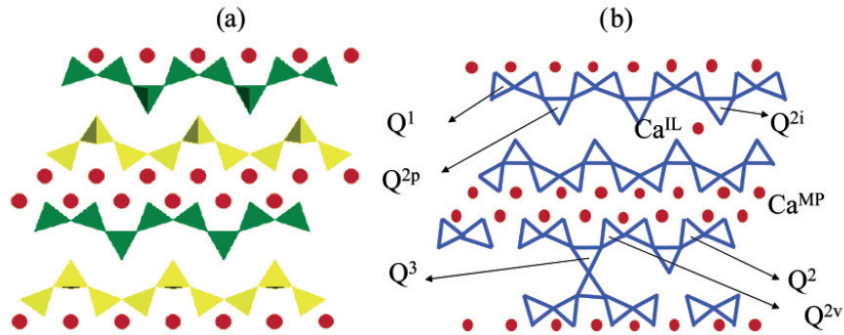
Figure 2.3 (a) Layered structure of tobermorite composed of a calcium sheet (red dots) which is flanked both sides with silicate chain (yellow and green), (b) Dreierketten structure, Q^1 is the end chains of Si tetrahedra. Q^2 is the silicon in middle chain which are coordinated by calcium sheet. Q^{2p} and Q^{2i} are not coordinated with calcium. Q^3 is the silicon tetrahedral which links two silicate chains in the interlayer space. Ca^{MP} is the calcium in Ca-O sheet and Ca^{IL} is the calcium in the interlayer space [31].

9

14 Å tobermorite is often used as a model structure for C-S-H. The Ca/Si (~0.83) of 14 Å tobermorite is different from the C-S-H of Portland cement system (~1.75), which limits the use of tobermorite as a model structure for C-S-H [33,37]. Consequently, many researchers have introduced defects into the system to try and approach a more realistic Ca/Si ratio. A defective 14 Å tobermorite structure where all the bridging silicates have been removed can have a maximum Ca/Si ratio of 1.5, which is still lower than the typical ratio in Portland cement. So, although a defective tobermorite is difficult to relate to C-S-H from Portland cement it had some success in representing synthetic C-S-H's at Ca/Si ratios <1.5. Above Ca/Si 1.5, many researchers have always invoked a second calcium rich phase. But recent work in our lab by Kumar et al. [20], we have developed a method to produce synthetic C-S-H at Ca/Si from 1.0-2.0 without a second phase. The synthetic samples in this Ca/Si range were consistent with the NMR results. C-S-H at high Ca/Si can be described by a defective 14 Å tobermorite with calcium being at the bridging silicate site and in the interlayer. Figure 2.4 shows the atomistic structure of C-S-H structure at Ca/Si 2.0 which we believe is the best representation of the atomistic structure of C-S-H to date. Population balance modeling has been used to confirm the absence of portlandite formation under these reaction conditions [21]. Portlandite is never supersaturated because of a kinetics limitation of its formation.
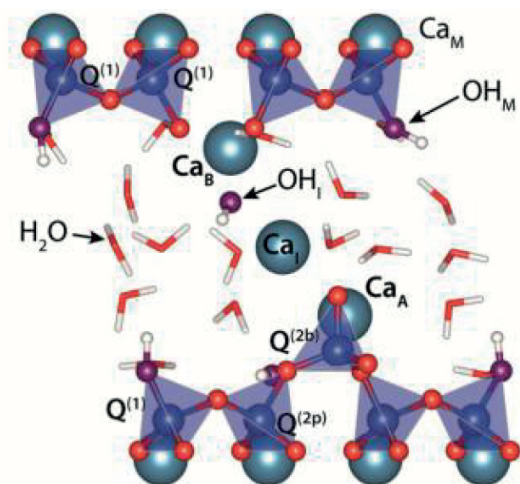
Figure 2.4 The atomistic structure of C-S-H structure at high Ca/Si showing calcium at the bridging site and in the interlayer [20].

2.3   Chemical admixtures

Chemical admixtures are chemical compounds added in concrete before or during mixing of Portland cement, aggregate and water [39,40]. There are five classes distinguished by their functional use, for example, water reducers, retarders, accelerators, superplasticizers and corrosion-inhibiting admixtures [39]. The chemical admixtures have been extensively used in the concrete industry to modify its properties in the fresh and hardened state. The admixture may interact with cement particles which influences the physico-chemical and mechanical properties of concrete. The beneficial effects from admixtures include controlled setting time and rheological properties, decreased water requirement and improved compressive strength [4,28,40]. Superplasticizers, which are high range water reducers, are commonly used in concrete to reduce water to cement ratio and improve fluidity to maintain workability of fresh concrete over time. The superplasticizers such as modified lignosulfonate, polynaphthalene sulfonate and polymelamine sulfonate disperse cement particles by adsorption on the surfaces. It has been generally believed, and is unfortunately still believed by some [11,20,2] that these molecules create an electrostatic repulsive effect due to their negative functional group backbone. However, at the high ionic concentrations found in cement pores solutions > 0.2 M the electrical double layer is significantly compressed and would have an effective thickness of around 0.5 nm at such concentrations [41]. Palacios et al. [41] showed clearly, using atomic force measurements, inter-particle force modelling and rheological modelling that the dominant repulsion mechanism even for these sulphonate superplasticizers is steric. Unfortunately, the general cement community assumed many years ago that a small change in zeta potential of around 10 mV could induce an electrostatic potential but never made any inter-particle force calculations. There can be an electrostatic contribution but Palacios et al. [41] showed clearly that steric is the dominant mechanism.

Polycarboxylate ether (PCE) is the new generation of superplasticizer which is commonly used in concrete. Its structure is comb copolymer which typically has carboxylate backbone and polyethylene oxide side chain. The carboxylate backbone can create an electrostatic effect to adsorb on cement surfaces. The long side chains of the ether group disperse the particles by a steric effect [31,38,41,42]. The advantage of the long side chains is that they are influenced by the ions in pore solutions. However, use of PCE can bring about a retardation in cement which is an unwanted secondary effect. Figure 2.5 shows the heat flow curve for Portland cement mixed with different PCE dosages [43]. The retardation is shown by the extended induction period. The slope of the acceleration period is also changed. This suggests that the interaction between PCE and cement grain can

modify the dissolution rate of anhydrous phase and nucleation and growth of hydrated phases [43,44] and is probably the main mechanism behind the retardation.
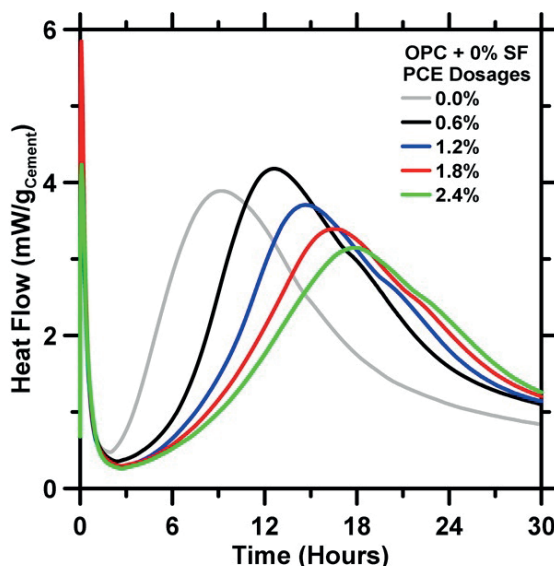
<u>Figure 2.5</u> Heat flow of Portland cement with different dosage of PCE [43].

2.4 Gluconate

Small molecules of various sugars such as maltodextrin, glucose, gluconate and glucitol are retarding admixtures which delay cement hydration by prolongation of the induction period [3,17,23–25]. The functional groups of these small molecules are representative of those found in PCE superplasticizers. As mentioned in Section 2.3, PCE is widely used in concrete but also shows the secondary effect of retardation. Therefore, several studies have been made on the effect of these small molecules on cement hydration in order to understand the mechanisms which are behind the PCE and cement particle interaction. Smith et al. [26] investigated the hydration behaviours in cement slurries with the presence of glucose, maltodextrin, and sucrose by using advanced solid-state NMR. The different hydration behaviours were influenced by alkaline stability of molecules and adsorption selectivity for different silicate or aluminate sites at heterogeneous cement surfaces, and binding strengths at surfaces of those molecules.

Gluconate is a salt of gluconic acid and a simple organic compound, sugar derivative. It is stable in highly alkaline solutions and is used as retarder in concrete [3,16,17,26,27]. The retardation has been postulated to be due to calcium complexation in pore solution or adsorption on cement grains or C-S-H surfaces. The gluconate can be used as an organic model to study interaction between

organic admixture and cement because of its functional groups such as COO$^-$ and OH representative of those found in PCE superplasticizers. The chemical structure of gluconate is shown in Figure 2.6.
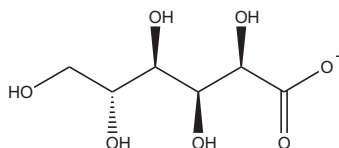
Figure 2.6 Chemical structure of gluconate.

Complex formation between gluconate and Ca^{2+} ions has been investigated for many applications such as dairy products and cement [29–31]. The complexation depends on pH, temperature and concentration because dissociation of the carboxylate group (COO$^-$) gives it a strong binding ability for Ca^{2+} ions. Figure 2.7 shows distribution diagram of calcium speciation as function of pH. Addition of gluconate to cementitious systems shows its adsorption onto both C$_3$S and C-S-H surfaces [25,32]. The adsorption of gluconate on C-S-H surface increases with higher Ca/Si ratios [32].
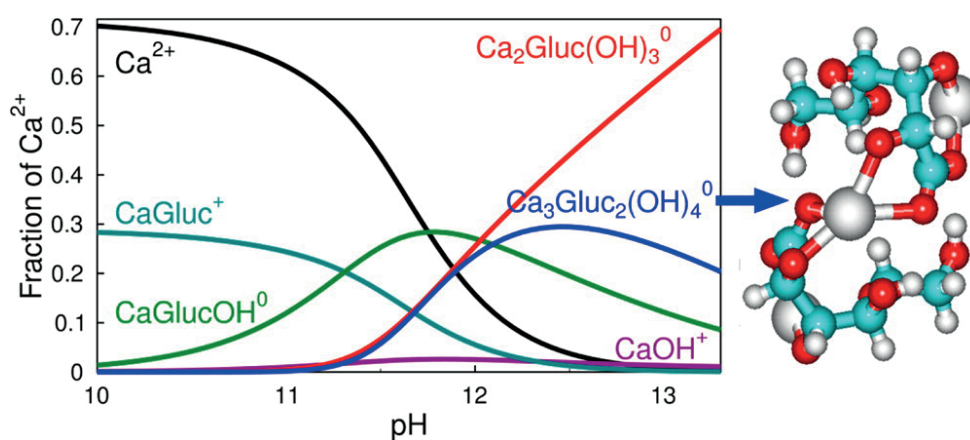
Figure 2.7 Distribution diagram of calcium speciation as function of pH [45].

Recent work supported by Nanocem (CP12) [10] has generated fundamental knowledge of a series of organic molecules on the effect of cement hydration e.g., the dissolution of anhydrous phases, nucleation and growth of hydrates [11–14]. The molecules, which differ by stereochemistry, functionality and charge, retard the hydration of pure C$_3$S and then enhance the quantity of C-S-H precipitated [13]. However, the mechanisms of these molecule are still not clearly understood by either their capacity to complex calcium in solution or their affinity to adsorb onto C-S-H. In fact, mole-

cules of a very similar size and structure (D-mannitol, D-glucitol, D-gluconate, Fig.2.8) gave very different retardation times.

(a)   (b)   (c)
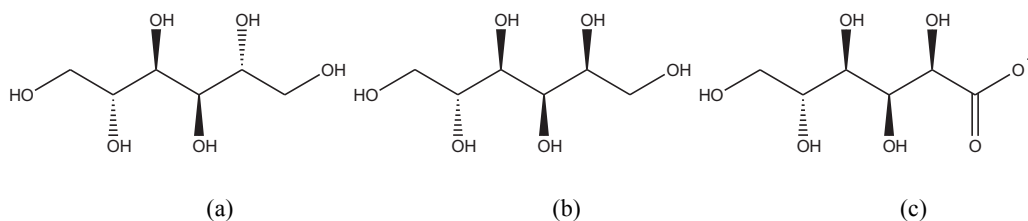
Figure 2.8 shows the chemical structure of (a) D-mannitol, (b) D-glucitol, and (c) D-gluconate.

Ma et al. [46] observed the effect of sodium gluconate on the cement hydration and performance of Portland cement. Sodium gluconate significantly delayed the hydration of cement by C_3S adsorption. When the dosage of sodium gluconate increased until 1.0% for convention Portland cement, the hydration kinetics was changed as shown in Figure 2.9. They suggested that 1.0% of sodium gluconate adsorbed on $CaSO_4.2H_2O$ which inhibited the dissolution of $CaSO_4.2H_2O$ and then AFt formation. Mota et al. [47] suggested that addition of gluconate together with Na_2SO_4 in white cement increased strength development because of less dense (and consequently higher volumes of) C-S-H formation. However, the mechanism of sodium gluconate on compressive strength of cement is still unclear. Different variation of D-gluconate concentration and complexation with calcium is studied in Chapter 5.
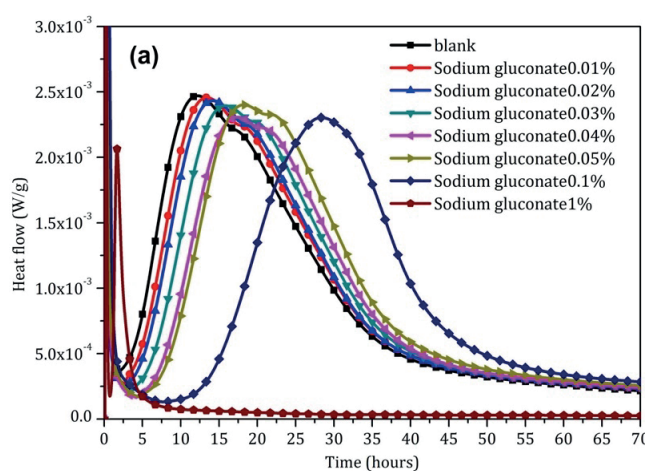
Figure 2.9 Heat flow of Portland cement with different dosage of sodium gluconate [46].

2.5   Filler effect

Supplementary cementitious materials (SCMs) are commonly used in blended cement and concrete by clinker replacement. Early age strength is mainly due to the hydration of clinker phase. There-fore, it is important to understand the mechanism of this reaction which is modified by the presence of SCMs. The reaction of SCMs usually starts after the main peak of the C_3S reaction. The SCMs particles such as quartz, fly ash or slag are thus relatively inert during the first hours of hydration in a paste containing ground clinker and SCMs [6,8,48].

Additionally, the inert materials of SCMs have a significant effect on cement hydration which refers to filler effect [8,49,50]. There are two main factors of this effect. Firstly, with presence of SCMs, the water to cement ratio is higher and they give relatively more space for the hydration products. Secondly, SCMs grain surfaces act as a nucleation sites for the heterogeneous nucleation of C-S-H [8,29]. The filler effect can be utilized to combat some known problems with high volume SCM use e.g. delayed setting and low early-age mechanical properties. The filler effect has been investigated by addition of quartz and slag in blended cement [29,48]. From the rate of heat evolution, it is clear that both quartz and slag increase the reaction (Fig 2.10).
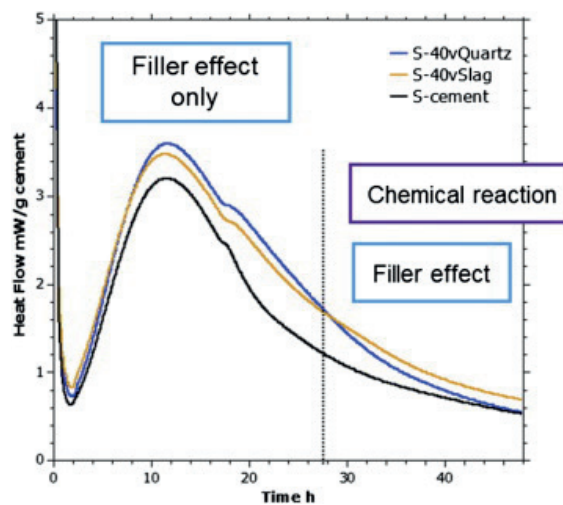
Figure 2.10 Rate of heat evolution normalized to clinker content for a Portland cement and the same cement substituted 40% by quartz or by slag [29].

Berodier et al. [48] reported the filler effect of SCMs in blended cements. The clinker replacement with quartz increases the rate of hydration reaction. Although quartz is non-reactive material, presence of nuclei on the quartz surface are observed by using scanning electron microscope (SEM) as shown in Figure 2.11. This confirms that quartz acts as a substrate for the heterogeneous nucleation of C-S-H. Comparison of the filler effect between quartz and limestone has been investigated by Kumar et al. [51]. They hypothesized that limestone is a better filler than quartz because of the higher dissolution of limestone providing Ca^{2+} and CO_3^{2-} ions in the system. Moreover, the dissolved carbonate ion was assumed to sorb on to the C-S-H gel and then OH^- from C-S-H was released in to the solution which increased the driving force for C-S-H growth. In this thesis, the effect of the presence of quartz and calcite on synthetic C-S-H growth is studied and presented in Chapter 6.
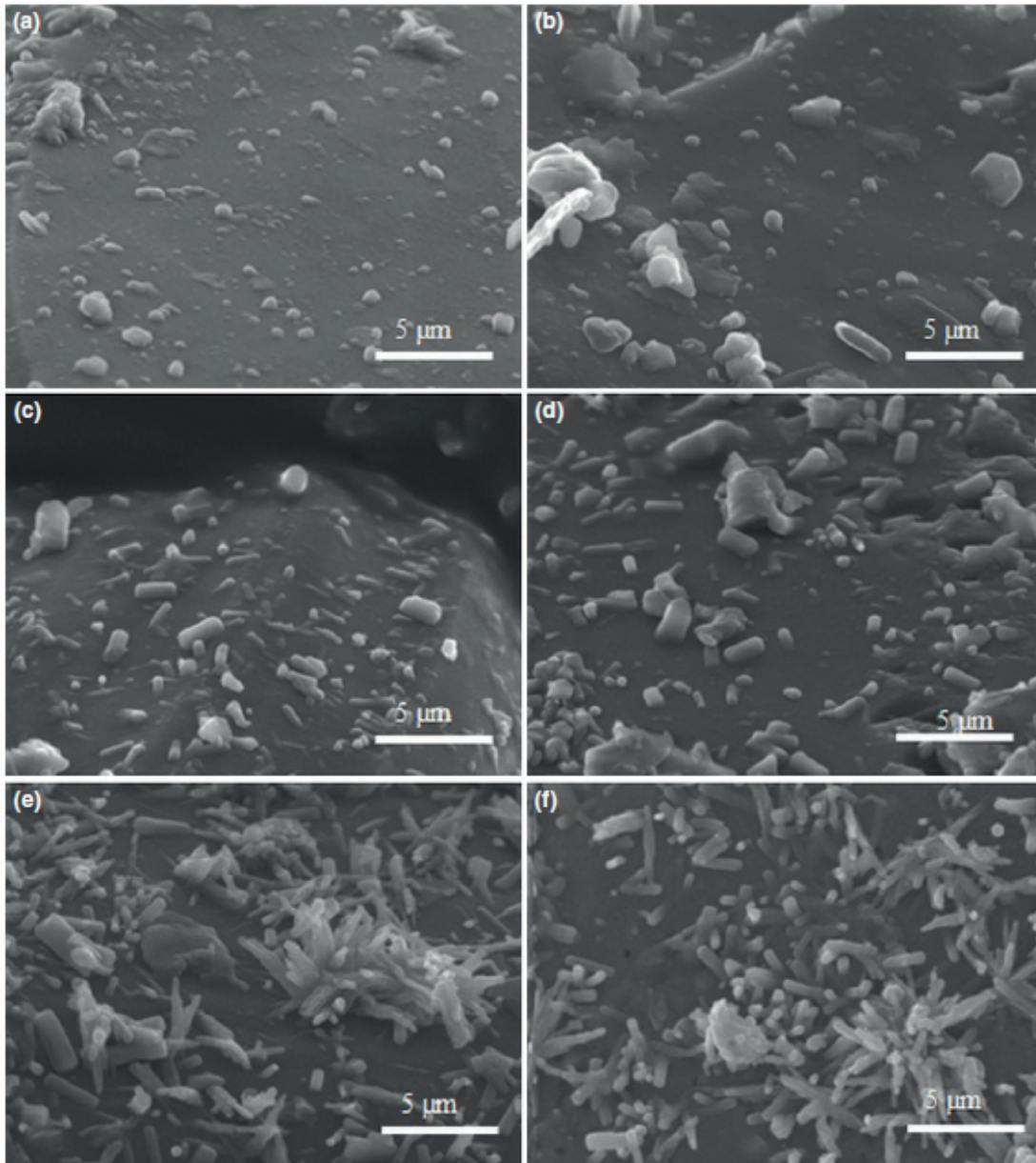
Figure 2.11 SEM micrograph of quartz surface on the left and cement on the right (a) and (b) after 5 min, (c) and (d) after 2 hour and (e) and (f) after 5 hour of hydration [48].

Chapter 3   Materials and methods

This chapter explains preparation of synthetic precipitated C-S-H using dropwise precipitation method. The preparation of synthetic C-S-H with introducing other ions, admixture and heterogeneous particles are shown in more details in each chapter. Characterization such as Inductively coupled plasma (ICP), Fourier-transform infrared spectroscopy (FTIR), Thermogravimetric analysis (TGA), X-Ray Diffraction (XRD), Transmission electron microscopy (TEM) and Scanning transmission electron microscope-energy dispersive x-ray (STEM-EDX) used extensively throughout the thesis.

3.1   Synthesis of calcium silicate hydrate (C-S-H)

Synthetic C-S-H was prepared via a dropwise method described in detail in [52]. A schematic diagram of this dropwise method is shown in Figure 3.1 (a). Before precipitation, the pH electrode (InLab®Expert Pro-ISM-IP67, *Mettler Toledo*) connected with benchtop pH meter (SevenExcellence pH Meter, *Mettlet Toledo*) was calibrated with standard solutions as shown in Table 3.1. Sodium metasilicate (Na_2SiO_3, S*igma-Aldric*h, CAS:6834-92-0) is placed in the main reactor (Part B, Fig.3.1) vessel and is purged with N_2 for 30 minutes before starting the reaction. Then calcium nitrate ($Ca(NO_3)_2.4H_2O$, *Fluka Chemicals,* CAS:13477-34-4) (Part A, Fig.3.1) is introduced into the vessel in a drop wise manner at a fixed rate and under N_2 atmosphere. The pH of the solution is adjusted by adding sodium hydroxide (NaOH, *Acros organic*, CAS:1310-73-2) in Part B to give a desired value for a particular Ca/Si ratio calculated from thermodynamic modelling [10]. The set up of the C-S-H synthesis is shown in Figure 3.1 (b). The reaction time was 3 hours. All solutions were prepared by using ultra-pure water previously boiled to remove the CO_2. The chemical glassware was washed with ultrapure water and dried under a laminar flow hood (Skanair®, Scan AG). After precipitation, the samples were washed with ultra-pure water mixed with ethanol (50:50 vol%) and followed by pure ethanol to remove unwanted ionic species in the precipitate. Then, samples were collected by vacuum filtration with 0.2 μm, 50 mm diameter of membrane filter, mixed Cellulose Ester ME24/21 STL (Whatman[TM], GE health care). Then, the sample was stored in polystyrene containers and then put in plastic zip lock bag before eventual drying and /or characterization.

(a)   (b)
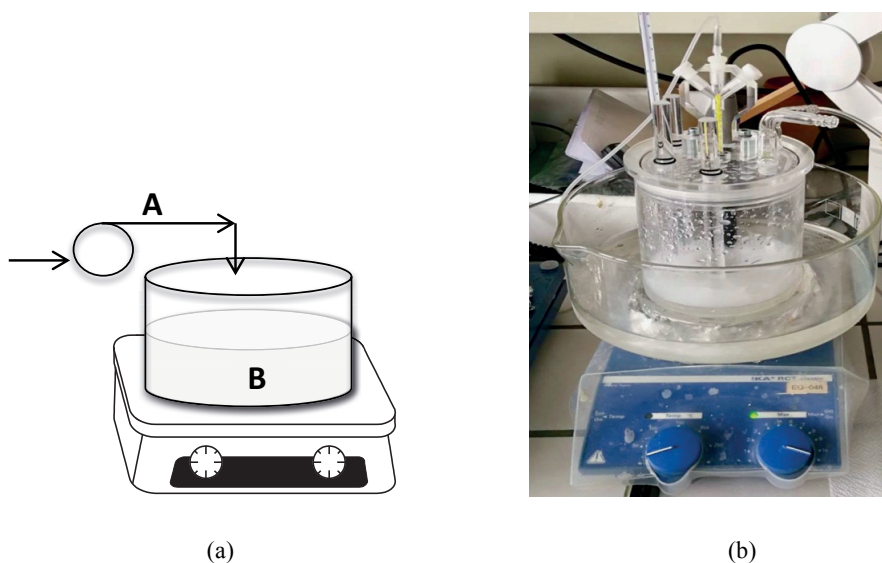
<u>Figure 3.1</u> (a) Diagram of dropwise method of synthetic C-S-H. A is calcium solution part and B is silicate solution part, (b) The set up of dropwise precipitation method. The reactor vessel is made out of PMMA and has both a diameter and height of 11cm. Maximum reaction volume is 1L.

3.2   Kinetics experiment of synthetic C-S-H

Kinetics data were collected during the dropwise precipitation using calcium ion selective (perfec-tION[TM], *Mettler Toledo*), pH (InLab[®]Expert Pro-ISM-IP67, *Mettler Toledo*) and conductivity (In-Lab[®] 731-ISM, *Mettler Toledo*) electrodes. The electrodes connected with benchtop pH meter (SevenExcellence pH Meter, *Mettlet Toledo*). The data were collected by EasyDirect™ pH Software. Before precipitation, all electrodes were calibrated with their standard solution as shown in Table 3.1.

Electrode	Standard solution
Calcium ion selective	10, 100 and 1,000 mg/L
pH	Buffer pH 4.0, 7.0 and 9.21
Conductivity	1413 μS/cm

<u>Table 3.1</u> Standard solution for each electrode.

The reactions were carried out under an N_2 atmosphere, and the pH was controlled at 12.0$\pm$0.2 by adding controlled amounts of 1.0 N NaOH standardized solution (*abcr GmbH,* CAS:1310-73-2). Temperature of the reaction was monitored by using sensor of pH electrode, which showed on the

screen of SevenExcellence benchtop meter. The calcium nitrate ($Ca(NO_3)_2.4H_2O$, *Fluka Chemicals,* CAS:13477-34-4), Part A in Figure 3.1 was constantly added to a solution of sodium silicate (Na_2SiO_3, S*igma-Aldric*h, CAS:6834-92-0), Part B in Figure 3.1 at a flow rate of 2.0±0.1 mL/min. After reaction time, the samples were washed and filtrated as the same procedure in Section 3.1.

3.3   Thermodynamic modelling

Thermodynamic modelling has been carried out using the Gibbs free energy minimisation program, GEM-Selektor v.3 (GEMS) [25,26]. This model is developed at PSI, Viligen and EMPA, Dubendorf. GEMS computes the equilibrium chemical speciation and activities of components in the pore solution and hydrate phase assemblage during cement hydration. GEMS was used to calculate and predict possible phases in our synthetic C-S-H system [20]. The database that we used for calculation in the thesis was *Cem18*.

3.4   Characterization methods

*3.4.1 Freeze dryin*g – This method was used to prepare dried samples in order to remove excess water before characterization e.g. XRD and TGA. The sample was performed by Alpha 1-2 LD plus, *Martin Christ Gefriertrocknungsanlagen GmbH*. The filtrated samples in polystyrene containers were kept in -80°C fridge overnight. Then, the samples were put in glass containers and then attached to freeze dryer valve for 24 hours. The samples were kept in polystyrene containers with lids and put them in plastic zip lock bag.

3.4.2 Inductively coupled plasma (ICP) – The stoichiometry of synthetic C-S-H was analysed by Inductively Coupled Plasma in the Optical Emission Spectroscopy mode (ICP-OES) which was performed on an ICPE-9000 series (Shimadzu) instrument. After washing and filtration, 0.1 g of the filtrated sample was dissolved in 8.0 mL of 65% HNO_3 (14.58 M), *Carlo Erba* and then in 2.0 mL of fuming 100% HNO_3 (22.43 M), *Merck KGaA*. The dissolved samples were diluted in HNO_3 (2.0 M), *Alfa Æsar* at x10, x100 and x1,000. Table 3.2 shows total volume of the dissolved samples and 2.0 M of HNO_3 of x10, x100 and x1,000 dilutions. After 24 hours, the diluted samples were filtered by using 10 mL of syringe together with 0.45 µm PTFE filter.

Dilution	Sample (μL)	2M HNO$_3$ (μL)
x10	1000	9000
x100	100	9900
x1000	10	9990

Table 3.2 Total volume of the dissolved samples and 2.0 M of HNO$_3$ of x10, x100 and x1,000 dilutions.

3.4.3 Fourier-transform infrared spectroscopy (FTIR)– After filtration, the filtrated samples were investigated by FTIR to identify the functional groups present in the precipitated C-S-H. The filtrated sample after washing were directly examined using a Nicolet 6700 from *ThermoFisher Scientific* with the range $450 - 4{,}000\text{cm}^{-1}$ (wavelength). The data were collected by *Omnic* software.

3.4.4 X-Ray Diffraction (XRD) - Data of synthetic C-S-H were collected using CuKα XRD (PANanalytical) analyses of wavelength λ=1,54 Å with a fixed divergence slit. The size of the slit is ½. Samples were placed in the sample holder and the patterns were collected between 5 and 70 degree 2θ. Scan step size is 0.0167113 degrees 2θ. The XRD pattern was recorded by *X'PERT Data Collector* software.

3.4.5 Thermogravimetric analysis (TGA) – TGA were performed on a Mettler Toledo, SDTA851 instrument. Samples (10-15 mg) were introduced in alumina crucible with a temperature ramp from 30-1000°C at 10°C/min under a nitrogen atmosphere.

3.4.6 Zeta potential – The zeta potential measurements were performed at 23-25°C using a NanoZS from Malvern Instruments. After washing and filtration of precipitated C-S-H, the suspensions were prepared by dispersing 2%w/v of solid in NaOH. The pH was controlled at 12.0±0.1. Prior to measuring, 1.0 mL of suspension was added into a disposable cuvette and inserted into the machine.

3.4.7 Transmission electron microscopy (TEM) The morphology of the synthetic C-S-H was investigated by using TEM, *Thermo Scientific™* Talos F200X scanning transmission electron microscope (STEM) with TEM mode. It was operated at an acceleration voltage of 200 kV. TEM images were collected and then exported by using TEM Imaging and Analysis (TIA) software. The samples were prepared by dispersing the precipitated C-S-H in isopropanol and treated in an ultrasonic bath for 15 minutes. The dispersed samples were dropped on to the charged grid (carbon films on 300 mesh grids copper, *Agar Scientific Ltd.*) and allowed to dry for few minutes.

3.4.8 Scanning transmission electron microscope-energy dispersive x-ray (STEM-EDX) - High-angle annular dark-field (HAADF) STEM measurement combined with EDX were used to investigate the elemental distribution. The elemental map of the samples was operated by Talos F200X scanning transmission electron microscope (STEM) with STEM-EDX mode. It was operated at an acceleration voltage of 200 kV. After STEM alignment, the elemental map was performed by using *Bruker Esprit 1.9* software. The samples were prepared with the same procedure as for TEM.

3.4.9 TEM- Tomography- The sample was dispersed in isopropanol and with gold particles as fiducial markers for the 3D reconstruction. The suspension was dropped on the TEM grid and the sample dried for few minutes. Tomograms were recorded on a transmission electron microscopy (Tecnai T12, FEI Company, Eindhoven, The Netherlands) at 120 kV from -65° to +65° tilt angles with increments of 1° using *SerialEM* (Mastronarde DN, 2005). Reconstructions were done with the freeware IMOD [53–55].

Chapter 4   Investigation of Iron (Fe^{3+} ions) on precipitated synthetic calcium silicate hydrate (C-S-H)

This chapter presents effect of iron (III) or Fe^{3+} ions on synthetic C-S-H by using the dropwise precipitation method. The effect of Fe^{3+} has been studied on precipitation of synthetic C-S-H. Thermodynamic modelling (GEMS) was used to predict expected phase formation under the experimental conditions studied. Characterization methods such as XRD, TGA, TEM and STEM-EDX were used to investigate the effect of Fe^{3+} on the precipitated product. The aim of this work is to better understand the effect of Fe^{3+} on the growth of precipitated synthetic C-S-H.

4.1   Introduction

Supplementary cementitious materials (SCMs) such as fly ash, calcined clays, ground granulated blast furnace slag and silica fume have been commonly used for clinker substitution in concrete or blended with Portland cement. The percentage of clinker replacement (approx. 5-20%) has been increased in recent years in concrete production in order to reduce CO_2 emissions linked to the production of clinker [5,6,9,27]. Each of these materials have different chemical compositions which results in different reactivities and different hydrated phases. Using SCMs makes concrete more sustainable, however, interaction of SCMs with Portland cement can affect performance at early ages, which often reduces strength, an undesired behaviour [4,6,8].

The major anhydrous phases in Portland cement, are alite (Ca_3SiO_5) and belite (Ca_2SiO_4). The minor phases are calcium aluminate ($Ca_3Al_2O_6$), ferrite ($Ca_2(Al,Fe)_2O_5$), calcite ($CaCO_3$) and gypsum ($CaSO_4$) [6,27,56,57]. When cement reacts with water, various ions (e.g. Ca, Si, Al, Fe and hydroxide) release continuously into the pore solution forming various hydration products [27,57]. The main hydration products are calcium silicate hydrate (C-S-H), calcium hydroxide (CH), ettringite, calcium monosulphoaluminate or calcium monocarboaluminate. Typically, Portland cement contains approximately 2-5% of Fe_2O_3. Fe-containing phases such as Fe-containing ettringite, AFm

phases are less stable, which can transform to stable Al-Fe siliceous hydrogarnet phases during hydration [56,58,59]. Furthermore, ferrihydrite often formed as an intermediate phase in the early stage of hydration can transform with time to form siliceous hydrogarnet [56].

Calcined clay minerals which when used in cement and concrete can lower the clinker factor but are often associated with relatively high Fe_2O_3 the content (0.3-15.4%) [60] which depends on the source of material. Chakchouk et al. [17] reported 5.87% of Fe_2O_3 in Tunisian clay and Danner et al. [61] found 10.6% of calcined marl in Norway. Ghorbel and Samet [19] investigated pozzolanic activity of kaolin by varying iron contents in blended white cements. The pozzolanic activity was enhanced when adding iron up to 2.7% Fe_2O_3, where the compressive strength increased with a higher consumption of portlandite. Moreover, a dense structure of C-S-H and ettringite containing iron was observed.

C-S-H is the major hydration product and the most important component in concrete [20,35,62]. The volume of C-S-H is up to 70% of fully hydrated paste [63]. It is a poorly crystalline non-stoichiometric material, which is difficult to characterize and describe at an atomistic level. ^{29}Si NMR has been the most relevant method to study Si arrangement in C-S-H [20,62,64,65]. This technique can distinguish between Si monomers (Q^0) and Si connected to a number X of other Si species (Q^X). The silica arrangement in C-S-H is parallel linear rows of dimers of silica tetrahedral more or less bridged by a third tetrahedron. Such a "dreierketten" structure is similar to the structure observed in some naturally occurring minerals such as tobermorite. 14 Å tobermorite is composed of Ca layers which are terminated on each side by Si chains. Both Ca^{2+} and water can be found between the calcium-silicate layers. Furthermore, foreign ions such as Fe^{3+}, Al^{3+} and Zn^{2+} may be incorporated into C-S-H [63,66,67]. However, there are fundamental questions that need to be addressed in order to fully understand the effect of such ions on the growth of C-S-H, is being addressed in this study for the case of Fe^{3+} for example - does iron substitute calcium in the C-S-H structure or does iron precipitate as a second phase e.g. ferryhidrite or hydrogarnet, or does it simply adsorb on the surface of C-S-H?

The precipitation method is an attractive tool to prepare synthetic C-S-H and will allow us to identify the effect of individual parameters on nucleation and growth of synthetic C-S-H. Kumar et al. [20] have recently reported that uniform synthetic C-S-H with controlled Ca/Si ratios can be produced using a well-designed reactor with different precipitation modes. The Ca/Si molar ratio of synthetic C-S-H were controlled between 1.0 and 2.0 without the formation of any secondary phases. The aim of this work is to investigate the effect of Fe^{3+} on the growth of synthetic C-S-H in well controlled conditions by using the dropwise method described by Kumar et al. [20]. This will pro-

vide fundamental understanding on the role of Fe^{3+} on key factors like C-S-H formation which may influence early age often modified while using SCMs containing iron.

4.2   Materials and Methods

Synthesis of pure phase C-S-H

The synthetic C-S-H was prepared via the dropwise method described in detail in Chapter 3. 0.1 M of sodium silicate (Na$_2$SiO$_3$, S*igma-Aldric*h, CAS:6834-92-0) at pH 13.5 was present in the vessel and 0.2 M of calcium nitrate (Ca(NO$_3$)$_2$.4H$_2$O, *Fluka Chemicals,* CAS:13477-34-4) at pH 6.5 was introduced into the vessel in a drop wise manner at a fixed rate (2.17 ml/min). The diagram of dropwise precipitation method is shown in Chapter 3, Figure 3.1. The pH of the solutions was adjusted by using sodium hydroxide (NaOH, *Acros organic*, CAS:1310-73-2) as indicated by Kumar et al. [20] to give a C-S-H with a 2/1, Ca/Si ratio. The total reaction time was 3 hrs. All solutions were prepared by using ultra-pure water previously boiled to remove the CO$_2$. After precipitation, the samples were washed with ultra-pure water mixed with ethanol (50:50 vol%) and followed by pure ethanol to remove unwanted ionic species in the precipitate. Then, samples were collected by vacuum filtration and stored as wet pastes in polystyrene containers.

Synthesis of C-S-H with Fe^{3+}

Iron (III) nitrate (Fe(NO$_3$)$_3$.9H$_2$O, *Acros Organics*) solutions at pH 2.5 were investigated at 1.0 and 4.0 mM concentration that was placed in either the silicate solution or the calcium solution. Experimental conditions are shown in Table 4.1 and 4.2. A pre-precipitation of an Fe phase was observed in the initial Fe containing solution with pH's ≥ 11 (Table 4.1). The experimental conditions were then modified in order to avoid the pre-precipitation as shown in Table 4.2. The synthetic C-S-H with Fe^{3+} was synthesized via the dropwise method in the same manner as for the synthesis of the pure phase C-S-H, i.e. by adding dropwise initial solution I to initial solution II that was already in our reaction vessel.

Sample	Initial solution I			Initial solution II		
	Ca(NO$_3$)$_2$.4H$_2$O	Fe(NO$_3$)$_3$.9H$_2$O	pH	Na$_2$SiO$_3$	Fe(NO$_3$)$_3$.9H$_2$O	pH
CSH	0.2 M	-	6.5	0.1 M	-	13.5
Fe_A1	0.2 M	1.0 mM	11.0	0.1 M	-	13.5
Fe_A2	0.2 M	4.0 mM	11.0	0.1 M	-	13.5
Fe_B1	0.2 M	-	6.5	0.1 M	1.0 mM	13.5
Fe_B2	0.2 M	-	6.5	0.1 M	4.0 mM	13.5

Table 4.1 Experimental conditions of synthetic C-S-H with pre-precipitation of Fe in initial solutions.

Sample	Initial solution I			Initial solution II		
	Ca(NO$_3$)$_2$.4H$_2$O	Fe(NO$_3$)$_3$.9H$_2$O	pH	Na$_2$SiO$_3$	Fe(NO$_3$)$_3$.9H$_2$O	pH
Fe_C1	0.2 M	1.0 mM	2.5	0.1 M	-	13.5
Fe_C2	0.2 M	4.0 mM	2.5	0.1 M	-	13.5

Table 4.2 Experimental conditions of synthetic C-S-H without pre-precipitation of initial Fe containing solution.

Characterization methods

The morphology of samples was observed using transmission electron microscope (Thermo Scientific™ Talos F200X scanning transmission electron microscope (STEM) at high-resolution mode at 200 kV. TEM images were collected and then exported by using TEM Imaging and Analysis (TIA) software. The samples were prepared by dispersing the precipitated C-S-H in isopropanol and treated in an ultrasonic bath for 15 minutes. The dispersed samples were dropped on to the charged grid (carbon films on 300 mesh grids copper, *Agar Scientific Ltd.*) and allowed to dry for few minutes. High angle annular dark field (HAADF) scanning transmission electron microscopy (STEM) measurements combined with EDX were used to make an elemental mapping of the samples. Details were shown in Chapter 3, Section 3.4.8.

Synthetic C-S-H precipitates were dissolved in concentrated HNO$_3$ in order to determine the Ca/Si ratio and Fe content by inductively coupled plasma (ICP) on an ICPE-9000 series (Shimadzu) instrument. The sample preparation for ICP was described in Chapter 3, Section 3.4.2. For characterisation by XRD and TGA the C-S-H samples were freeze-dried for 24 hours after washing which was explained in Chapter 3, Section 3.4.1. The diffractogram of the freeze-dried powder was measured using CuKα XRD (PANanalytical) analyses of wavelength λ=1,54 Å with a fixed divergence

slit. The size of the slit is ½. The patterns were scanned between $5° < 2\theta < 70°$ degree. Thermogravimetric analysis (TGA) were performed on a Mettler Toledo SDTA851 instrument using a temperature ramp from 30-1000°C at 10°C/min under a nitrogen atmosphere. The data presented is typical of two replicates.

Thermodynamic modelling has been carried out using the Gibbs free energy minimisation program GEMS [25,26]. This software package GEMS v.3 has been developed to compute the chemical speciation of the pore solution and hydrate phase assemblage during cement hydration. In our work, *Cem18* database was used for thermodynamic calculation. GEMS predicts possible equilibrium phases in our synthetic C-S-H system in the presence of Fe^{3+}.

4.3   Results

Morphology

TEM micrographs of synthetic C-S-H –with and without Fe^{3+} are shown in Figure 4.1 and 4.2. All samples show C-S-H with a nanofoil-like morphology. Some spherical nanoparticles (200 nm) were also observed for Fe_A2 (Fig.4.2(a)) and Fe_B2 (Fig.4.2(b)), the samples prepared with high initial concentrations of Fe^{3+}. To determine the composition of synthetic C-S-H with Fe^{3+}, HAADF-STEM measurement combined with EDX were used. The observed elemental distributions are shown in Figure 4.3 and 4.4. HAADF image of Fe_C2 in Figure 4.3 shows homogeneous nanofoil morphology of synthetic C-S-H with 4.0 mM of Fe^{3+}. The distribution of Ca, Si and O were relatively uniform. The Fe were observed on the elemental map shows the presence of Fe over the whole sample but, some bright spots (around 30 nm) can be observed (red circle in Fig.4.3, Fe) possibly suggesting some ultrafine Fe containing particles on the C-S-H foils. The Fe_B2 (Fig.4.4) shows a mixture of nanofoils and spherical nanoparticles. In the elemental maps from the STEM-EDX, the presence of Fe is only observed in the spherical nanoparticles. The distribution of Ca, Si, and O are detected in both nanofoils and nanoparticles which were also relatively uniform.

(a)

(b)

(c)

(d)
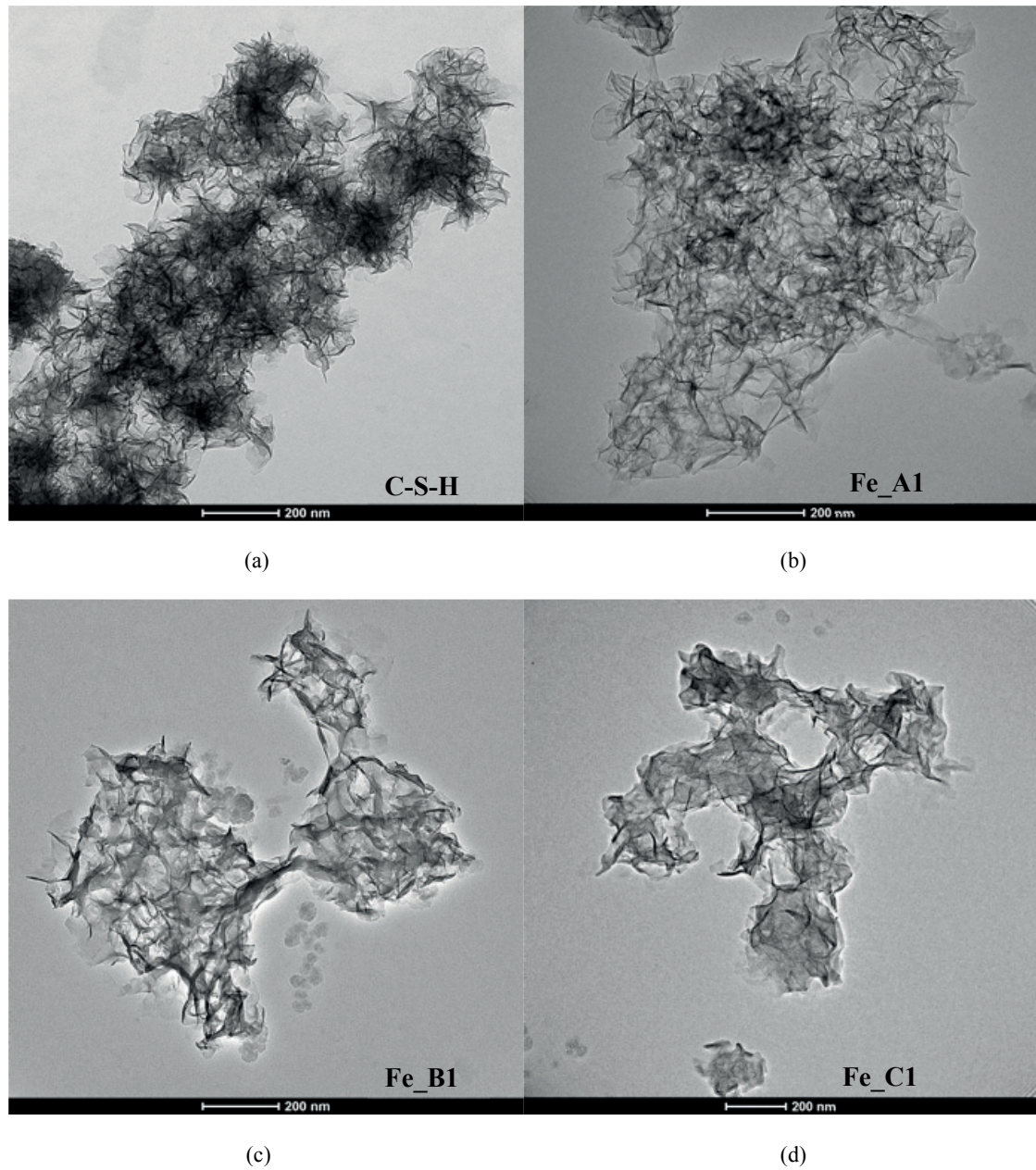
Figure 4.1 Morphology of synthetic C-S-H (a) CSH, synthetic C-S-H with low concentration of Fe^{3+} (b) Fe_A1, (c) Fe_B1, (d) Fe_C1.

(a)   (b)

(c)
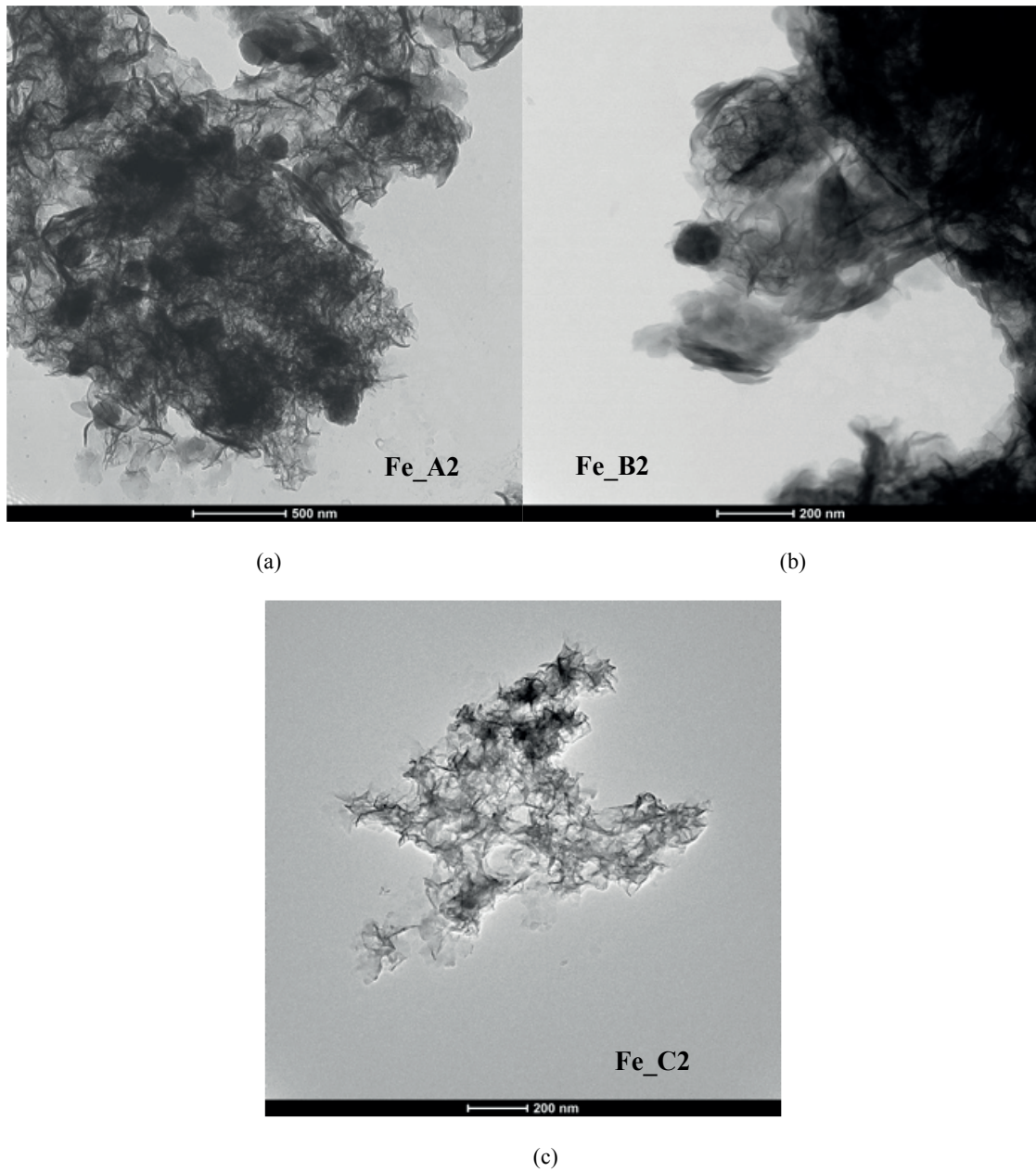
Figure 4.2 Morphology of synthetic C-S-H with high concentration of Fe^{3+} (a) Fe_A2, (b) Fe_B2, (c) Fe_C2.
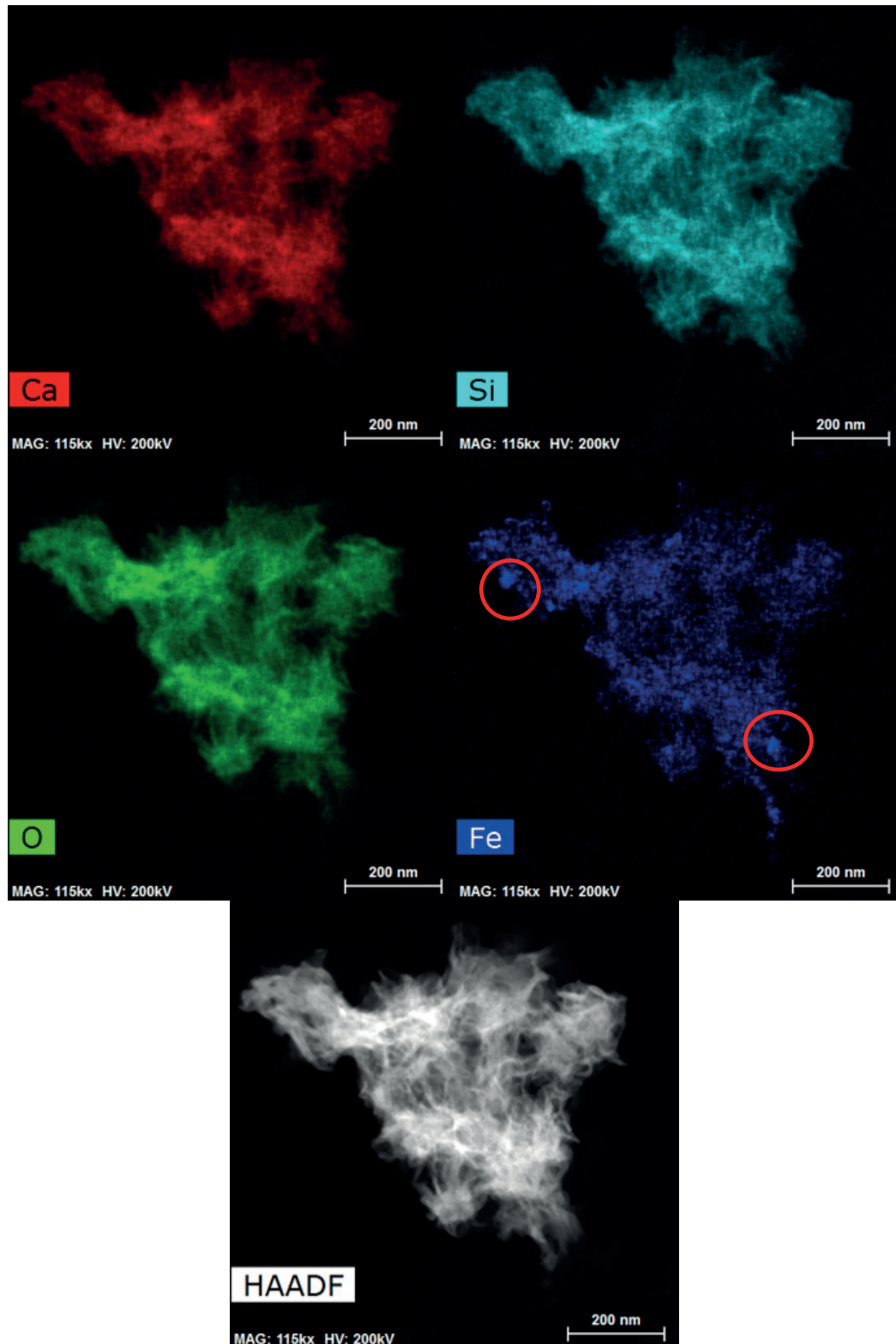
Figure 4.3 Elemental maps of synthetic C-S-H with high concentration of Fe^{3+} (Fe_C2).
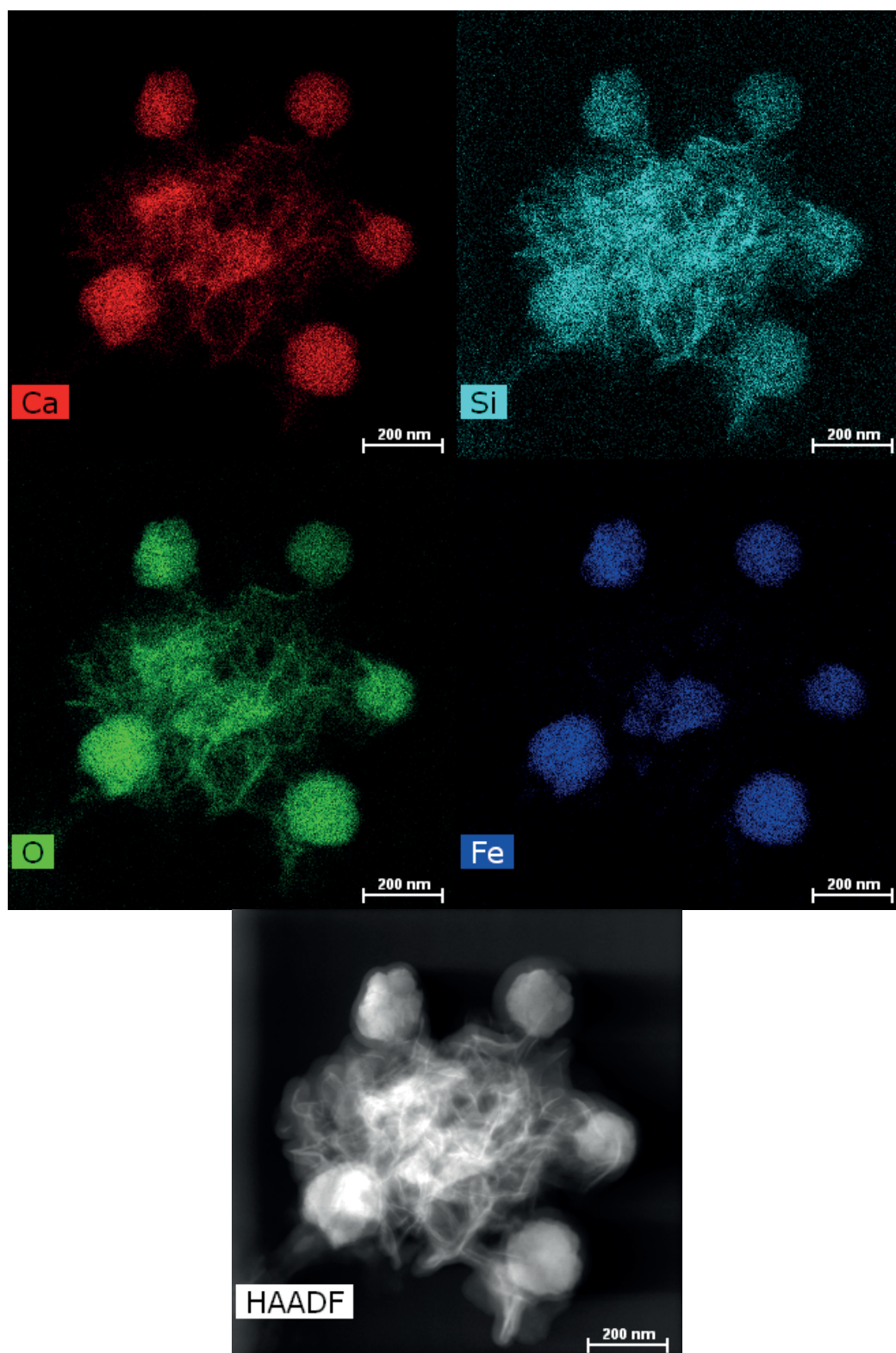
Figure 4.4 Elemental maps of synthetic C-S-H with high concentration of Fe^{3+} (Fe_B2).

Chemical compositions

The Ca/Si ratio and Fe content for the precipitated synthetic C-S-H with and without Fe^{3+} are shown in Table 4.3. The quantity of Fe in the samples depends on Fe^{3+} concentrations that were introduced in the reactions. At low concentration of Fe^{3+} the C-S-H shows 0.010-0.014 millimole (mM) of Fe and at high concentration of Fe^{3+} 0.039-0.048 mM of Fe per gram of sample, about 2-3% of the iron initially added to the reaction vessel. The presence of Fe^{3+} in the precipitation of the synthetic C-S-H leads to Ca/Si ratios in general lower than the pure C-S-H system. Fe_B2 at high Fe^{3+} concentration shows the lowest Ca/Si at around 1.2.

Sample	*Ca/Si*	*Fe/Si*	*Fe (mM)/ gram sample*
CSH	2.2 ± 0.6	-	-
Fe_A1	1.7 ± 0.3	0.0006	0.014
Fe_A2	1.7 ± 0.1	0.0027	0.048
Fe_B1	1.7 ± 0.3	0.0006	0.010
Fe_B2	1.2 ± 0.1	0.0025	0.039
Fe_C1	1.8 ± 0.1	0.0006	0.011
Fe_C2	2.2 ± 0.6	0.0027	0.039

Table 4.3 Ca/Si ratios and quantity of Fe per gram of sample.

XRD data

Initial Fe containing solutions of Fe_A1/A2 and Fe_B1/B2 were prepared by adjusting pH as shown in Table 4.1. The initial solution I and II were calcium and silicate solutions, respectively. Pre-precipitation occurred when pH in solution reached the designed pH as shown in Table 4.1. The colour of the pre-precipitation either in the initial solution I or II was dark brown. The XRD pattern of the pre-precipitation of Fe containing solution in the initial solution I and II are shown in Figure 4.5 which was an amorphous material. It could possibly be an amorphous material of Fe phase because of characteristic colour of Fe [68,69].
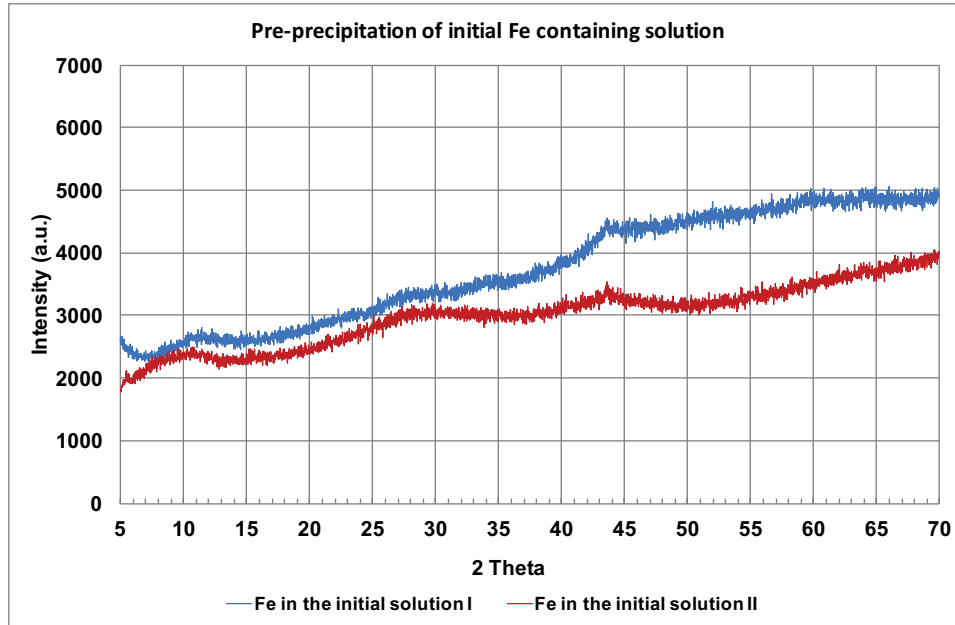
Figure 4.5 XRD patterns of pre-precipitations of Fe solid phase in the initial solution I and II.

XRD analysis results for the seven samples show amorphous materials and some crystalline peaks (Fig.4.6 and 4.7). A comparison of XRD analysis results for the seven samples (with and without Fe^{3+}) show some peaks around 16-18°, 29.2°, 33°, 50°, 55° and 67° (2θ), which correspond to dried synthetic C-S-H [62]. When comparing C-S-H in the presence of Fe^{3+} at low concentration (Fig.4.6), all samples shows similar pattern to C-S-H except for a small broad peak around 17° (2θ), which, according to recent results from Grangeon et al. [62], corresponds to the occupancy of Si atoms in bridging sites. We see that this shifts slightly to the left which could be due to replacement of Si by Fe at the bridging site. At the higher Fe^{3+} concentration, (Fig.4.7), the Fe_C2 sample also shows a similar pattern to pure C-S-H again with the small broad peak around 17° (2θ) shifting slightly to the left. Both Fe_A2 and Fe_B2 show more crystalline peaks at 17.4°, 20.0°, 26.8°, 28.7°, 33.0°, 35.2°, 39.6°, 44.7° and 52.9° (2θ), which correspond to siliceous hydrogarnet containing iron [70]. There are some small crystalline peaks of $NaNO_3$ at 23.2° and 48.4° and $Ca(OH)_2$ at 18.1°, 34.1° and 47.3° (2θ). Thermodynamic modelling using GEMS has been used to see what phases are expected at equilibrium and is discussed below.
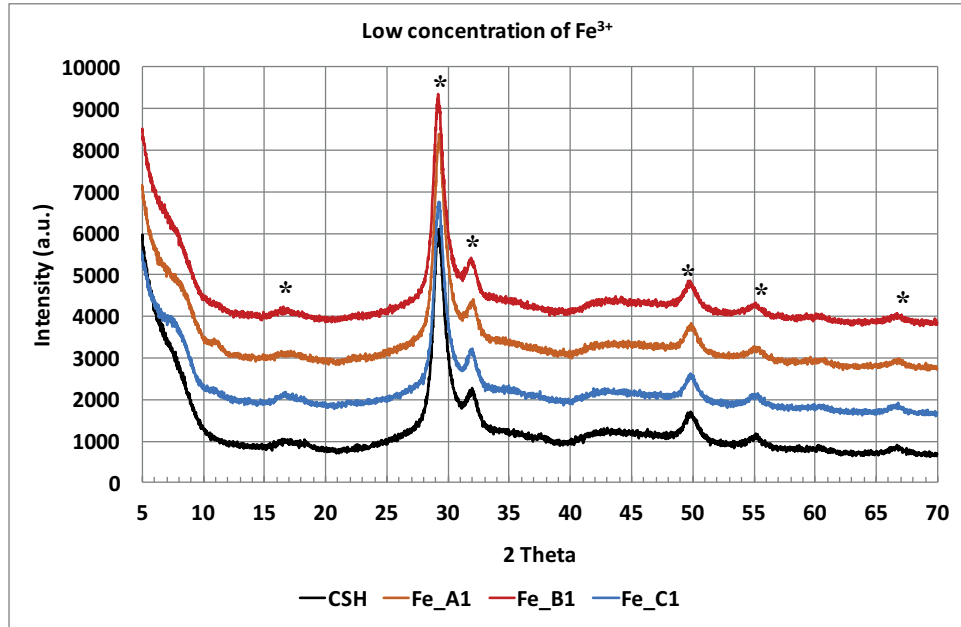
Figure 4.6 XRD patterns of synthetic C-S-H of low concentration of Fe^{3+} (* - C-S-H).
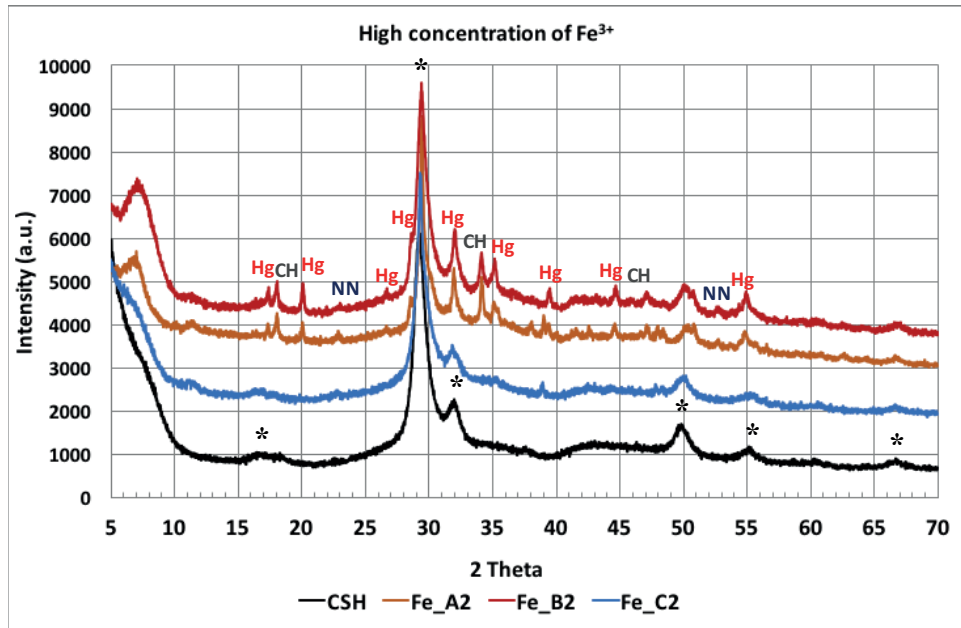
Figure 4.7 XRD patterns of synthetic C-S-H of high concentration of Fe^{3+} (* - C-S-H, Hg-siliceous hydrogarnet, CH-calcium hydroxide and NN-sodium nitrate).

TGA data

In cementitious materials, mass loss of samples up to 600ºC relate to the loss of water and above 600ºC corresponding to the loss of CO_2 [32]. All freeze-dried samples show the main weight loss in TGA curve at 80-150°C typical of interlayer water of C-S-H and the broad weight loss at 650-700°C could be due to poorly crystalline $CaCO_3$ (Fig.4.8 and 4.9). At high concentration of Fe^{3+} (Fig.4.9), there are weight loss at 320°C approximately 2 wt.-%, and 450°C approximately 5 wt.-%. It could be due to siliceous hydrogarnet containing iron [11] and $Ca(OH)_2$, respectively. When analyzing wet samples (without freeze drying) we do not see any $Ca(OH)_2$ or $CaCO_3$ suggesting some minor degradation and formation of $CaCO_3$ and $Ca(OH)_2$ can sometimes take place during the freeze-drying stage.
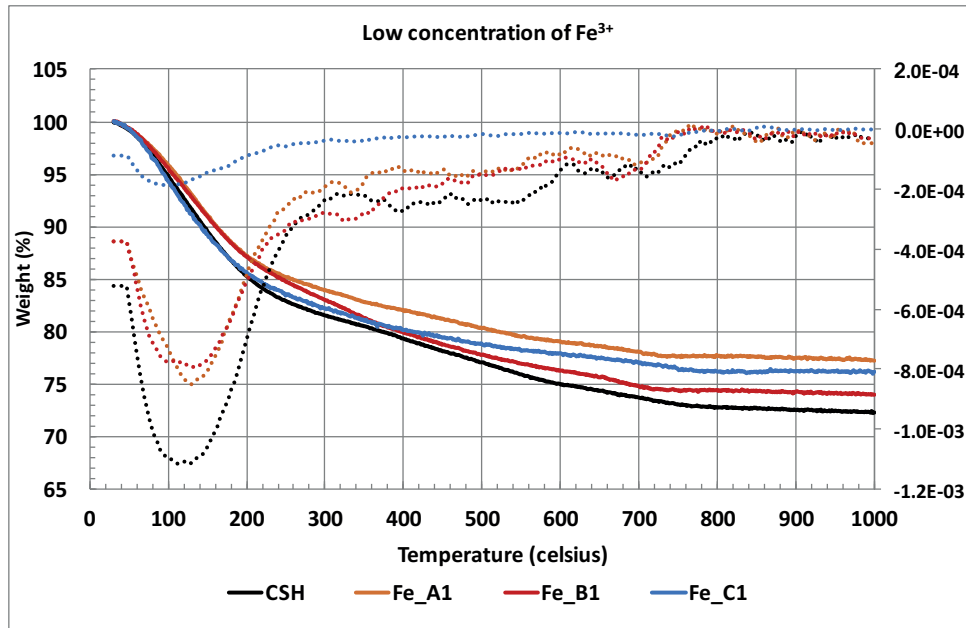
Figure 4.8 Thermogravimetric analysis (TGA) of synthetic C-S-H. Solid lines represents weight loss and dotted line represents first derivative of low concentration of Fe^{3+}.
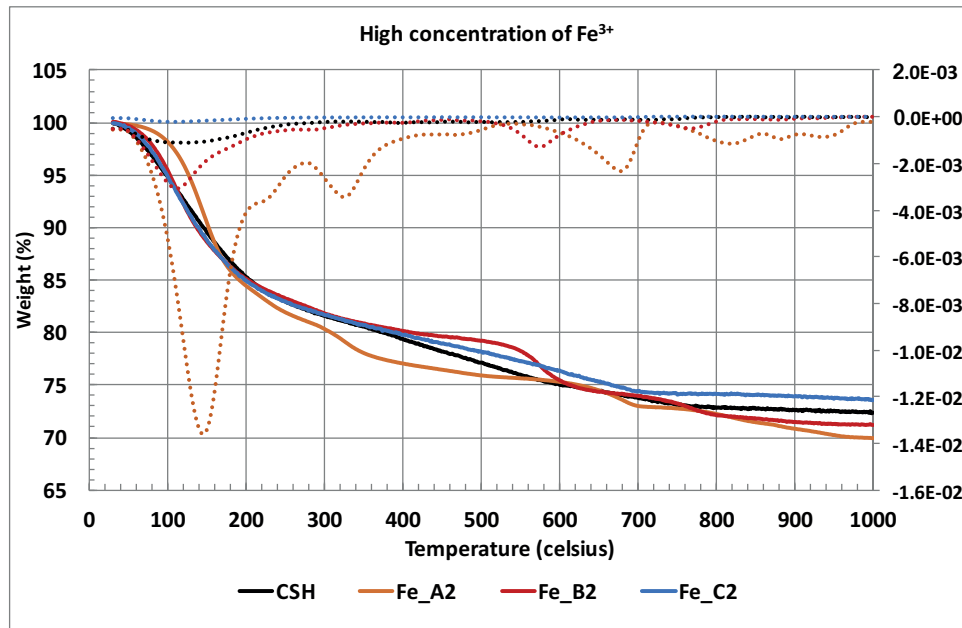
Figure 4.9 Thermogravimetric analysis (TGA) of synthetic C-S-H. Solid lines represents weight loss and dotted line represents first derivative of high concentration of Fe^{3+}.

Thermodynamic modelling, GEMS

Generally, Fe^{3+} is commonly used to prepare ferrihydrite in homogeneous solution which acts as a precursor of goethite synthesis [71–74]. The ferrihydrite is metastable forming at pH > 2.5 which can transform to more crystalline and stable phases. From Table 4.1, the pre-precipitation of an Fe phase was observed in the initial Fe containing systems whether in the calcium or silicate solutions, pH≥11. The thermodynamic modelling (GEMS) predicts iron species and phase of the initial Fe containing solution which are shown in Figure 4.10 and 4.11. The @ in Figure 4.10 and 4.11 represents a water molecule in the full chemical formula. The solid phase of the pre-precipitation of the initial solution (Fe_A1, Fe_A2, Fe_B1 and Fe_B2) is expected to be ferrihydrite (FeOOH) (Fig.4.10 (a) and 4.10 (b)). Table 4.4 shows the quantity of ferrihydrite calculated by GEMS. The quantity of this phase depends on concentration of Fe^{3+} and pH of the solution. At low pH (~2.5) of the initial Fe containing solution, there is no pre-precipitation of a solid phase. The iron species of the initial Fe containing solution without pre-precipitation present are shown in Figure 4.11. The major Fe species in the initial solution without solid phase is Fe^{3+}, Fe$_2$(OH)$_2^{4+}$ and FeOH^{2+}. The ferrihydrite (FeOOH) is not expected in the initial Fe containing solution of Fe_C1/C2.
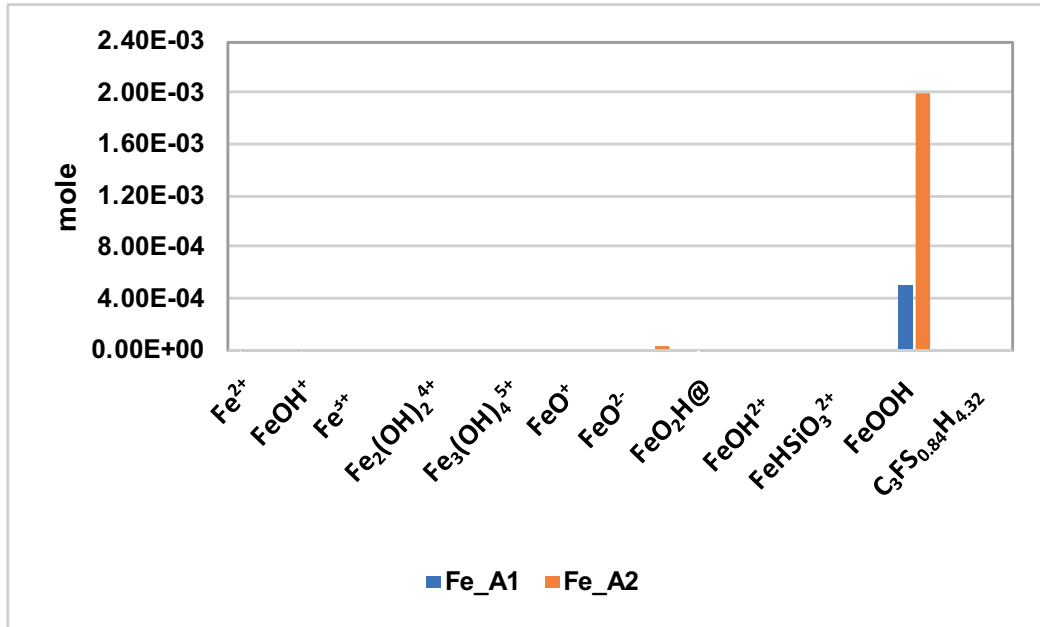
(a)
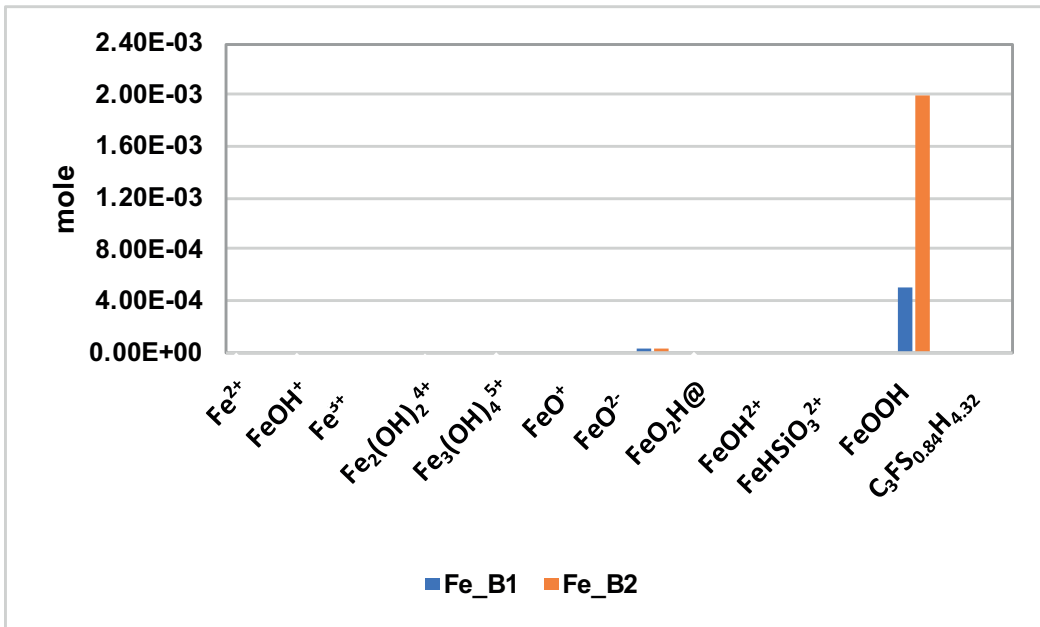
(b)

Figure 4.10 Iron species of the initial Fe containing solution predicted from GEMS at equilibrium state. (a) Fe_A1/A2, (b) Fe_B1/B2.
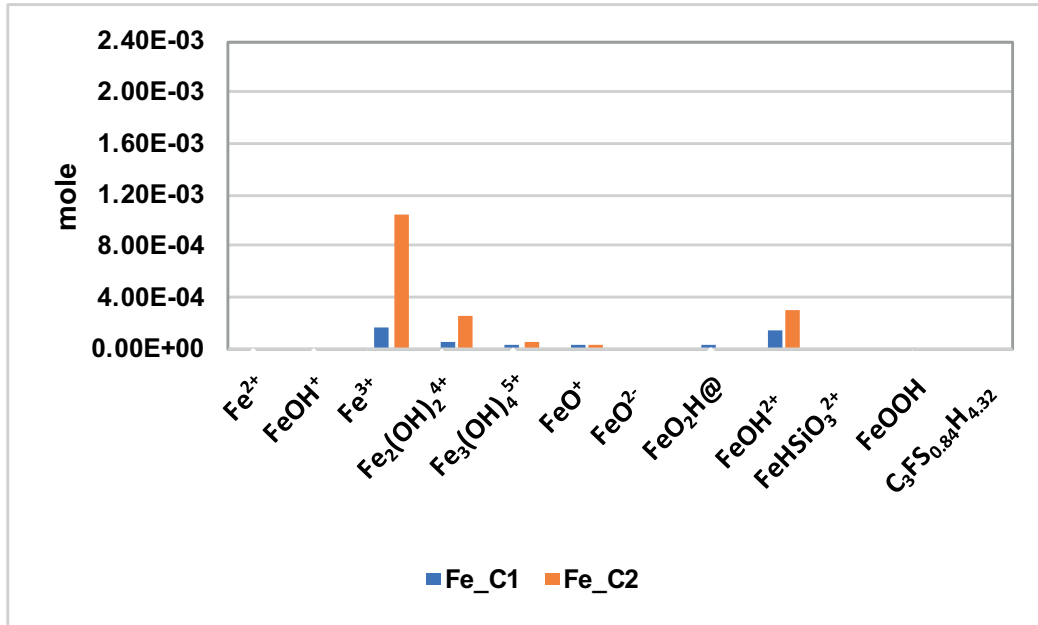
Figure 4.11 Iron species of the initial Fe containing solution predicted from GEMS at equilibrium state of Fe_C1/C2.

Sample	Ferrihydrite (mM)
Fe_A1	0.495
Fe_A2	2.004
Fe_B1	0.495
Fe_B2	2.004

Table 4.4 Amounts of pre-precipitation products of initial Fe containing solution calculated by GEMS.

The synthetic C-S-H system in the presence of Fe^{3+} were also modelled using GEMS. The possible solid phases and their quantities at equilibrium are shown in Table 4.5. GEMS only looks at final equilibrium point, thus there is no difference between initial Fe-containing solutions of calcium and silicate. C-S-H is the dominant solid phase in the system. With presence of Fe^{3+}, GEMS predicts a second phase, siliceous hydrogarnet phase, $C_3FS_{0.84}H_{4.32}$. The calculations from GEMS shows good agreement with our experiments with high Fe^{3+} concentration of Fe_A2 and Fe_B2.

Sample	C-S-H (mM)	$C_3FS_{0.84}H_{4.32}$ (mM)
CSH	15.0	-
Fe_A1	14.8	0.2
Fe_A2	13.6	1.0
Fe_B1	14.8	0.2
Fe_B2	13.6	1.0

Table 4.5 Possible phases in synthetic C-S-H experiments with the presence of Fe^{3+} calculated by GEMS.

Magnetic resonance

Magnetic resonance has been used to identify the iron site in the C-S-H structure by using electron paramagnetic resonance (EPR) and nuclear magnetic resonance (NMR). This was carried out in collaboration with Dr. Brennan Walder and Prof. Lyndon Emsley at the Institut des Sciences et Ingénierie Chimiques at EPFL.

Electron paramagnetic resonance (EPR)

The local distribution of iron in these samples was analysed by magnetic resonance. Figure 4.12 shows low temperature X-band EPR spectra of iron containing C-S-H samples prepared with and without prior precipitation of ferrihydrite phases. The EPR spectrum of the latter sample, Fe_C1, is dominated by a tall feature centered around an apparent g value of $g_{eff} = 4.3$. From this feature, a prominent wing extends toward lower field values, terminating at $g_{eff} = 9.7$. Signals in this region have a long history in the literature of silicates [75] and the $g_{eff} = 4.3$ signal in particular has been attributed to isolated Fe^{3+} ions which substitute for Si^{4+} in tetrahedral coordination as a network former, as first described in the pioneering work of Castner et. al. [76]. Toward higher field, a less distinct roll is visible as a minor feature, centered around $g_{eff} = 2$, which covers nearly the entire baseline to the upper end of the field sweep range (0.6 T, $g_{eff} = 1.1$). This feature may be due to solvated $[Fe(H_2O)_6]^{3+}$ trapped in pores but unassociated with the C-S-H structure. More likely, it is the result of spin-spin coupling between centers in regions of higher iron density or nanoparticles, as is well-documented for a wide variety of iron-doped systems. The EPR spectrum of sample Fe_B2, containing iron-rich nanoparticles, supports this interpretation: the broad feature at $g_{eff} = 2$, now appearing as a rolling Gaussian line shape, dominates the spectrum. The tall feature around $g_{eff} = 4.3$ due to isolated Fe^{3+} is a minor feature in comparison to the roll but remains visible none-

theless, suggesting that the C-S-H foils do contain Fe^{3+} but at a lower level rendering them dark in STEM-EDX.
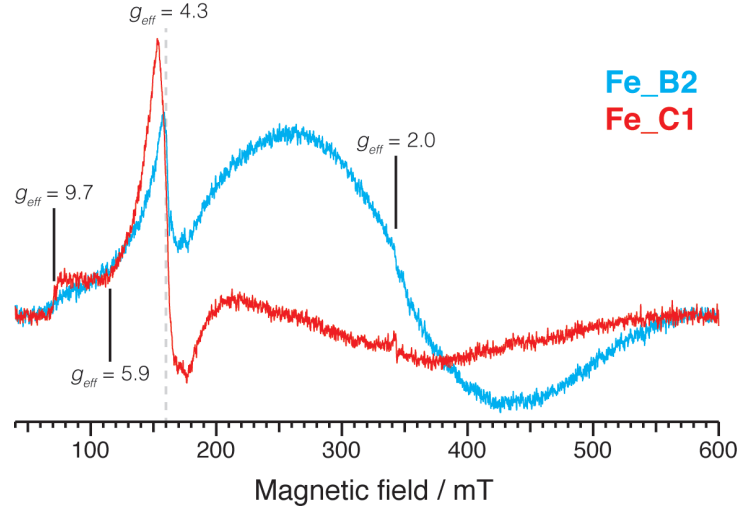
Figure 4.12 X-band EPR ($\omega_0/2\pi$ = 9.60 GHz) spectra at 100 K of C-S-H samples synthesized with a high concentration of Fe^{3+} with prior precipitation of ferric species at a high Fe^{3+} concentration (4.0 mM in starting solution), Fe_B2 and without prior precipitation at a low Fe^{3+} (1.0 mM in starting solution), Fe_C1.
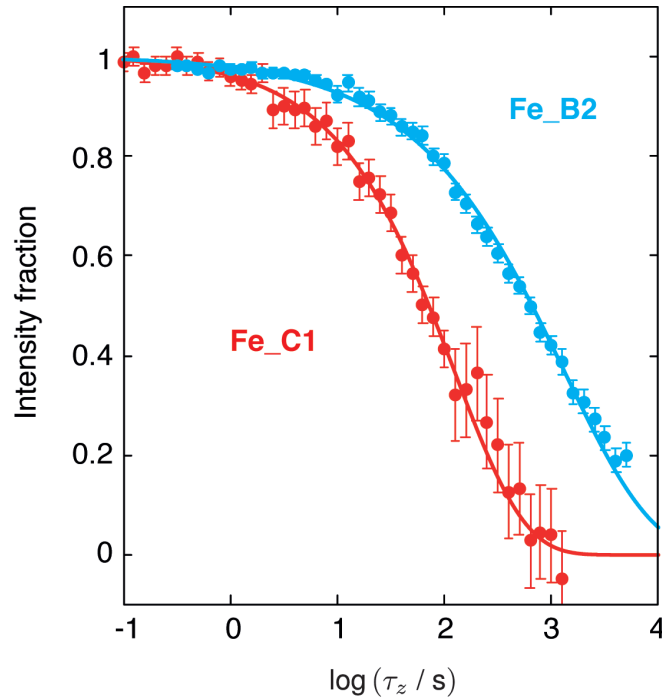
Figure 4.13 Semilog plot of the intensity of ^{29}Si signals as a function of the longitudinal storage interval τ_z for C-S-H samples Fe_B2 and Fe_C1 at 100 K in the z-filtered CP experiment. Points signify data, and the curves the best fit to a stretched exponential decay function. Best fit parameters: Fe_C1, T = 125 ± 11 s, β = 0.67 ± 0.05; Fe_B2, T = 1320 ± 90 s, β = 0.53 ± 0.03.

Nuclear magnetic resonance (NMR)

As has been discussed extensively in the literature, the features observed in the X-band EPR spectra of ferric ions in silicates are suggestive of certain iron environments, but they are not unique fingerprints. To provide supporting evidence for the role of iron as a network former in C-S-H, we investigated the relaxation of ^{29}Si nuclei by means of ^{29}Si CP-MAS NMR, which provides signals that are selective for the silicates in the C-S-H phase. Figure 4.13 shows the decay of the CP-MAS NMR signal as a function of a longitudinal storage interval τ_z during which the NMR signal decays to zero. The decay of such signals is governed by factors such as the concentration of relaxing agents, motional dynamics, and nuclear spin diffusion. For NMR nuclei in a rigid solid, being relaxed by dilute, uniformly, and randomly distributed paramagnetic centers (such as Fe^{3+}), the decay of such signal is predicted to be governed by a stretched exponential, with a stretching parameter of $\beta = 0.5$.

$$S(\tau_z) = A \exp\left(-\tau_z/T\right)^{\beta}$$

This is a common situation for ^{29}Si in silicate glasses being relaxed by paramagnetic impurities. For frozen Fe_B2 at 100 K, this is indeed the stretching parameter we observe. This evidence supports the EPR in suggesting that the iron centers in the C-S-H phase are incorporated much as they are in silicate glass frameworks, where they are known to be network formers. Stretching parameters between 0.5 and 1 result when any of the above assumptions regarding the distribution of paramagnetic centers breaks down. For frozen Fe_C1, it is likely that the β parameter of around 0.7 that we analyse is a consequence of an increasingly high iron content in the silicate matrix such that the assumption of dilute paramagnetic centers is no longer valid. The increased iron content of the C-S-H phase in Fe_C1 relative to Fe_B2 is also inferred through strong signal bleaching such that much lower signal-to-noise ratios of the ^{29}Si CP-MAS NMR spectrum are observed for the Fe_C1 sample, despite the fact that the iron concentration of the sample is nominally lower. This suggests that the majority of the Fe signal comes from an Fe rich phase e.g. the siliceous hydrogarnet phase, seen in the XRD and in the STEM-EDX for these Fe_B2 samples.

4.4   Discussion

In real Portland cement, ferrite is major Fe phase which reacts with water forming ettringite, ferrihydrite and siliceous hydrogarnet containing iron. The ferrihydrite converts to more stable siliceous hydrogarnet in a few hours with increasing pH in pore solution because of its metastable nature [56,59]. Fe enriched-kaolinite in blended white cement improves pozzolanic activity. The optimum level is 2.7% Fe_2O_3 [19]. A dense structure of C-S-H containing iron was found. At higher Fe_2O_3 contents, the pozzolanic activity decreased and also a new phase of $AlCaFeS(OH)_5$ was observed.

From our results, the effect of Fe^{3+} on the synthetic C-S-H was investigated at 1.0 and 4.0 mM via a dropwise precipitation method. The precipitated C-S-H is the major phase and a second phase is siliceous hydrogarnet (Table 4.5) is sometimes observed. For Fe_A1 and Fe_A2, adding NaOH at pH 11.0 in Ca and Fe solution leads to the pre-precipitation of ferrihydrite, which was observed by XRD (Fig.4.5) and predicted by the thermodynamic modelling (GEMS calculations) (Fig.4.10). When the suspension of ferrihydrite in calcium drops into the silicate solution, the metastable ferrihydrite can transform to the more stable phase of siliceous hydrogarnet, $C_3FS_{0.84}H_{4.32}$. This is also in agreement of GEMS calculation. When adding NaOH in Si and Fe solution (Table 4.1, Fe_B1 and Fe_B2), the iron could be in the form of a pre-precipitation of ferrihydrite, which was observed by XRD (Fig.4.5), as well as contributing to the formation of Fe (III) silicate complexes [74]. After introducing of Ca solution into suspension of ferrihydrite and Fe (III) silicate complexes, then siliceous hydrogarnet phase is seen to form, which is in agreement of GEMS prediction.

Without pre-precipitation of Fe phase (Fe_C1 and Fe_C2), no siliceous hydrogarnet is seen. As GEMS calculation at equilibrium state, our experiments have the same concentrations of chemicals in the system but different pH of initial solutions. So, we can observe only the different ionic speciations of the initial solutions. Figure 4.11 presents iron species of the Fe containing solution at equilibrium state calculated by GEMS. The major iron specie of Fe_C1 and Fe_C2 is Fe^{3+}, $Fe_2(OH)_2^{4+}$ and $FeOH^{2+}$. However, after mixing, only precipitated C-S-H is formed with no second phase of siliceous hydrogarnet. It could be the reaction of C-S-H is faster than hydrogarnet, which has a two-stage reaction, first precipitation of ferrihydrite and transformation of ferrihydrite to hydrogarnet. This also happens in Portland cement [56,59,77].

The synthetic C-S-H with and without Fe^{3+} were characterized by XRD, TGA, TEM and STEM-EDX. The results confirm that the precipitated synthetic C-S-H is the major phase of seven samples. The Fe contents in samples are 0.010-0.014 mM (0.06-0.08%) of low Fe^{3+} concentration and 0.039-0.048 mM (0.22-0.27%) of high Fe^{3+} concentration per gram of sample. However, the Ca/Si ratios

of precipitated synthetic C-S-H with presence of Fe^{3+} are slightly decreased when compared to the pure synthetic C-S-H. This maybe by the substitution of Fe^{3+} in the C-S-H structure or interlayer or the iron could be adsorbing onto the C-S-H surface. From XRD and TGA, Fe^{3+} does not show a great effect on nucleation and growth of synthetic C-S-H (interlayer or structure), although ionic radius of Fe^{3+} (0.645Å) is smaller than Ca^{2+} (0.99Å) and could thus possibly substitute in the Ca sites either in the main layer structure or the newly identified bridging sites in the interlayer [7]. This has to be further investigated to better understand the decrease in the Ca/Si ratio.

To try and distinguish where iron is or can be incorporated into C-S-H structure, EPR and ^{29}Si NMR relaxation data have been used. The results of EPR strongly suggested that Fe substituted Si^{4+} in the C-S-H structure as shown peak, g_{eff} = 4.3 in Figure 4.12. This signal is particularly strong for the Fe_C1 sample prepared without the prior precipitation of ferrihydride. For the Fe_B2 samples (Fig.4.12), the signal was dominated by the broad signal at g_{eff} around 2 suggesting an iron rich environment as would be expected for the iron containing siliceous hydrogarnet found in the phase by XRD. There is however still a small component of the g_{eff} = 4.3 signal indicating that even if the majority of the Fe has been consumed in the ferrihydride precipitation there is still enough iron in the solution to be incorporated into the C-S-H. ^{29}Si NMR relaxation data confirmed the incorporation of the Fe into the silicate chain of C-S-H with the relaxation signal similar to that seen in silicate glasses resulting from paramagnetic impurities as shown in Figure 4.13. Fe_C1 showed strong signal bleaching compared to Fe_B2, even though Fe content in Fe_C1 sample was lower than Fe_B2 sample, indicating a high degree of Fe incorporation into the silicate chains. Further work is being carried out to try and determine the exact number of Fe sites in the silicate chains.

4.5   Conclusions

The precipitation of synthetic C-S-H was performed via dropwise method in the presence of Fe^{3+}. The addition of Fe^{3+} to synthetic system results in precipitation of C-S-H and sometimes siliceous hydrogarnet, $C_3FS_{0.84}H_{4.32}$ depending on the concentration of Fe^{3+} and the pH. The formation of ferrihydrite as a pre-precipitation phase when the initial solutions before precipitation was observed by XRD and predicted by thermodynamic modelling. This was due to the adjustment of the pH with NaOH to control the stoichiometry of the C-S-H to be precipitated. A system was then devised to allow the precipitation of C-S-H in the presence of Fe^{3+} without any pre-precipitation. In the presence of Fe^{3+}, the Ca/Si ratios of precipitated synthetic C-S-H are always slightly decreased. The morphology of synthetic C-S-H –with and without Fe^{3+} always shows a nanofoil like morphology.

EPR and ^{29}Si NMR relaxation data strongly supported that Fe^{3+} is incorporated into the silicate chains in the C-S-H sturcture.

The second phase of Fe (C$_3$FS$_{0.84}$H$_{4.32}$) is clearly seen after precipitation at 4.0 mM when the Fe is in either the calcium or the silicate solution before precipitation, i.e with the formation of ferrihydrite and it is distributed as fine nanoparticles, < 200 nm, with a spherical morphology. The presence of Fe in these nanoparticles was confirmed by STEM-EDX. When there was no pre-precipitaion of ferrihydrite, no formation of C$_3$FS$_{0.84}$H$_{4.32}$ was observed at either concentration investigated but very small (< 20 nm) iron rich phases were observed in the STEM-EDX. This suggests that the formation of C$_3$FS$_{0.84}$H$_{4.32}$ passes through ferrihydrite as an intermediate phase and needs time to reach the thermodynamic equilibrium.

Chapter 5 Effect of D-gluconate on nucleation and growth of synthetic C-S-H

This chapter investigates the effect of D-gluconate on nucleation and growth of precipitated C-S-H. The goal of this work is to understand effect of the D-gluconate as a representative molecule with similar functional groups as typical admixtures or superplasticizers on the nucleation and growth of synthetic C-S-H. The characterization of the precipitated C-S-H with and without the presence D-gluconate was investigated. Kinetics data was collected using an in-situ calcium electrode and the morphology of the resulting precipitated C-S-H were observed. To better understand the role of D-gluconate and its complexation with Ca both before and during the precipitation of synthetic C-S-H attempts to valid the conflicting complexation constants found in the literature were also made.

5.1 Effect of D-gluconate on nucleation and growth of synthetic Calcium Silicate Hydrate (C-S-H)

This section is reformatted from an ACI proceeding published in 12th International Conference on Superplasticizers and Other Chemical Admixtures in Concrete, 2018.

Effect of D-gluconate on nucleation and growth of synthetic Calcium Silicate Hydrate (C-S-H)

Jirawan Siramanont and Paul Bowen

Powder Technology Laboratory, Institut des Matériaux, Ecole Polytechnique Fédérale de Lausanne (EPFL), CH-1015 Lausanne, Switzerland

Biography: Jirawan Siramanont, PhD student of Materials Science and Engineering, École Polytechnique Fédérale de Lausanne, Switzerland. She received her B.Sc. from Department of Chemistry and M.Sc. from Petrochemistry and Polymer Science, Faculty of Science, Chulalongkorn Uni-

versity, Thailand. After graduation, she has worked in Siam Research and Innovation Co., Ltd, Siam Cement Group in Thailand for 8 years. Her research interests include synthesis and characterization of calcium silicate hydrate and admixtures in cement.

Prof. Bowen has a BSc in Physics (Imperial College (UK)), and a Ph.D. in Physical Chemistry (University of Cambridge (UK)). He worked in industry for 4 years before moving to EPFL, Switzerland in 1987. He has been at the Powder Technology Laboratory (Materials Institute) since 1988. He has over 200 publications and has co-authored an undergraduate textbook on ceramics. His research interests are powder synthesis, powder characterization, colloidal processing and atomistic modelling of surfaces and interfaces.

5.1.1 Abstract

Calcium Silicate Hydrate (C-S-H) was synthesized with and without D-gluconate in controlled conditions and environment via a dropwise precipitation method. The presence of D-gluconate seems to affect the synthetic C-S-H precipitation. D-gluconate can adsorb on C-S-H and also complex with Ca^{2+} in solution. The C-S-H stoichiometry in the presence of D-gluconate is different compares to the pure synthetic C-S-H. The underlying structure of all samples characterized by FTIR and XRD are similar. With the addition of D-gluconate the C-S-H showed higher weight losses (0.8-4.7%) than the pure synthetic C-S-H. Primary particles show a nanofoil-morphology with or without addition of D-Gluconate. The D-gluconate modifies the agglomeration patterns, forming hollow square or cuboid aggregates. Higher concentrations of D-gluconate in synthetic C-S-H accentuate this square aggregate shape possibly because of a preferential adsorption onto the synthetic C-S-H basal plane.

Keywords: calcium silicate hydrate; D-gluconate; precipitation; morphology; agglomeration.

5.1.2 Introduction

Concrete is extensively used in the construction industry including buildings, bridges, dams, tunnels, and roads. It is traditionally made by mixing cement, water, and aggregate. Concrete production has a significant carbon footprint due to the high quantities used and this is expected to double in the next 30 years [1,2]. To reduce CO_2 emissions, clinker substitution, replacing clinker by supplementary cementitious materials (SCMs) is a promising strategy. SCMs such as slag, fly ash, clay, limestone, etc. are already in use for clinker replacement for a portion of Portland cement in

concrete or mixed with clinker to produce cement. However, the level of SCMs replacement is limited because of their lower reactivity, which diminishes performance at early ages [5,6,9,78].

Calcium Silicate Hydrate (C-S-H) is the major hydration product of Portland cement, which is a contributor to the important properties of concrete such as strength and durability. In Portland cement systems, there are various anhydrous phases such as tricalcium silicate, dicalcium silicate, aluminate and ferrite. These react with water to form various hydration products such as C-S-H, portlandite, ettringite, calcium monosulphoaluminate or calcium monocarbo-aluminate.

The effect of the admixtures on the hydration of cement is a key topic in modern cement technology as we try and reduce the clinker content. The retardation effect of polycarboxylate superplasticizers could not be explained simply by either their capacity to complex calcium in solution or their affinity to adsorb onto C-S-H. Nalet and Nonat [11–14] studied a series of organic molecules, representative of functional groups seen in typical processing admixtures (polycarboxylate superplasticizers and retardation admixtures), on the effect of cement hydration e.g., the dissolution of anhydrous phases, the nucleation and growth of hydrates. The molecules, which differ by stereochemistry, functionality and charge, first retard the hydration of pure C_3S and then enhance the quantity of C-S-H precipitated. Again, the effect could not be explained simply by either their capacity to complex calcium in solution or their affinity to adsorb onto C-S-H. In fact, molecules of a very similar size and structure gave very different retardation times. Recent work on the adsorption of polycarboxylate based superplasticizers (PCEs) indicates that the main retardation mechanism is the slowing down of dissolution [44]. Furthermore, the impact of PCEs, with varying pH (10.4 – 13.8), on the nucleation and growth of synthetic C-S-H has very recently been investigated [79], using a synthetic precipitation route similar to that developed by Kumar et al. [20]. The pH conditions affect morphology, nanostructure and Ca/Si molar ratio of synthetic C-S-H with presence of PCEs.

The precipitation method is an attractive tool to prepare synthetic C-S-H. As mentioned above Kumar et al. [20] have recently demonstrated that uniform synthetic C-S-H can be produced in well controlled conditions by using a dropwise method. The Ca/Si molar ratios of synthetic C-S-H were controlled between 1.0 and 2.0 without the formation of any secondary phase. In the current work, we will use this synthetic precipitation system to identify effects of D-gluconate on the growth of precipitated synthetic C-S-H. The chemical structure of D-gluconate is shown in Figure 5.1.
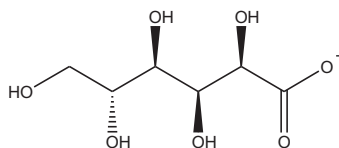
Figure 5.1 Chemical structure of D-gluconate chosen for the investigation.

5.1.3 Research significance

With the introduction of supplementary cementitious materials to reduce the amount of clinker, and hence the carbon footprint of cement, the use of chemical admixtures play a key role in concrete. The chemical admixture can modify the hydration process and consequently early age strength. A better understanding of these effects can also be elucidated from well controlled precipitation of synthetic C-S-H in the presence of chosen organic molecules representative of the most important functionalities in chemical admixtures.

5.1.4 Experimental Investigation

Synthesis of C-S-H

The synthetic C-S-H was synthesized via the dropwise method, as shown schematically in Figure 5.2. Solutions were prepared using boiled deionized water. Before precipitation, pH electrode (In-Lab®Expert Pro-ISM-IP67, *Mettler Toledo*) connecting with benchtop pH meter (SevenExcellence pH Meter, *Mettler Toledo*) was calibrated with standard solution as shown in Chapter 3, Table 3.1. The reaction vessel contained 100 mL of 0.1 M sodium silicate (Na_2SiO_3, S*igma-Aldric*h, CAS:6834-92-0), the pH was adjusted with sodium hydroxide (NaOH, *Acros organic*, CAS:1310-73-2) to reach an initial pH of 13.5. Calcium nitrate, (100 mL of 0.2 M ($Ca(NO_3)_2$.$4H_2O$, *Fluka Chemicals,* CAS:13477-34-4) were constantly added to silicate solution at 2.2 mL/min into the stirred tank. The samples were collected after 3 hours. The precipitates were then vacuum filtered and washed with an ultra-pure water/ethanol, 50/50 mixture.
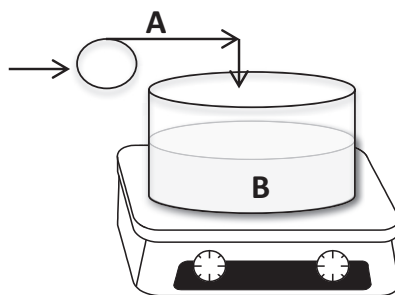
Figure 5.2 Diagram of dropwise precipitation method of synthetic C-S-H.

Synthesis of C-S-H with D-gluconate

The effect of D-gluconate on synthetic C-S-H was investigated with varying concentrations between 3 and 12 mM. The D-gluconate (*Merck KGaA*, CAS:1527-07-1) was mixed in the silicate solution and the pH was adjusted with sodium hydroxide (NaOH, *Acros organic*, CAS:1310-73-2) to reach an initial pH of 13.5. The synthetic C-S-H with D-gluconate was prepared using the same dropwise method as for the pure synthetic C-S-H. The experimental conditions are shown in Table 5.1.

Sample	A	B		Ratio of D-gluconate/C-S-H ($\mu g/g$)	pH
	Ca(NO$_3$)$_2$.4H$_2$O	Na$_2$SiO$_3$	D-gluconate		
C-S-H	0.2 M	0.1 M	-	-	13.5
GN03	0.2 M	0.1 M	3 mM	5.89	13.5
GN06	0.2 M	0.1 M	6 mM	11.78	13.5
GN12	0.2 M	0.1 M	12 mM	23.56	13.5

Table 5.1 Experimental conditions of synthetic C-S-H in the presence of D-gluconate.

Characterization methods

ICP – The chemical compositions were analysed by Inductively Coupled Plasma in the Optical Emission Spectroscopy mode (ICP-OES). It was performed on ICPE-9000 series, Shimadzu. After washing and filtration, 0.1 g of the filtrated sample was dissolved in 8.0 mL of 65% HNO$_3$ (14.58 M), *Carlo Erba* and then in 2.0 mL of fuming 100% HNO$_3$ (22.43 M), *Merck*. The dissolved sam-

ples were diluted in HNO_3 (2.0 M), *Alfa Æsar* at x10, x100 and x1,000. Total volume of the dissolved sample and 2.0 M HNO_3 are shown in Chapter 3, Table 3.2.

FTIR – The filtrated samples were investigated by Fourier-transform infrared spectroscopy (FTIR) to identify the functional groups present in the precipitated C-S-H with and without D-gluconate. Samples were examined using a Nicolet 6700 from ThermoFisher Scientific with the range 450 – 4,000 cm^{-1} (wavelength). The data were collected by *Omnic* software.

XRD – Data of synthetic C-S-H were collected using CuKα XRD (PANanalytical) analyses of wavelength λ=1,54 Å with a fixed divergence slit. The size of the slit is ½. Samples were placed in the sample holder and the patterns were collected between 5 and 70 degree 2θ. Scan step size is 0.0167113 degrees 2θ. The XRD pattern was recorded by *X'PERT Data Collector* software.

TGA - Thermogravimetric analysis (TGA) were performed on a Mettler Toledo SDTA851 instrument. Samples were freeze-dried during 24 hours prior to measurement. The preparation of freeze-dried sample is shown in Chapter 3, Section 3.4.1. The freeze-dried samples were put in an alumina crucible with a temperature ramp from 30-1,000°C at 10°C/min under a nitrogen atmosphere.

TEM and STEM-EDX - The morphology of the synthetic C-S-H was investigated by using TEM, Thermo Scientific™ Talos F200X scanning transmission electron microscope (STEM). The samples were prepared by dispersing the precipitated C-S-H in isopropanol and treated in an ultrasonic bath for 15 minutes. The dispersed samples were dropped on to the charged grid and allowed to dry for few minutes. HAADF-STEM measurement combined with EDX were used to investigate the elemental distribution. The elemental map was operated by STEM-EDX mode. Details was shown in Chapter 3, Section 3.4.8.

5.1.5 Experimental, results and discussion

The Ca to Si ratios (Ca/Si) are shown in Table 5.2 for different amounts of D-gluconate. Here we see that in the presence of D-gluconate a lower Ca/Si ratio than the pure synthetic C-S-H is observed. This could be due to either complexation of Ca^{2+} in solution [11,45] or adsorption onto the C-S-H during growth and nucleation effecting the stoichiometry.

Sample	Ca/Si
C-S-H	2.2 ± 0.6
GN03	1.8 ± 0.1
GN06	1.7 ± 0.1
GN12	1.9 ± 0.1

Table 5.2 Ca/Si ratios from ICP measurements of synthetic C-S-H with different D-gluconate concentrations.

FTIR spectra of synthetic C-S-H with different amounts of D-gluconate are shown in Figure 5.3. The main characteristic peaks of C-S-H are located in the range between 850 (Q1), 980 (Q2), and 670 (Si-O-Si) cm^{-1} of the precipitated C-S-H. All sample of the precipitated C-S-H with and without D-gluconate show the Q2 and Q1 bands. Carbonate bands are exhibited at 900 cm^{-1} and in the range at 1,400-1,500 cm^{-1} due to the presence of carbonate due to CO_2 taken up by the solid upon exposure to the atmosphere for the FTIR measurement. There is no observation of a portlandite ($Ca(OH)_2$) peak at 3,640 cm^{-1}.

The XRD pattern of C-S-H with D-gluconate at 3 mM showed some minor unidentified peaks as seen in Figure 5.4. All samples show peaks around 29.3°, 33°, 50°, 55° and 67° (2θ) as previously observed for synthetic C-S-H [80]. There are no crystalline peaks corresponding to $Ca(OH)_2$ or $CaCO_3$.
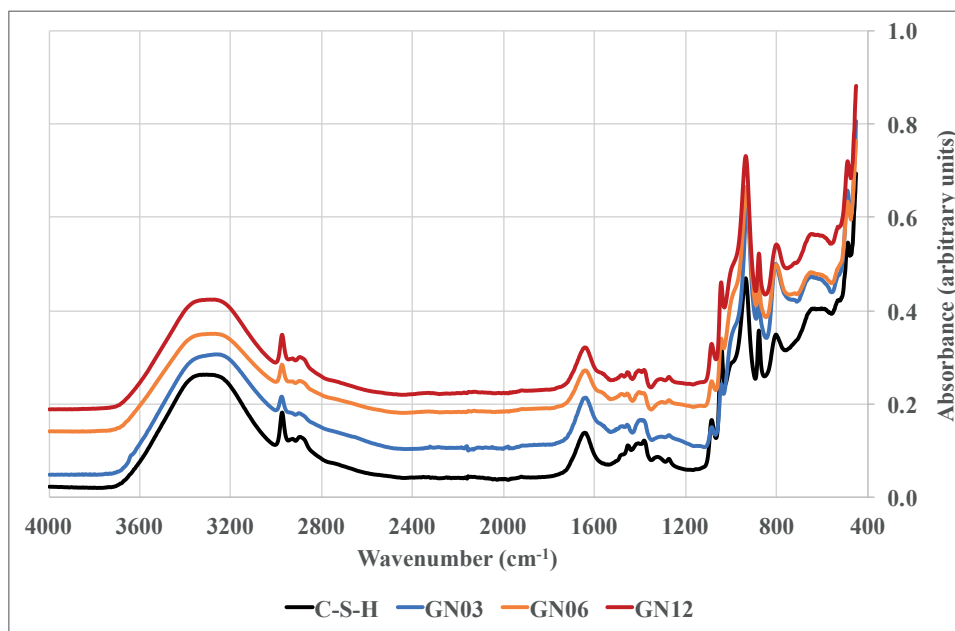
Figure 5.3 FTIR spectra of C-S-H, and samples GN03, GN06 and GN12 made in the presence of D-gluconate.
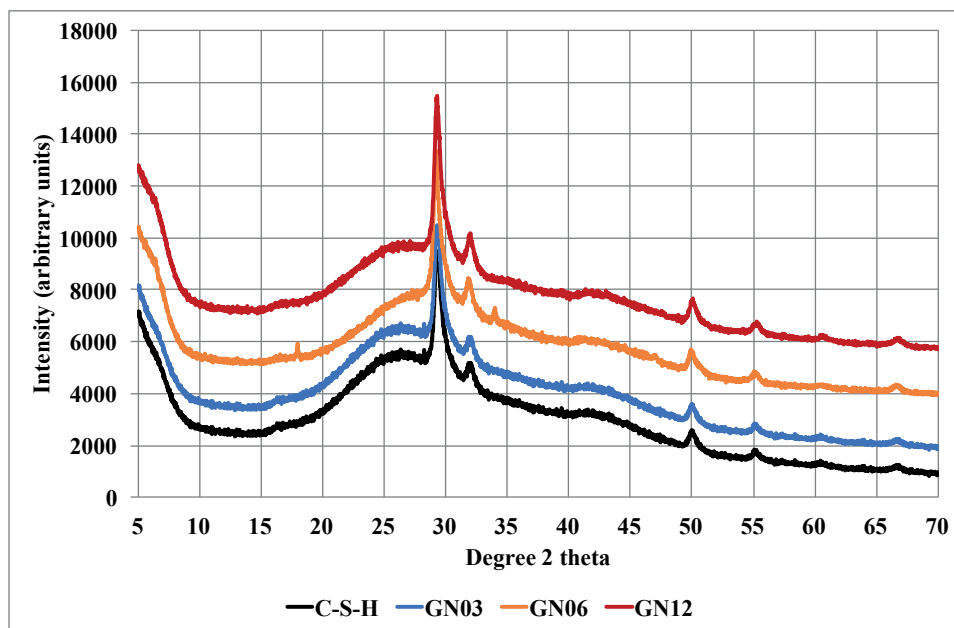
Figure 5.4 XRD patterns of C-S-H, GN03, GN06 and GN12 made in the presence of D-gluconate.

Thermogravimetric analysis (TGA) was used to determine the weight loss of freeze dried samples as shown in Figure 5.5. The C-S-H and GN06 are almost identical suggesting very little D-gluconate present. The GN12 shows more weight loss which indicates a higher amount of D-gluconate present. The main loss occurred at 80-150°C typical of C-S-H water loss [66]. The broad weight loss at 300 – 600°C are due to D-gluconate and bound water in the sample. The weight loss at 650-700°C could be due to poorly crystalline $CaCO_3$ due to CO_2 contamination during sample handling and measurement. There is no clear weight loss of $Ca(OH)_2$, which would show a feature at 450°C. Addition of D-gluconate at 6 mM (GN06) and 12 mM (GN12) show higher weight loss than pure synthetic C-S-H, presumably due to adsorption of D-gluconate on the C-S-H surface.
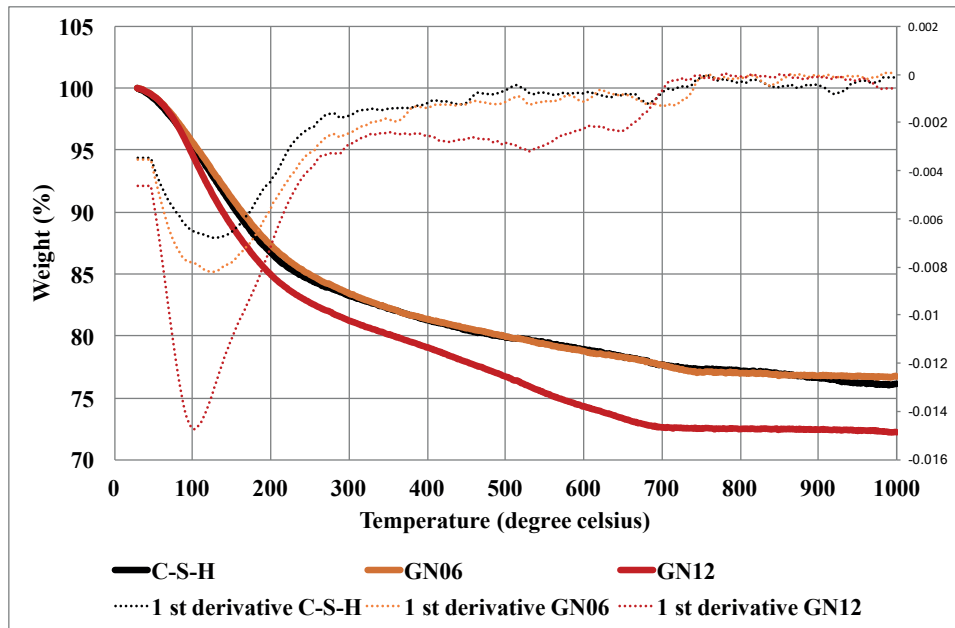
Figure 5.5 Thermogravimetric analysis (TGA) of C-S-H, GN06 and GN12 (1 degree celsius = 33.8 degree farenheit) made in the presence of D-gluconate.

Morphological analysis –TEM analysis shows nanofoil like morphology for all samples (Fig.5.6). The aggregate morphology is progressively modified as the D-gluconate concentration increases forming more and more open agglomerates with the highest concentration showing organized square-like shapes in Figure 5.6 (d). The D-gluconate, which had negative charge, was able to complex with Ca^{2+} ions present on the C-S-H surface by forming cation bridging complexes [81]. The aggregate morphology could be due to the adsorption of D-gluconate on precipitated C-S-H, which could change surface energy and surface charge of C-S-H and hence the way the primary C-S-H particles interact. Such a morphology suggests an anisotropic adsorption of the D-gluconate onto the foil-like C-S-H. Furthermore, Nicoleau et al. [82] suggested that the aggregation of synthetic C-S-H was driven by adsorption of polymers such as either along a line, or in a plane on single particles. However, the polymer was able to desorb and re-adsorb onto newly precipitated C-S-H particles which effected the aggregated structures.

Therefore, a first hypothesis of our results would be that the D-gluconate adsorbs onto the basal plane preferentially giving a steric hindrance between basal planes of the C-S-H primary particles initially leading to more open agglomerates which is shown in Figure 5.6 (b). Then, as the concentration of the D-gluconate increases this repulsion between basal planes gets larger where it does not adsorb onto the foil edges. When the D-gluconate desorbed and re-adsorbed onto newly precipi-

tated C-S-H, then these can approach each other and form end-on aggregates which may form these square-like aggregates as shown in Figure 5.6 (d).

HAADF-STEM measurement combined with EDX were used to investigate the elemental distribution of square aggregation pattern of synthetic C-S-H with D-gluconate. Figure 5.7 shows high-angle annular dark-field image of GN12, which shows the square aggregation pattern of nanofoils. The elemental distribution maps of Ca, Si, and O are detected in nanofoils which relate to the composition of synthetic C-S-H and suggest no significant modifications.
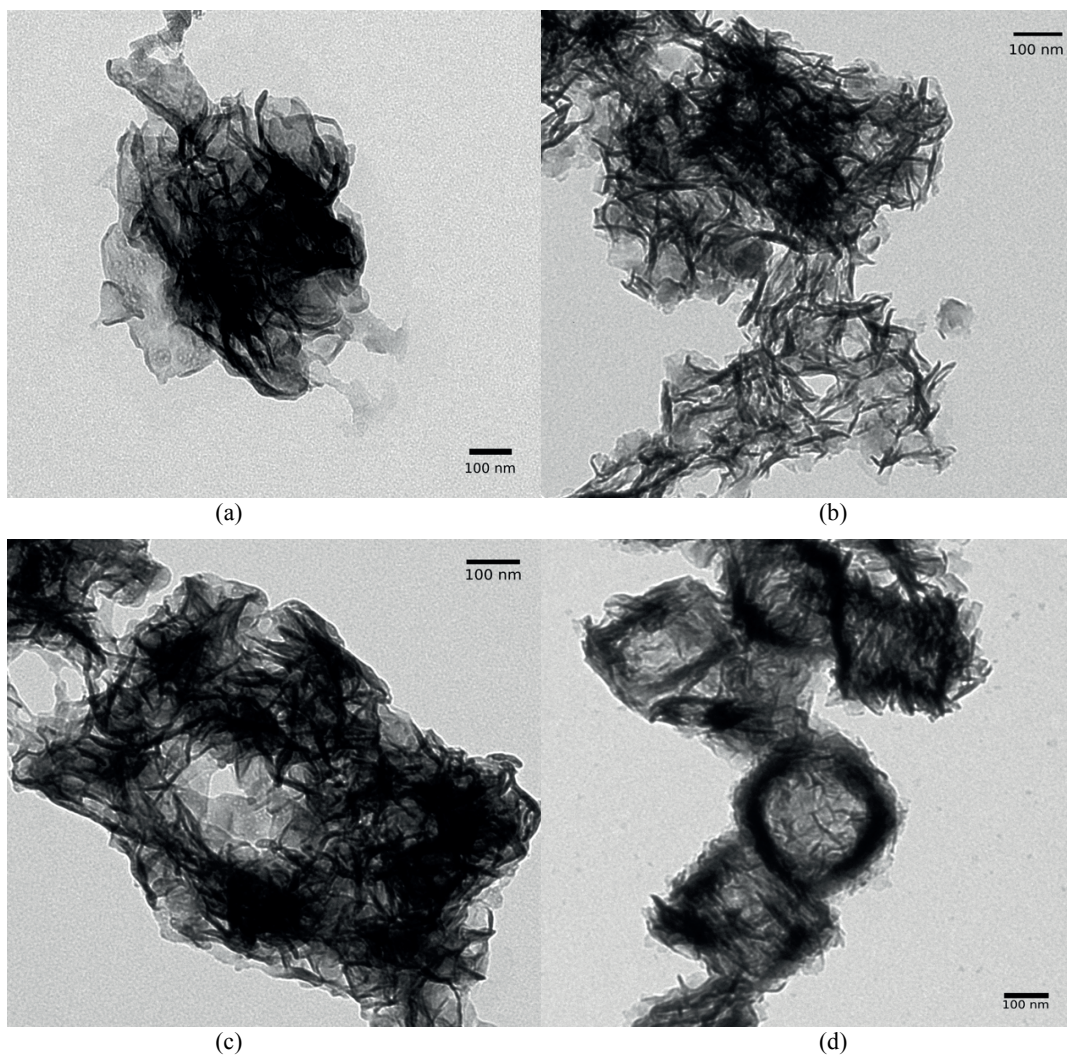
Figure 5.6 TEM micrographs of (a) C-S-H, (b) GN03, (c) GN06 and (d) GN12.
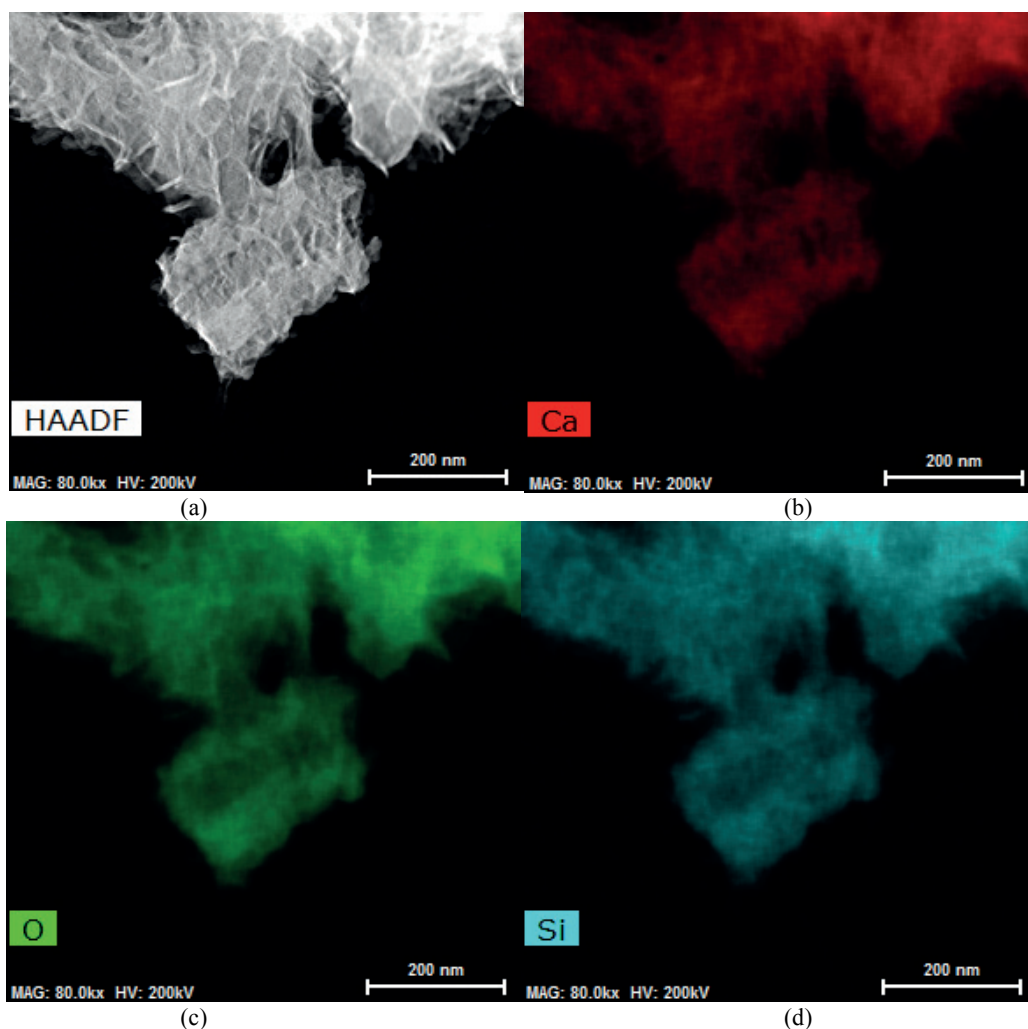
Figure 5.7 STEM-EDX images of GN12, (a) HAADF-STEM images, (b, c and d) elemental maps of Ca, O and Si, respectively.

5.1.6 Conclusions

Synthetic C-S-H with D-gluconate was prepared using a dropwise precipitation method in a well-mixed stirred tank reactor. The addition of D-gluconate to the synthetic system did not interfere with the precipitation of C-S-H but the Ca/Si ratios were slightly lower than the pure synthetic C-S-H. This may be due to complexation with Ca^{2+} or from adsorption onto the growing C-S-H. From FTIR and XRD, D-gluconate did not show a great impact on the underlying synthetic C-S-H structure with characteristic absorption bands and XRD reflections remaining similar. The TGA curves show the weight loss of samples made in the presence of D-gluconate is higher than pure synthetic C-S-H, especially for the higher D-gluconate concentrations. The morphology of synthetic C-S-H –

with and without D-gluconate always shows a nanofoil like morphology. However, the D-gluconate significantly modifies the agglomeration patterns, suggesting adsorption on basal planes of the foil-like C-S-H. Further work at lower solution concentrations is planned to try and investigate effects on the kinetics of nucleation and growth.

5.1.7 Further research

In cementitious systems, the range of total calcium concentration is from 10^{-4} M to 2×10^{-2} M [26]. Our system has much higher initial reactant concentration and hence relatively rapid kinetics, even with the dropwise addition method typical experiments are conducted in less than 3 hours. To approach real systems, lower supersaturations with lower initial concentrations of calcium nitrate and sodium silicate solutions will be used in order to investigate the effect of small polyol admixtures on the nucleation and growth of precipitated synthetic C-S-H. This will allow us to identify effects of individual parameters e.g. competition of ionic species or molecules in the synthetic precipitation system. Also work on quantifying the degree of complexation of Ca^{2+} with the D-gluconate is planned such that thermodynamic modelling will be made and to see if the complexation with calcium can help explain the modification in the Ca/Si ratio. These lower concentrations will also allow us to follow the kinetics of the reaction by measuring the amount of free Ca^{2+} ions using a calcium selective electrode. At the concentrations used in the present study, it was not possible.

5.1.8 Acknowledgement

5.2 Effect of D-gluconate on morphology of synthetic C-S-H and kinetics analysis

This section is planned to be submitted to an international journal.

5.2.1 Introduction

The effect of admixtures on the hydration of cement is a key topic in modern cement technology as we try and reduce the clinker content. For example, synthetic calcium-silicate-hydrate (C-S-H) has been used to accelerate hydration of cement by seeding [83]. Comb-like polymers, which contain ethylene glycol side chains and carboxylate or phosphate groups, were used as dispersants for these synthetic C-S-H seeds to improve their suspension properties [79,82,84]. Often these dispersants or superplasticizers (SPs) induce a retardation of the hydration of Portland cement. Marchon et al. [85] suggest that the adsorption of the SPs onto the clinker slowing down dissolution is the key factor in retardation. The effect of small organic molecules on the heat release of C_3S and white cement has been recently studied in detail by Nalet et al. [11,12,14]. They investigated the heat release of C_3S hydration in the presence of small organic molecules (e.g. D-mannitol, D-galacitol, D-glucitol, D-gluconate and D-galactarate) using isothermal calorimetry. The maximum heat flow of C_3S with the presence of these molecules were all delayed with the highest to lowest delay times in the following order, D-galactarate > D-gluconate > D-glucitol > D-galacitol > D-mannitol. The effect could not be explained simply by either their capacity to complex calcium in solution or their affinity to adsorb onto C-S-H. In fact, the size and structure of these molecules are very similar but gave very different retardation times. This leaves some fundamental questions that need to be addressed to better understand these retardation mechanisms, for example, how does the adsorption of molecules on clinker phase disrupt the dissolution process, can they also modify the nucleation process, either by adsorption, complexation or stabilizing pre-nucleation clusters (embryos) and/or adsorption onto stable nuclei interfering with C-S-H growth.

In real Portland cement system, there are various anhydrous phases forming various hydration products. Calcium-silicate-hydrate (C-S-H) is the major binding phase in concrete formed during the hydration of cementitious materials. C-S-H has variable stoichiometry which Ca/Si ratios from 1.2 to 2 and is poorly crystalline material [35]. It is difficult to characterise their structures by traditional X-ray diffraction methods. Kumar et al. [20] have recently developed a synthetic approach by precipitation which allows any stoichiometry from 1 to 2 to be formed as single-phase of uniform C-S-H particles. The set-up also allows the collection of kinetics data (e.g. Ca^{2+} activity as a func-

tion of time). Therefore, using a synthetic precipitation system will allow us to try and identify effects of individual parameters on nucleation and growth of precipitated C-S-H and this is the question we shall investigate in this paper.

D-gluconate is a small organic molecule, stable at high pH and has representative functional groups seen in typical processing admixtures (polycarboxylate superplasticizers and retardation admixtures). As discussed above D-gluconate generates a retarding effect on the cement hydration. It delays the hydration by extending the induction period [13,14,46,86,87]. The aim of this paper is to investigate the effect of D-gluconate on the nucleation and growth of precipitated synthetic C-S-H by using the dropwise precipitation method recently introduced by Kumar et al. [20]. We also investigate the complexation of D-Gluconate with calcium under our experimental conditions to see which of the data published in the literature [88] best fits our experimental conditions to enable us to consider the complexation effects of the nucleation and growth of precipitated synthetic C-S-H.

5.2.2 Materials and methods

Heat flow release of cement hydration

Heat flow release of OPC type I with and without D-gluconate was monitored by isothermal calorimetry (*TAM AIR*) at 20ºC. 20 g of cement powder was mixed with 8.0 ml of deionized water for OPC type I and 8.0 ml of aqueous solution for cement with D-gluconate (*Merck KGaA*) (w/c = 0.4). The concentration of D-gluconate was 12 mM (0.01 wt% of OPC type I), for which we observed the strong effect on the aggregation of C-S-H in Section 5.1. The pastes were mixed for 2 min at 750 rpm and then immediately capped and inserted in the machine.

Calcium complexation with D-gluconate

Calcium complexation of the D-gluconate was investigated using a calcium ion selective electrode (perfectION^{TM}, *Mettler Toledo*) at pH 11.0$\pm$0.1 in order to avoid precipitation of Ca(OH)$_2$. The pH was monitored by using pH electrode (InLab$^®$Expert Pro-ISM-IP67, *Mettler Toledo*). These electrodes connected with benchtop pH meter (SevenExcellence pH Meter, *Mettler Toledo*). The data were collected by EasyDirect™ pH Software. The electrodes were calibrated before experiments by using standard solutions which shown in Chapter 3, Table 3.1. The D-gluconate (*Merck KGaA*, CAS:1527-07-1) solutions (50 mL) investigated were 20, 100 and 200mM. Before introducing D-gluconate to the reactor a 0.02 M solution of calcium nitrate (Ca(NO$_3$)$_2$.4H$_2$O, *Fluka Chemicals,* CAS:13477-34-4) was placed the in vessel purged with N$_2$ for 30 min. Then, the D-gluconate was

added in a dropwise manner with a constant flow rate of 2.0 ± 0.1 mL/min to a reaction vessel of 250 mL containing 50 mL of the 0.02 M calcium nitrate solution. All solutions in the experiment were prepared by using boiled deionized water. The reactions were performed under flowing N_2 at 10mL/min. The value of free calcium ion concentration was measured as a function of admixture concentration. Thermodynamic modelling has been carried out using the Gibbs free energy minimisation program GEMS. GEMS calculates complexation between calcium and D-gluconate.

Precipitation of synthetic C-S-H with and without D-gluconate

Section 5.1 showed the effect of D-gluconate on precipitated synthetic C-S-H which modified the aggregation pattern of synthetic C-S-H with D-gluconate. At 12 mM of D-gluconate in silicate solution showed strong aggregation pattern of synthetic C-S-H. Therefore, the effect of D-gluconate on precipitated synthetic C-S-H when premixing in calcium solution at the same concentration of D-gluconate (12 mM) was observed in this section.

The synthetic C-S-H with and without D-gluconate was synthesized via the dropwise method as described in Section 5.1 as shown schematically in Figure 5.2. Solutions were prepared using boiled deionized water. Before precipitation, pH electrode (InLab®Expert Pro-ISM-IP67, *Mettler Toledo*) connecting with SevenExcellence pH Meter, *Mettler Toledo* benchtop meter was calibrated with standard solution as shown in Chapter 3, Table 3.1. The reaction vessel contained 100 mL of 0.1 M sodium silicate (Na_2SiO_3, S*igma-Aldric*h, CAS:6834-92-0), the pH was adjusted with sodium hydroxide (NaOH, *Acros organic*, CAS:1310-73-2) to reach an initial pH of 13.5. Calcium nitrate ($Ca(NO_3)_2.4H_2O$, *Fluka Chemicals,* CAS:13477-34-4) solution, (100 mL of 0.2 M) was constantly added to silicate solution at 2.2 ± 0.1 mL/min into the stirred tank. The samples were collected after 3 hours. The precipitates were then vacuum filtered and washed with an ultra-pure water/ethanol, 50/50 mixture. In the presence of D-gluconate, the synthetic precipitated C-S-H with D-gluconate was also performed using the dropwise method. The addition of 12 mM of D-gluconate in either the calcium (0.2M) or silicate (0.1M) solution was studied. The precise experimental conditions are present in Table 5.3.

Sample	A		B		pH
	Ca(NO$_3$)$_2$.4H$_2$O	D-gluconate	Na$_2$SiO$_3$	D-gluconate	
C-S-H	0.2 M	-	0.1 M	-	13.5
CaGN	0.2 M	12 mM	0.1 M	-	13.5
SiGN	0.2 M	-	0.1 M	12 mM	13.5

Table 5.3 Experimental conditions of synthetic C-S-H in the presence of D-gluconate.

Kinetics experiment of synthetic C-S-H

Kinetics data were collected during the dropwise precipitation using calcium ion selective (perfec-tION^{TM}, *Mettler Toledo*), pH (InLab$^®$Expert Pro-ISM-IP67, *Mettler Toledo*) and conductivity (In-Lab$^®$ 731-ISM, *Mettler Toledo*) electrodes. The electrodes connected with benchtop pH meter (SevenExcellence pH Meter, *Mettler Toledo*). The data were collected by EasyDirect™ pH Soft-ware. Before precipitation, all electrodes were calibrated with their standard solution as shown in Chapter 3, Table 3.1.

In the kinetics experiment, calcium (Ca(NO$_3$)$_2$.4H$_2$O, *Fluka Chemicals,* CAS:13477-34-4) and sili-cate (Na$_2$SiO$_3$, S*igma-Aldric*h, CAS:6834-92-0) solution were diluted x10 of C-S-H precipitation experiments. At high pH (e.g. pH 13.5), calcium ions in the solution complexed and gave high complexation of CaOH$^+$ and low Ca^{2+}, making it difficult to follow accurately the kinetics. So, pH in the kinetics experiments was controlled at 12.3. The reactions were carried out under an N$_2$ at-mosphere, and the pH was controlled by adding controlled amounts of 1.0 N NaOH standardized solution (*abcr GmbH*, CAS:1310-73-2). This was carried out for C-S-H without the D-gluconate, when the D-gluconate solution was premixed in silicate solution (SiGN_I) or in the calcium solu-tion (CaGN_I). The calcium solution with and without D-gluconate was constantly added to a solu-tion of sodium silicate with and without D-gluconate at a flow rate of 2.0±0.1 mL/min. The exper-imental conditions are shown in Table 5.4.

Sample	A		B		pH
	Ca(NO$_3$)$_2$.4H$_2$O	D-gluconate	Na$_2$SiO$_3$	D-gluconate	
C-S-H_I	0.02 M	-	0.01 M	-	12.3+ 0.1
CaGN_I	0.02 M	12 mM	0.01 M	-	12.3+ 0.1
SiGN_I	0.02 M	-	0.01 M	12 mM	12.3+ 0.1

Table 5.4 Experimental conditions for the collection of kinetics data for synthetic C-S-H in the presence of D-gluconate.

Characterization methods

The characterization methods were distributed in three groups as shown below.

- *Chemical and compositional analysis*

Inductively Coupled Plasma (ICP) – The chemical compositions were analysed by Inductively Coupled Plasma in the Optical Emission Spectroscopy mode (ICP-OES). It was performed on ICPE-9000 series, Shimadzu. After washing and filtration, 0.1 g of the filtrated sample was dissolved in 8.0 mL of 65% HNO$_3$ (14.58 M), *Carlo Erba* and then in 2.0 mL of fuming 100% HNO$_3$ (22.43 M), *Merck*. The dissolved samples were diluted in HNO$_3$ (2.0 M), *Alfa Æsar* at x10, x100 and x1,000. Total volume of the dissolved sample and 2.0 M HNO$_3$ are shown in Table 3.1.

Thermogravimetric analysis (TGA) - TGA were performed on a Mettler Toledo SDTA851 instrument. Samples were kept at -80°C for 24 hours and then freeze-dried during 24 hours prior to measurement. The dried samples were put in an alumina crucible with a temperature ramp from 30-1,000°C at 10°C/min under a nitrogen atmosphere.

- *Phase and morphological analysis*

X-ray diffraction (XRD) - XRD data of the synthetic C-S-Hs were collected using CuKα XRD (PANanalytical) analyses of wavelength λ=1,54 Å with a fixed divergence slit. The size of the slit is ½. Samples were placed in the sample holder and the patterns were collected between 5 and 70 degree 2θ. Scan step size is 0.0167113 degrees 2θ. The XRD pattern was recorded by *X'PERT Data Collector* software.

Transmission electron microscopy (TEM) - The morphology of the synthetic C-S-H was investigated by using TEM, Thermo Scientific™ Talos F200X scanning transmission electron microscope (STEM) with TEM mode. It was operated at an acceleration voltage of 200 kV. The sam-

ples were prepared by dispersing the precipitated C-S-H in isopropanol and treated in an ultrasonic bath for 15 minutes. The dispersed samples were dropped on to the charged grid and allowed to dry for few minutes.

TEM-tomography - Three-dimensional representations of samples were observed by using tomograms recorded in a TEM. The sample was dispersed in isopropanol and with gold particles as fiducial markers for the 3D reconstruction. The suspension was dropped on the TEM grid and the sample dried for few minutes. Tomograms were recorded on a transmission electron microscopy (Tecnai T12, FEI Company, Eindhoven, The Netherlands) at 120 kV from -65° to $+65^{o}$ tilt angles with increments of 1° using SerialEM (Mastronarde DN, 2005). Reconstructions were done with the freeware *IMOD* [53–55].

- *Surface analysis*

Zeta potential – The zeta potential measurements were performed at 23-25°C using a NanoZS from Malvern Instruments. After washing and filtration of precipitated C-S-H, the suspensions were prepared by dispersing 2%w/v of solid in NaOH. The pH was controlled at 12.0 ± 0.1. Prior to measuring, 1.0 mL of suspension was added into a disposable cuvette and inserted into the machine.

5.2.3 Results

Heat flow release of cement hydration

The heat flow curves (Fig.5.8) show the impact of the D-gluconate on the hydration of the OPC type I cement. With presence of 0.01% of D-gluconate, the hydration kinetics of Portland cement significantly changed by extending the induction period. It confirms that the molecule significantly delays the hydration, which also was observed by Ma et al. [46]. This was also seen for the hydration of C_3S by Nalet et al. [14]. It could be due to adsorption of D-gluconate on dissolution sites of cement particles slowing down the dissolution rate [44,46]. Moreover, slope of the first peak relating to the acceleration or post-induction period, associated with the precipitation of C–S–H gel and CH was slightly changed.
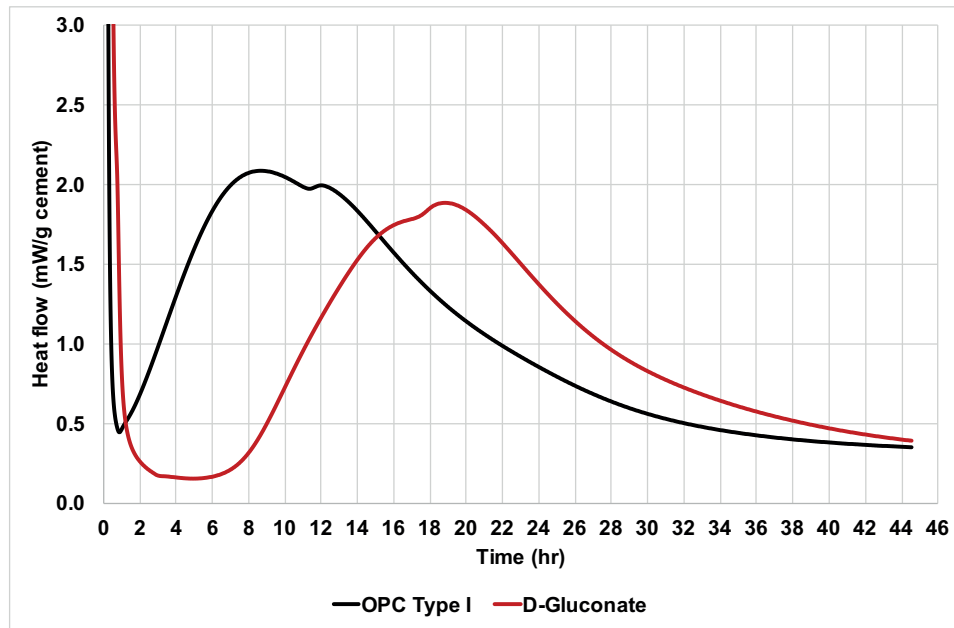
<u>Figure 5.8</u> Heat flow curves of OPC type I with and without D-gluconate, w/c = 0.4, 0.01% wt. of solids.

Calcium complexation with D-gluconate

The value of free calcium ion concentration measured as a function of added calcium with different D-gluconate concentrations (20, 100 and 200 mM) at pH 11.0 ± 0.1 is shown in Figure 5.9. The dotted line in the Figure 5.9 is the amount of calcium added in the system calculated from the flow rate. Figure 5.9 shows that the D-gluconate reveals a strong complexation with calcium. Increasing the concentration of D-gluconate also gives a higher complexation between calcium and D-gluconate. Two repetitions were carried out for all three concentrations. The complexation between calcium and D-gluconate has been calculated by using thermodynamic model GEMS (in collaboration with Prof. Barbara Lothenbach from EMPA, Dubendorf). Our results fits the data of Kutus et al. [88] and we will use this for future thermodynamic modelling. The results of thermodynamic model GEMS calculation are shown in Chapter8, Section 8.1.
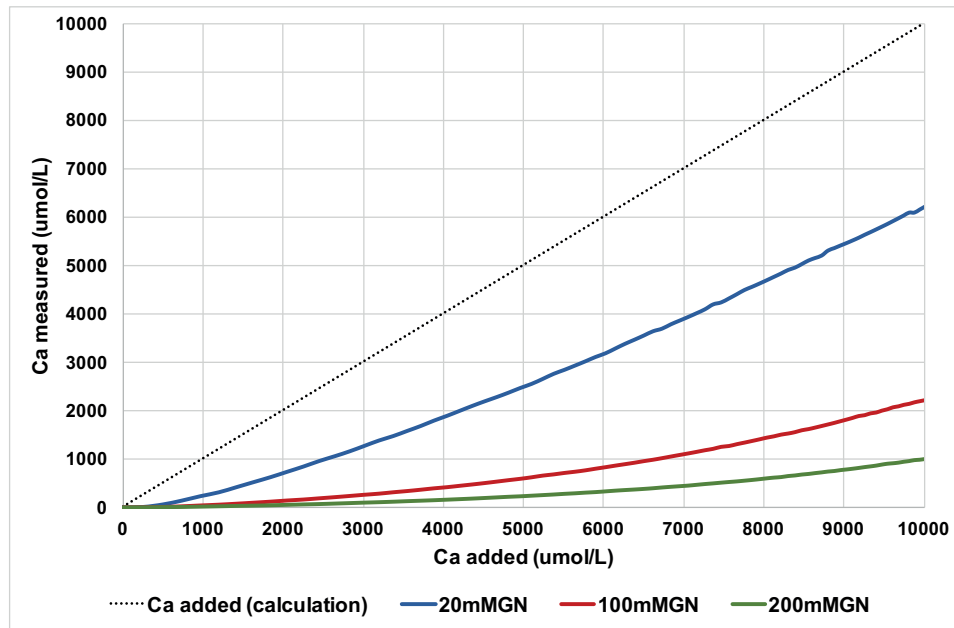
Figure 5.9 Calcium ion concentration measured as a function of D-gluconate concentrations at pH 11.0±0.1.

Precipitation of synthetic C-S-H with and without D-gluconate

Table 5.5 shows stoichiometry of the synthetic C-S-H precipitated with and without D-gluconate which was determined by ICP. The Ca/Si ratios of synthetic C-S-H systems with presence of D-gluconate were slightly decreased when compared to the pure synthetic C-S-H (within the large error shown for the pure C-S-H, the results are averages from three dilutions and three separate precipitation experiments). From XRD (of the non-dried samples), the D-gluconate did not show significant changes compared with the pure synthetic C-S-H (Fig. 5.10), showing only characteristic broad signals typical of precipitated synthetic C-S-H [62] and no secondary phases. The TGA data for the different precipitated samples are shown in Figure 5.11. The main weight loss of precipitated C-S-H with and without D-gluconate occurred at 80-250°C typical of water loss from C-S-H [32]. The broad weight loss at 300 - 600°C could be due to D-gluconate and bound water in the sample. Poorly crystalline $CaCO_3$ shows the weight loss at 650-700°C. This is assumed to occur due to CO_2 contamination during sample handling and measurement (freeze drying and placement in the TGA). Addition of D-gluconate shows higher weight losses than pure C-S-H in the 300-600°C range. This could be due to the adsorption of D-gluconate onto the precipitating C-S-H surface [81]. However, there is no difference observed for synthetic C-S-H in the presence of D-gluconate between premixing either in the calcium or the silicate solutions (Fig.5.11).

Sample	Ca/Si
C-S-H	2.2 $\pm$ 0.6
CaGN	1.9 $\pm$ 0.1
SiGN	1.9 $\pm$ 0.1

Table 5.5 Ca/Si ratios from ICP measurements of synthetic C-S-H with 12 mM of D-gluconate.
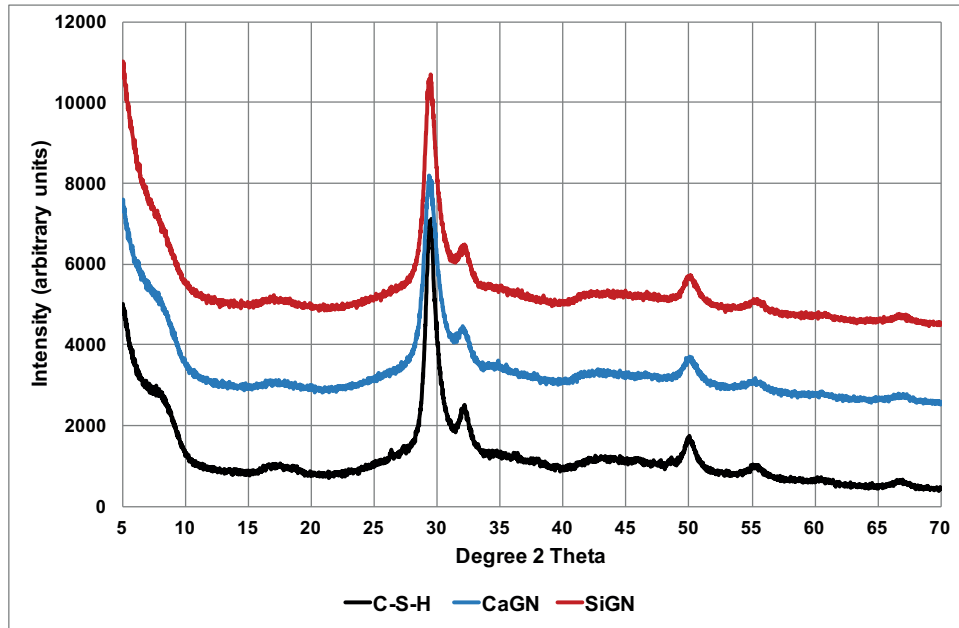
Figure 5.10 XRD pattern of C-S-H, CaGN and SiGN, of wet samples.
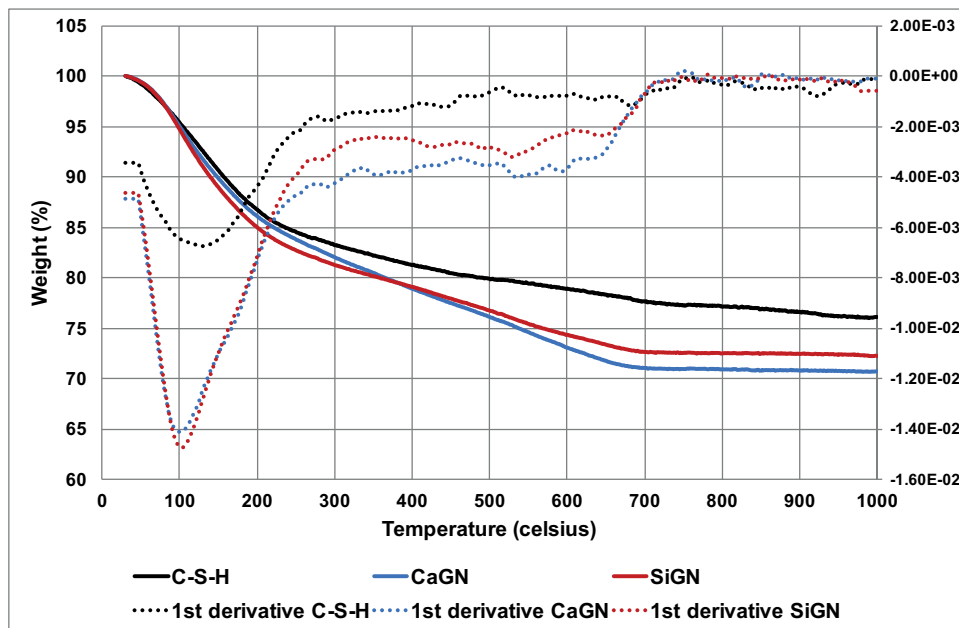
Figure 5.11 Thermogravimetric analysis (TGA) of C-S-H, CaGN and SiGN of freeze-dried samples.

Morphology analysis of synthetic C-S-H form the precipitation experiments

The morphology of synthetic C-S-H –with and without D-gluconate always showed nanofoil like morphology as shown in Figure 5.12. As seen in Section 5.1 (Fig.5.6), the D-gluconate when pre-mixed in the silicate solution modifies C-S-H the agglomeration patterns (Fig. 5.12).
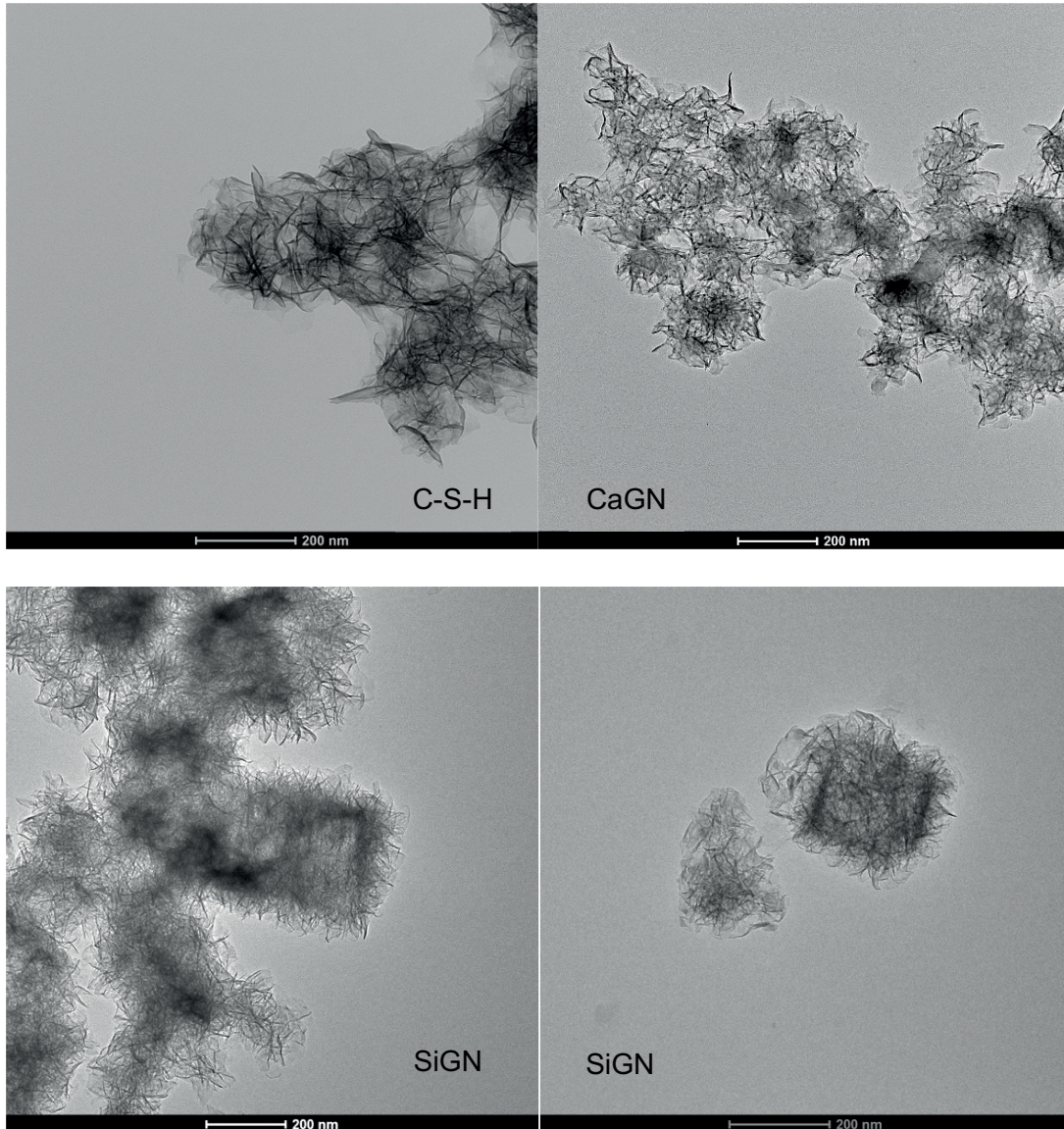
Figure 5.12 TEM micrographs of C-S-H, CaGN and SiGN.

To investigate the aggregation pattern in more detail, the SiGN precipitation product was observed using TEM tomography. The tomogram was created by making a series of TEM images. Tomograms of the SIGN sample shows a very interesting 3-dimensional structure in Figure 5.13 of the assumed square aggregation pattern observed in normal TEM mode (Fig.5.12 and Fig.5.6) which is a bi-pyramidal cage-like structure. This can be seen more clearly in the video available at the referenced link [89].

The morphology of precipitated C-S-H is not affected much by adding D-gluconate when premixed with calcium nitrate. It is unclear why the aggregation pattern of C-S-H with D-gluconate in the sodium silicate observed in SiGN, is not seen for the CaGN. It could be due to the complexation of D-gluconate and calcium ions during this process prior to precipitation [45,88], modifying its interaction with the C-S-H. Although D-gluconate can complex with the calcium ion, the concentration of calcium nitrate (0.2M) is only slightly reduced by ~8.7% of total calcium concentration [45,88] in the system and thereby there is still plenty of calcium to react with silicate species in the system forming C-S-H. But the gluconate is now already complexed (~90%) [45,88] and there is less available to possibly adsorb onto the C-S-H surface and induce this bi-pyramidal structure. Further work, atomistic modelling for the adsorption of D-gluconate onto C-S-H surfaces needs to be carried out to further elucidate this interesting agglomeration phenomenon. Such structures could perhaps be used for the incorporation of active molecules and used as drug delivery vehicles.
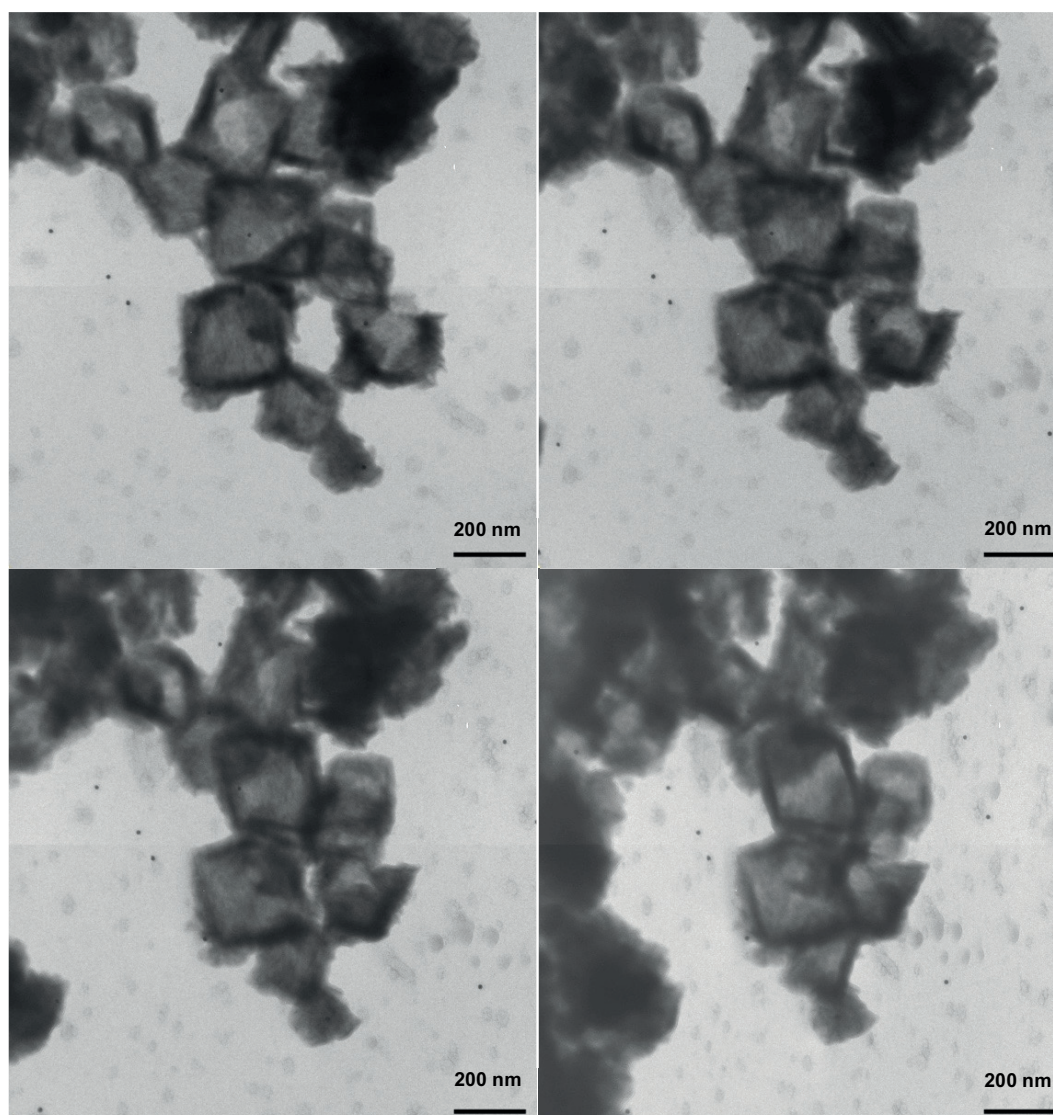
Figure 5.13 Single shots from the TEM tomogram of SiGN.

Kinetics experiment of synthetic C-S-H

Characterization

The zeta potential of the samples collected after washing and redispersion in NaOH at pH 12.0 ± 0.1 is shown in Figure 5.14. The pure C-S-H_I showed the highest negative charge at -16.3 mV. With presence of D-gluconate, the zeta potential presented a slightly more positive charge than C-S-H_I of -13.2 mV and -11.9 mV, for SiGN_I and CaGN_I respectively. This could be due to the D-gluconate adsorption onto the precipitated C-S-H surfaces.
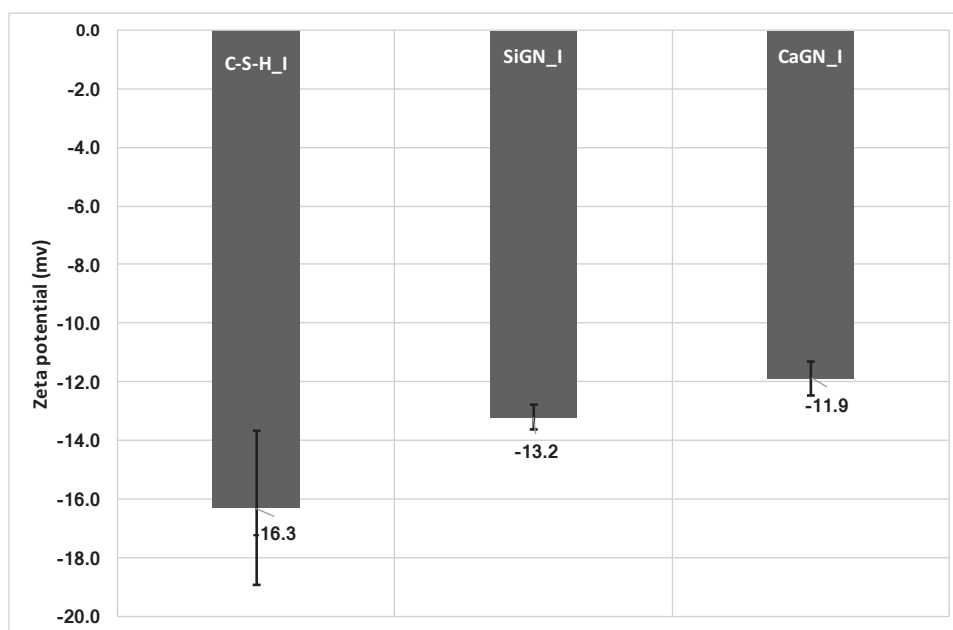
Figure 5.14 Zeta potential of C-S-H_I, CaGN_I and SiGN_I at pH 12.0.

 TGA was used to determine weight loss of D-gluconate as shown in Figure 5.15. The samples were freeze-dried for 24 hours prior to measurement. All samples showed the curves which is similar to Figure 5.11. The main weight loss between 80-250 °C which relates to typical water loss from C-S-H [32]. The broad weight loss at 300 - 600°C could be due to bound water in the sample of C-S-H_I and D-gluconate with bound water of SiGN_I and CaGN_I. Poorly crystalline $CaCO_3$ is also observed with the weight loss at 650-700°C. This is assumed to occur due to CO_2 contamination during sample handling and measurement. The zeta potential and TGA, confirm that D-gluconate adsorbs on precipitated C-S-H surfaces (as expected from the results of Nalet et al. [11,12,14]).
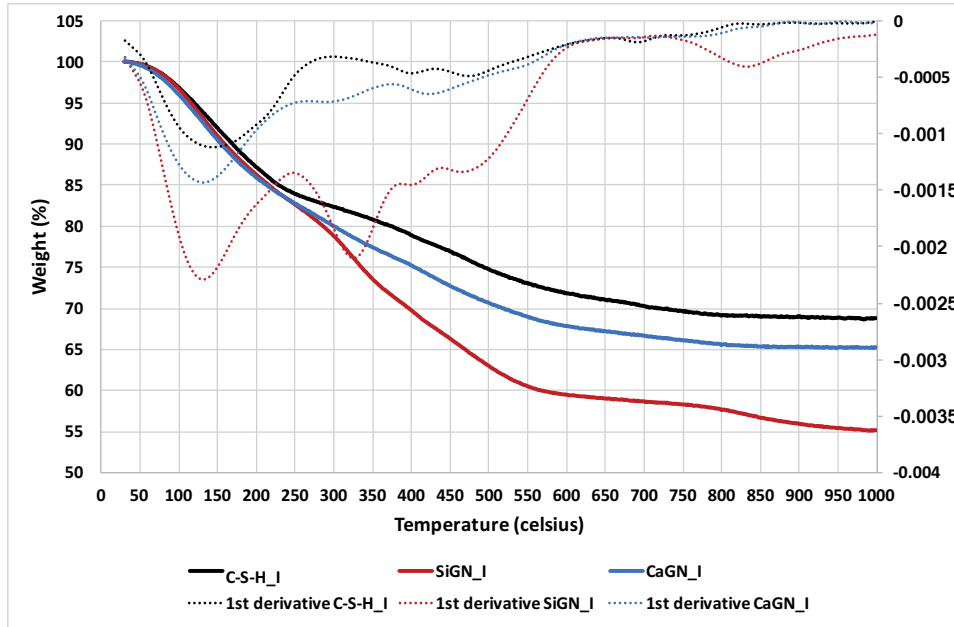
Figure 5.15 Thermogravimetric analysis (TGA) of C-S-H_I, CaGN_I and SiGN_I.

Morphology analysis of synthetic C-S-H form the kinetics experiment

TEM was used to monitor the morphology of the precipitated C-S-H with and without D-gluconate. The samples from the kinetics experiments at pH 12.3 are shown in Figure 5.16. The morphology of C-S-H_I is nanofoil, which is typical of the dropwise synthetic C-S-H. Both the CaGN_I and SiGN_I show a mixed morphology, which is a mixture of nanofibrils or needles and nanoparticles. Because of this unexpected difference in morphology complimentary experiments were carried out the same low concentration of the kinetics experiments but at a higher pH around 13.5. All samples show a nanofoil morphology (Fig.5.17). The SiGN_I (Fig.5.17) shows the square-like aggregation pattern, which is similar to SiGN (Fig. 5.12) at high concentration of calcium and silicate solutions.
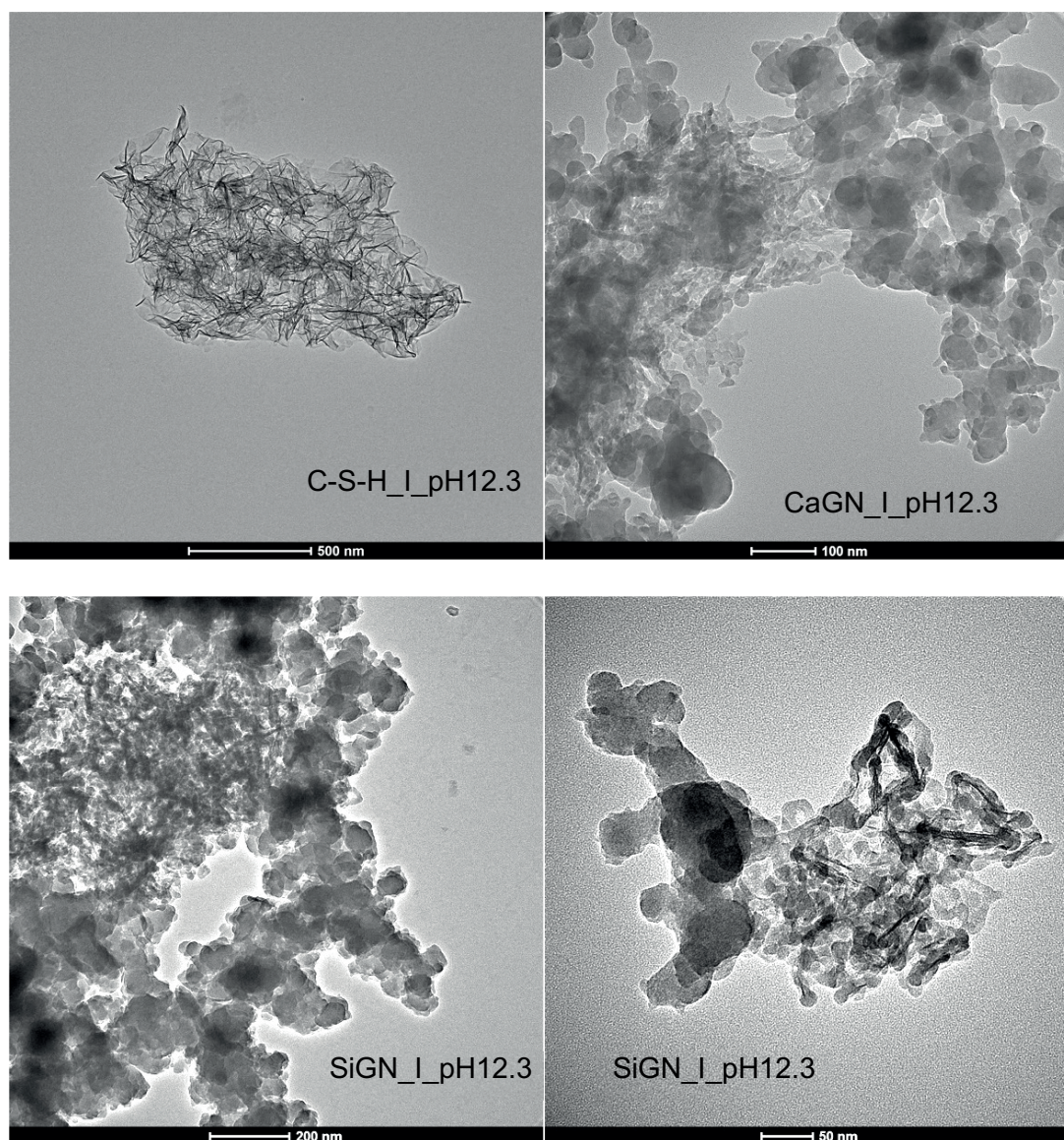
Figure 5.16 TEM images of C-S-H_I, CaGN_I and SiGN_I at pH 12.3.
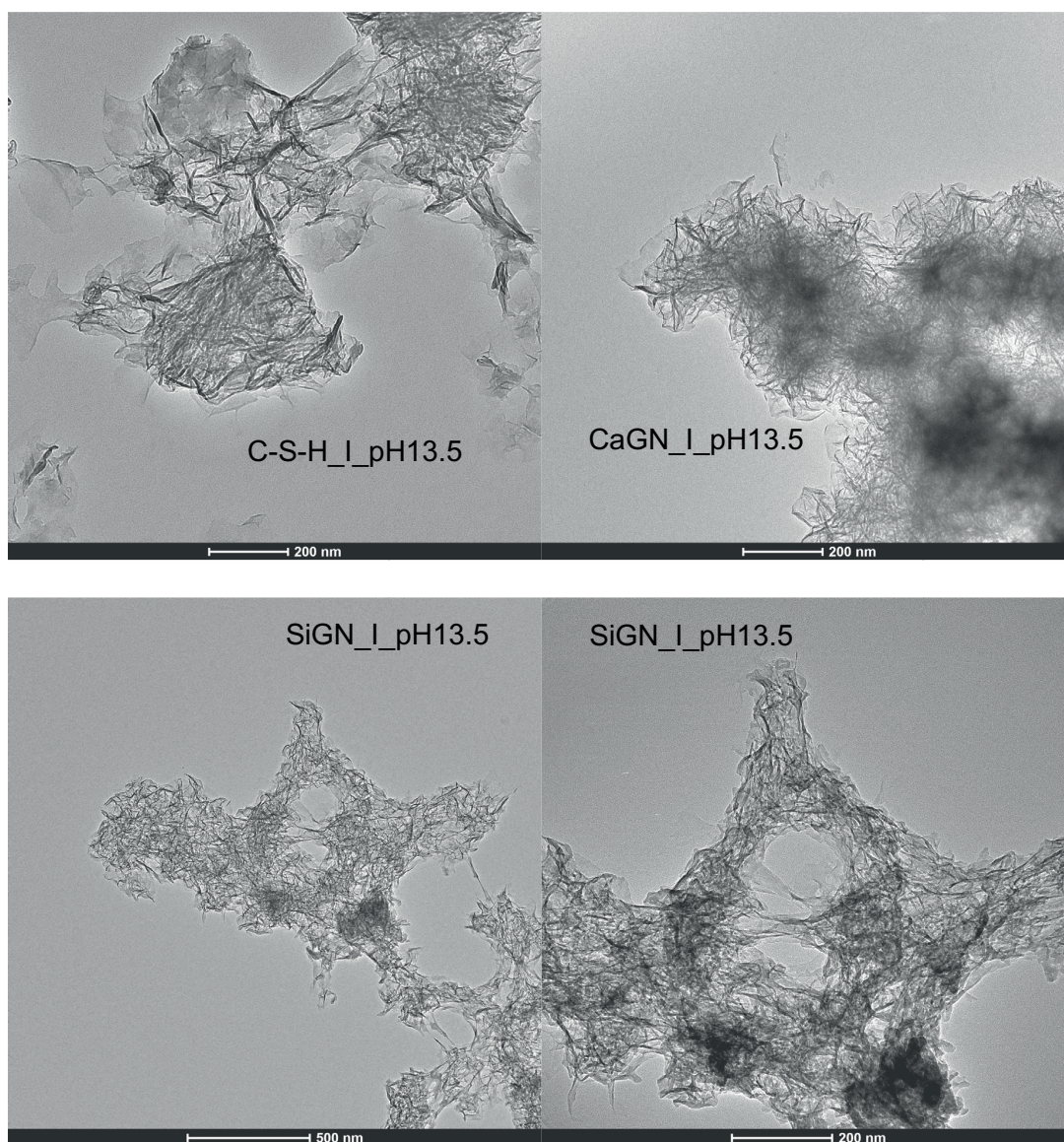
Figure 5.17 TEM images of C-S-H_I, CaGN_I and SiGN_I at pH 13.5.

Kinetics data

All samples (C-S-H_I, CaGN_I and SiGN_I) show lower amounts of free calcium ion concentration when compared with the amount of added calcium (dotted line) because of calcium consumption in different phenomena, e.g. complexation (with Silicate, D-gluconate, nucleation and growth of C-S-H (Fig.5.18). The free calcium concentration of pure C-S-H gradually increased until it reaches a critical point at 1,800 μmol/L of added calcium, where a change in slope was observed, coincident with a sudden change in the turbidity of the solution in the reactor. This was interpreted as the nucleation event for the synthetic C-S-H. Then, the calcium consumption rate is faster than the calcium addition rate as shown by the slight drop in calcium activity followed by a horizontal portion of the Ca^{2+} data. Then, at around 4,300 μmol/L, the calcium concentration increases as the consumption rate falls below that of the addition rate presumable as a result of a change in the dominating mechanism at that point in time e.g. the end of secondary nucleation and the start of slow growth of C-S-H, as previously reported by kinetics modelling of plate-like synthetic C-S-H [21].
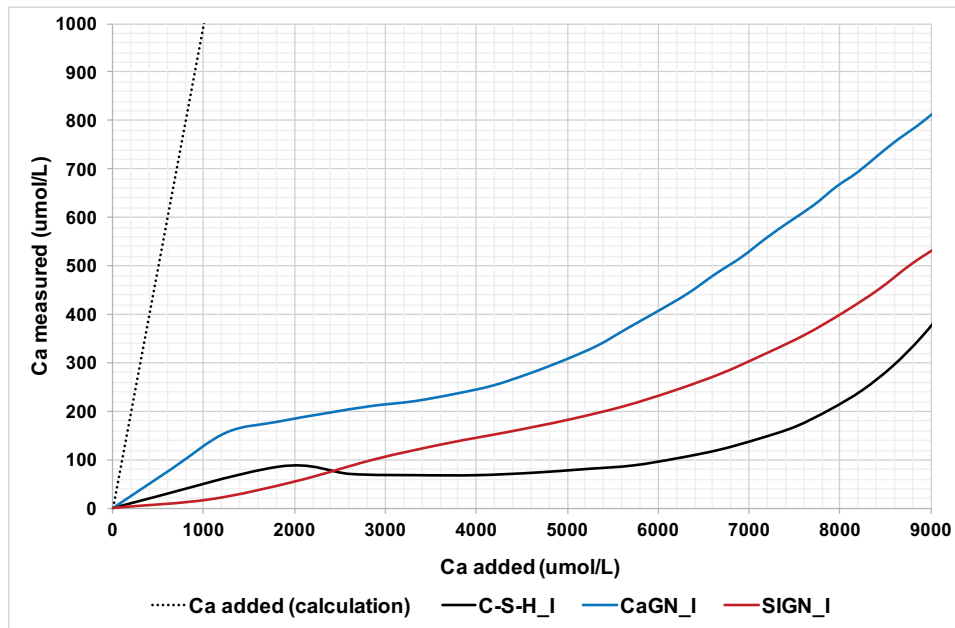
Figure 5.18 Early C-S-H precipitation curve of C-S-H_I, CaGN_I and SiGN_I.

At the beginning, the SiGN_I data shows the lowest amount of free calcium ion concentration. The slope slightly increases as time evolves. It could be both either due to the D-gluconate, silicate ions complexing with calcium or reacting with calcium. The free calcium concentration of SiGN_I is higher than pure C-S-H at 2,300 μmol/L of added calcium, which could imply an even slower growth of C-S-H in this regime because of adsorption of D-gluconate onto the C-S-H surface. For

CaGN_I, it shows the highest of measured free calcium ion concentration. The calcium consumtion rate of CaGN_I was slower than C-S-H_I and SiGN_I. This suggests that the D-gluconate in calcium nitrate solution, is complexed prior to being dropped into the sodium silicate solution. When this mixture of D-gluconate and calcium solution was added to the reactor, silicate species may react with free calcium to form C-S-H but with the quantity already complexed with calcium, the supersaturation is reduced and thus nucleation rates are reduced and thus consumption rate is reduced. At later ages the consumption is lower than both previous cases presumably because of a lower amount of C-S-H, giving less available surface for secondary nucleation and growth as well as possible hindrance of growth because of adsorbed D-gluconate. Because of the mixed morphology, the kinetics data cannot be directly used in the population balance modelling (PBM) recently used to follow the precipitation pathway of synthetic C-S-H. In Chapter 5, Section 5.3, the precipitation method for kinetics data collection is modified to try and produce single morphology particles which will eventually allow the use of the PBM method to better interpret the kinetics and precipitation pathway of synthetic C-S-H in the presence of D-gluconate.

5.2.4 Discussion

D-gluconate is a small organic molecule which shows a strong retardation effect on cement hydration. The premixing of D-gluconate in calcium or silicate solution of synthetic C-S-H did not interfere with the precipitation of C-S-H but the Ca/Si ratios were slightly lower than the pure synthetic C-S-H. This may be due to complexation with Ca^{2+} or from adsorption onto the growing C-S-H. The D-gluconate does not show a great effect on the underlying synthetic C-S-H structure with XRD reflections remaining similar. The TGA curves show the weight loss of samples made in the presence of D-gluconate is higher than pure synthetic C-S-H indicating adsorption of D-gluconate on the growing C-S-H. The morphology of synthetic C-S-H with and without D-gluconate always shows a nanofoil like morphology. Compared to CaGN, only SiGN significantly modifies the aggregation pattern of nanofoils, suggesting adsorption on basal planes of the foil-like C-S-H [81,82]. Then, D-gluconate could modify the aggregation pattern of precipitated C-S-H growth by desorption and re-adsorption onto newly precipitated C-S-H surfaces. The aggregation pattern showed a very interesting 3-dimensional bi-pyramidal structure which was clearly seen with TEM tomography.

For kinetics data collection, the dilution of calcium and silicate solution were necessary, whereas the concentration of D-gluconate remained the same as previous experiments. The experimental

conditions are shown in Table 5.4. The kinetics data of synthetic C-S-H with and without the D-gluconate was collected. The different premixing conditions (in calcium or silicate solution) D-gluconate changed the kinetics. The zeta potential and TGA confirm that D-gluconate adsorbs on the precipitated C-S-H, slightly decreasing the negative charge on the surface and an increasing weight loss between 300-600°C. The D-gluconate modifies the morphology of synthetic C-S-H produced at pH 12.3 showing a mixed morphology of nanofibrils/needles and nanoglobules. However, increasing the pH of the synthetic system at 13.5 shows a single morphology of nanofoils. This could be due to the competitive complexation ability on calcium between the D-gluconate and dormant silicate species at different pH. Additionally, the relative concentration of the aqueous silicate species is not same at different pH conditions. $[SiO(OH)_3]^-$ becomes the dominant species at pH 12.3 and $[SiO_2(OH)_2]^{2-}$ become dominant species at pH 13.5 [90]. However, it does not affect the morphology of C-S-H without D-gluconate, which is nanofoil at both 12.3 and 13.5. The presence of D-gluconate at pH 12.3 seems to modify the nucleation and growth of precipitated C-S-H. It could be due to the charge of the dominant silicate species. The charge of $[SiO(OH)_3]^-$ is weaker than $[SiO_2(OH)_2]^{2-}$. So, D-gluconate may be able to compete better with $[SiO(OH)_3]^-$ than $[SiO_2(OH)_2]^{2-}$ for the complexation with available calcium.

However, kinetics data at pH 13.5 cannot be collected because of the limitation of calcium ISE electrode. Further work is planned to find experimental conditions which give us a single morphology of synthetic C-S-H with and without the D-gluconate. Then, the kinetic-population balance model [21] will be used to investigate effects on the kinetics of nucleation and growth.

5.2.5 Conclusion

In summary, D-gluconate gave a strong retardation in Portland cement assumed to be due to adsorption on dissolution sites of cement particles which slowed down the dissolution rate. The complexation between calcium and D-gluconate has been studied by using a calcium ion selective electrode. Increasing the concentration of D-gluconate showed higher calcium complexation in the solution. The data have been evaluated by using the thermodynamic modelling package GEMS which gives a best fit to the data of Kutus et al. [88]. Our results will be used for future thermodynamic modelling.

The effect of D-gluconate premixed in either the calcium or silicate solutions on precipitated synthetic C-S-H has been investigated. For characterization, ICP and XRD did not show significantly change with presence of D-gluconate in the synthetic system compared to pure synthetic C-S-H. However, TGA showed higher weight loss in the presence of D-gluconate compared to pure syn-

thetic C-S-H because of the adsorption of D-gluconate on the C-S-H surface. The morphology of synthetic C-S-H with and without presence of D-gluconate was observed to be nanofoils. The aggregation pattern of SiGN has been investigated by TEM-tomography which showed a 3-dimensional of bi-pyramidal cage-like structure. However, premixed D-gluconate in calcium solution did not show the aggregation pattern of nanofoils attributed to the pre-complexation with calcium.

For the kinetics analysis of synthetic C-S-H, the presence of D-gluconate in the premixed solutions showed different kinetic behaviors. The presence of D-gluconate in the calcium solution gave the slowest consumption of calcium during both nucleation and growth period of the C-S-H formation. This was attributed to the complexation with D-gluconate lowering the supersaturation for C-S-H nucleation and consequently also slowing down growth. Zeta potential measurements showed a less negative surface charge of synthetic C-S-H in the presence of D-gluconate (CaGN_I and SiGN_I) compared to pure synthetic C-S-H (C-S-H_I). It confirmed the adsorption of D-gluconate on precipitated C-S-H surfaces. The D-gluconate modified the morphology of synthetic C-S-H at different pH's. TEM images showed mixed morphology of nanofibrils and nonoglobules (CaGN_I and SiGN_I) at pH around 12.3, whereas the morphology of the pure C-S-H_I was nanofoils. Increasing pH to 13.5, the morphology of precipitated C-S-H with presence of D-gluconate also showed nanofoils. This difference was explained by the different silicate species at these pHs and the competition for complexation with calcium with D-gluconate, which observed the mixed morphology.

5.3   Kinetics analysis of single morphology of synthetic C-S-H in the presence of presence of D-gluconate

Section 5.2 investigated the effect of D-gluconate on synthetic C-S-H. The kinetics data at pH 12.3 was collected. However, the morphology of the precipitated C-S-H in the presence of D-gluconate was a mixture of nanofoils and nanoglobules, which does not allow kinetics modelling using the population balance modelling (PBM) approach developed in our group. Consequently, there was a need to find experimental conditions which give a single morphology of synthetic C-S-H in the presence of D-gluconate. This was achieved and kinetics data were collected and will be investigated by using the population balance model (PBM) approach in collaboration with Mohammad Reza Andalibi (PSI) for a future publication in an international journal.

5.3.1 Introduction

Concrete is the most widely used construction material in the world. It has a significant carbon footprint because of the very high quantity used. Supplementary cementitious materials (SCMs) are alternative materials such as fly ash, slag, and calcined clay which have been generally used to replace clinker content in order to reduce CO_2 emissions [6,8,9]. Portland cement is a complex system, there are several hydrated products such as C-S-H, calcium hydroxide (CH), ettringite, calcium monosulphoaluminate or calcium monocarboaluminate. These phases have been formed in the system from the dissolution of several anhydrous phases [16,27,57].

Calcium silicate hydrate (C-S-H) is the major hydration product and the most important phase in cement. This phase contributes 50-60% by volume of hardened cement paste and it is responsible for early age strength of cement and long term evolution of concrete structures [20,22]. C-S-H is a poorly crystalline material which has varying stoichiometry (Ca/Si molar ratio from 0.8-2.2) [35,91,92]. It is difficult to characterize at an atomistic level. Therefore, much research has concentrated on synthetic C-S-H - a simpler system than Portland cement allowing for better interpretations of mechanisms behind cement hydration [7, 12–18]. In recent work, from Kumar et al. [20], homogeneous synthetic C-S-H with Ca/Si molar ratio up to 2.0 have been prepared by using a dropwise precipitation method.

Population balance equation (PBE) is a mathematical framework to describe the development of particle formation during the processing or over time [97–100]. PBE simulation combined with an optimization code for equilibrium speciation calculations considering solid/liquid equilibrium ex-

plains nucleation, growth, dissolution, and aggregation of particles together within a single framework. The PBE simulation were successfully applied on particulate materials precipitating from aqueous solutions such as $BaTiO_3$ [99,100] and $CaCO_3$ polymorphs [98]. Primary nucleation, secondary nucleation and molecular growth of synthetic C-S-H with Ca/Si = 2.0 [20] has been described by Andalibi et al. [21] by using a computational model based on a PBE approach. The model tracked nucleation (primary and secondary) events and growth in the synthetic C-S-H system giving much insight into how supersaturation evolves in time and how the different processes dominate at different times.

This chapter will focus on collecting kinetics data of synthetic C-S-H in the presence of D-gluconate which has a single morphology, to allow kinetics analysis using the PBE approach. The complexation of D-gluconate will also be taken into account in the PBE modelling using the results from Kutus et al. [88] confirmed in Chapter 5.2 as being a good representation of our D-gluconate system. The dropwise precipitation method with in-situ Ca selective, pH and conductivity electrodes will be used to prepare and collect kinetics data of synthetic C-S-H formation with and without D-gluconate. This method will allow us to investigate the effect of D-gluconate on nucleation and growth of precipitated C-S-H. Samples were qualitatively analyzed by TEM and STEM-EDX.

5.3.2 Materials and methods

Kinetics experiments on synthetic C-S-H

Kinetics experiments were performed with the dropwise precipitation method using the same protocol as in Chapter 3, Section 3.2. A schematic of the dropwise method is shown in Chapter 3, Figure 3.1. The experimental setup combined with calcium ion selective (perfectION^{TM}, *Mettler Toledo*), pH (InLab$^®$Expert Pro-ISM-IP67, *Mettler Toledo*) and conductivity (InLab$^®$ 731-ISM, *Mettler Toledo*) electrodes. The electrodes are connected with benchtop pH meter (SevenExcellence pH Meter, *Mettlet Toledo*). The data were collected by EasyDirect™ pH Software. Before precipitation, all electrodes were calibrated with their standard solutions as shown in Chapter 3, Table 3.1.

The calcium ($Ca(NO_3)_2.4H_2O$, *Fluka Chemicals,* CAS:13477-34-4) solution (Part A) is always constantly added to the silicate solution (Part B). With presence of the 1.2 mM of D-gluconate (*Merck KGaA*, CAS:1527-07-1), the D-gluconate solution was premixed in either the 0.01 M, 50 mL silicate (Na_2SiO_3, S*igma-Aldric*h, CAS:6834-92-0) solution or the 0.02 M, 50 mL calcium solution. The reactions were carried out under an N_2 atmosphere. The pH was controlled at around 11.0 ± 0.2

or 12.0 ± 0.2 by adding calculated amounts of 1.0 N NaOH standardized solution (*abcr GmbH, CAS:1310-73-2*). The experimental conditions are shown in Table 5.6.

Sample	A		B		pH
	$Ca(NO_3)_2.4H_2O$	D-gluconate	Na_2SiO_3	D-gluconate	
C-S-H_II	0.02 M	-	0.01 M	-	11.0 ± 0.2
CaGN_II	0.02 M	1.2 mM	0.01 M	-	11.0 ± 0.2
SiGN_II	0.02 M	-	0.01 M	1.2 mM	11.0 ± 0.2
C-S-H_III	0.02 M	-	0.01 M	-	12.0 ± 0.2
CaGN_III	0.02 M	1.2 mM	0.01 M	-	12.0 ± 0.2
SiGN_III	0.02 M	-	0.01 M	1.2 mM	12.0 ± 0.2

Table 5.6 Experimental conditions of synthetic C-S-H in the presence of D-gluconate.

Characterization methods

Transmission electron microscopy (TEM) The morphology of the synthetic C-S-H was investigated by using TEM, *Thermo Scientific™* Talos F200X scanning transmission electron microscope (STEM) with TEM mode. It was operated at an acceleration voltage of 200 kV. TEM images were collected and then exported by using TEM Imaging and Analysis (TIA) software. The samples were prepared by dispersing the precipitated C-S-H in isopropanol and treated in an ultrasonic bath for 15 minutes. The dispersed samples were dropped on to the charged grid (carbon films on 300 mesh grids copper, *Agar Scientific Ltd.*) and allowed to dry for few minutes.

Scanning transmission electron microscope-energy dispersive x-ray (STEM-EDX) - High-angle annular dark-field (HAADF) STEM measurement combined with EDX used to investigate the elemental distribution. The elemental map of the samples was operated by Talos F200X scanning transmission electron microscope (STEM) with STEM-EDX mode. It was operated at an acceleration voltage of 200 kV. After STEM alignment, the elemental map was performed by using *Bruker Esprit 1.9* software. The samples were prepared using the same procedure as for the TEM.

The stoichiometry of synthetic C-S-H was analysed by Inductively Coupled Plasma in the Optical Emission Spectroscopy mode (ICP-OES) which was performed on an ICPE-9000 series (Shimadzu) instrument. After washing and filtration, 0.1 g of the filtrated sample was dissolved in 8.0 mL of 65% HNO_3 (14.58 M), *Carlo Erba* and then in 2.0 mL of fuming 100% HNO_3 (22.43 M), *Merck KGaA*. The dissolved samples were diluted in HNO_3 (2.0 M), *Alfa Æsar* at x10, x100 and x1,000.

Chapter 3, Table 3.2 shows total volume of the dissolved samples and 2.0 M of HNO_3 of x10, x100 and x1,000 dilutions. After 24 hours, the diluted samples were filtered by using 10 mL of syringe together with 0.45 μm PTFE filter.

5.3.3 Results and discussion

Morphology analysis

The morphology of synthetic C-S-H with and without D-gluconate at pH 11.0 ± 0.2 is shown in Figure 5.19. TEM images show a nanoglobular morphology. It seems the size of the pure synthetic C-S-H (100-300 nm) is larger than C-S-H with presence of D-gluconate (50-100 nm), suggesting influence on the nucleation rate. HAADF image and elemental map of SiGN_II is shown in Figure 5.20. Elemental map shows homogeneous distribution of Ca, Si and O in the nanoglobules which corresponds to a C-S-H composition.
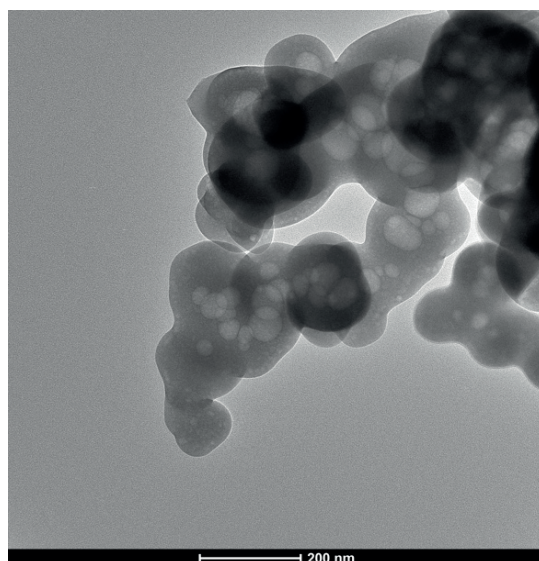
(a)
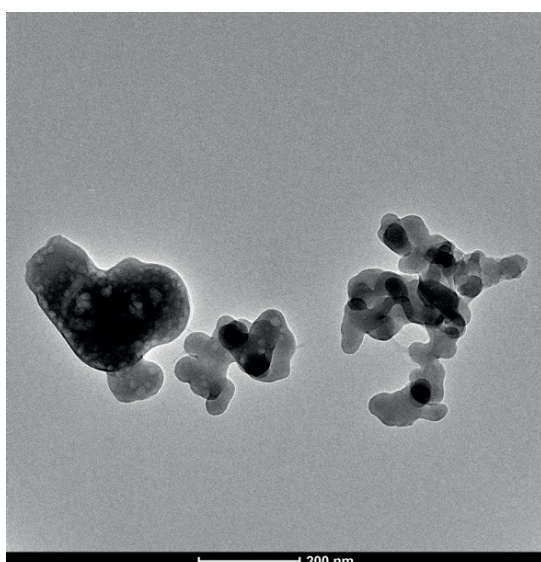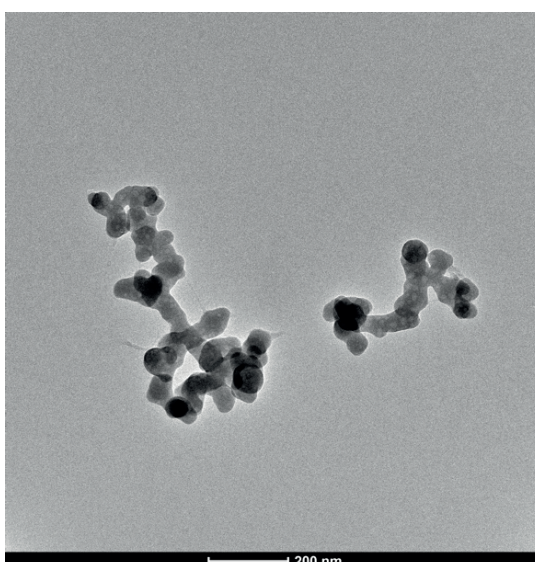
(b)   (c)

Figure 5.19 TEM images of synthetic C-S-H at pH 11.0±0.2, (a) pure synthetic C-S-H, (b) SiGN_II and (c) CaGN_II.
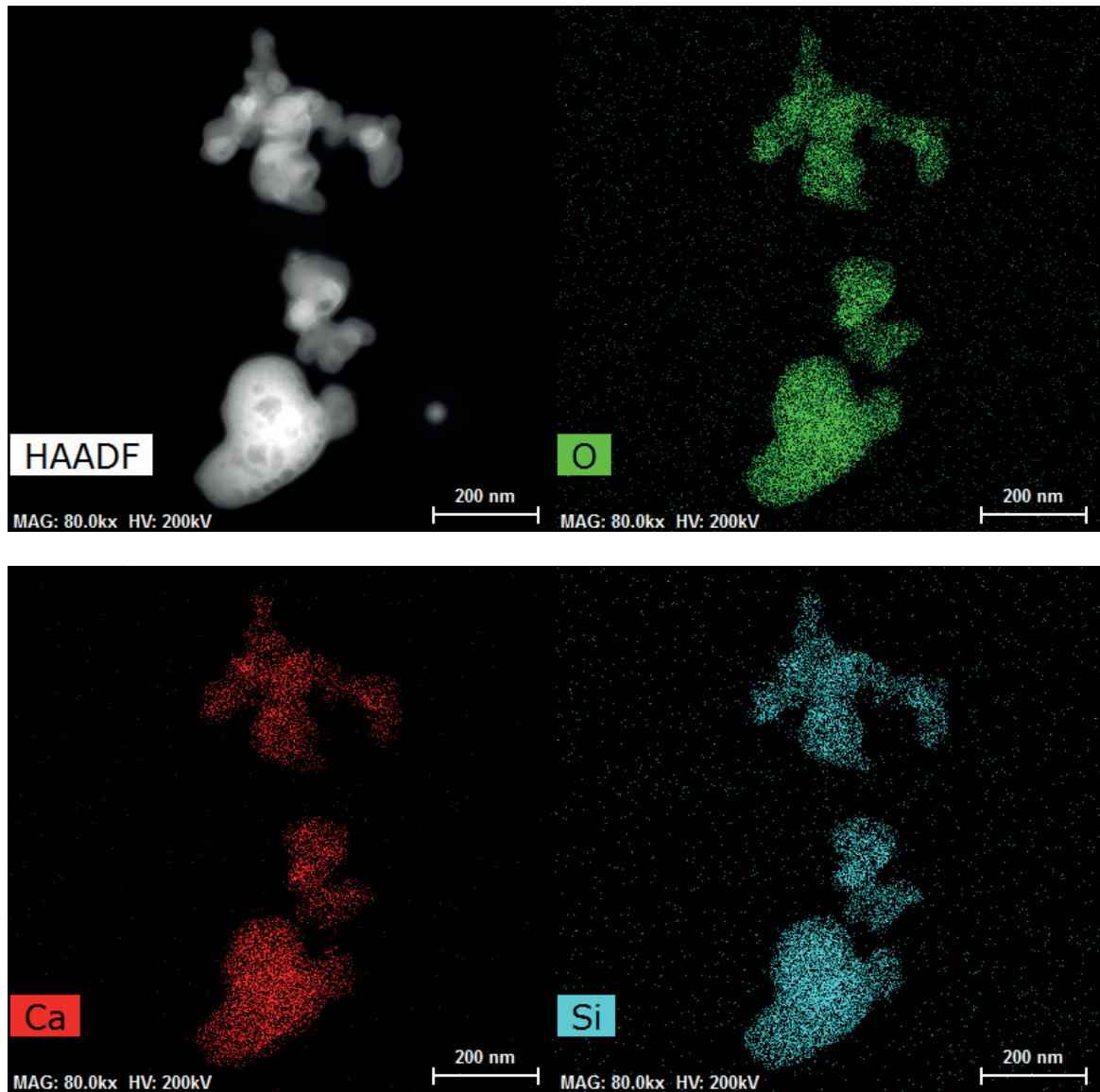
Figure 5.20 HAADF image and elemental map of synthetic C-S-H with presence of D-gluconate (SiGN_II) at pH 11.0±0.2.

When increasing pH up to 12.0±0.2, the C-S-H_III, SiGN_III and CaGN_III all present a nanofoil morphology as shown in Figure 5.21, 5.22 and 5.23, respectively. With presence of D-gluconate (SiGN_III and CaGN_III), the square aggregation (probably bi-pyramidal in 3D) pattern were shown in Figure 5.22 (b) and 5.23 (b), which is similar to Section 5.2 in Figure 5.12. It could be due to D-gluconate complexation with calcium modifies nucleation and growth of C-S-H formation. HAADF images and elemental maps of C-S-H_III and CaGN_III are shown in Figure 5.24 and 5.25, respectively. The HAADF images present nanofoils of C-S-H_III and CaGN_III. It is clearly seen that elemental maps of Ca, Si and O shows homogeneous distribution of the elements without any obvious secondary phases.
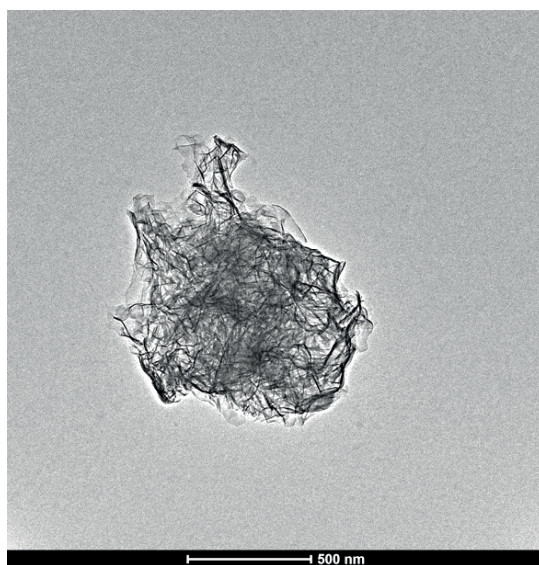
Figure 5.21 TEM image of synthetic C-S-H without D-gluconate at pH 12.0±0.2.

(a)   (b)
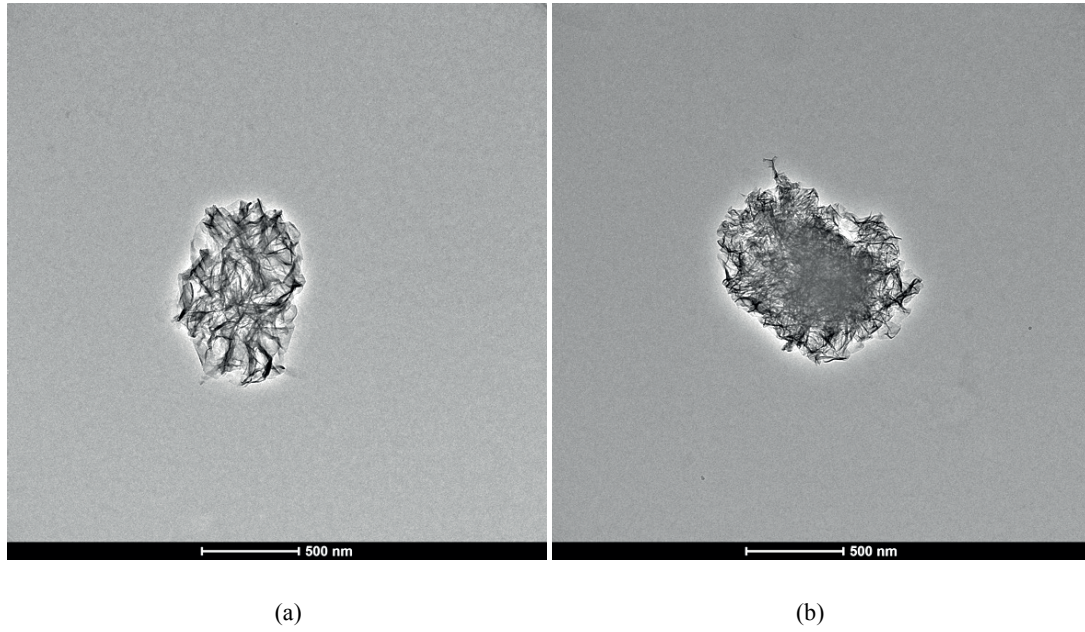
Figure 5.22 TEM images of synthetic C-S-H with presence of D-gluconate (SiGN_III) at pH 12.0±0.2.

(a)   (b)
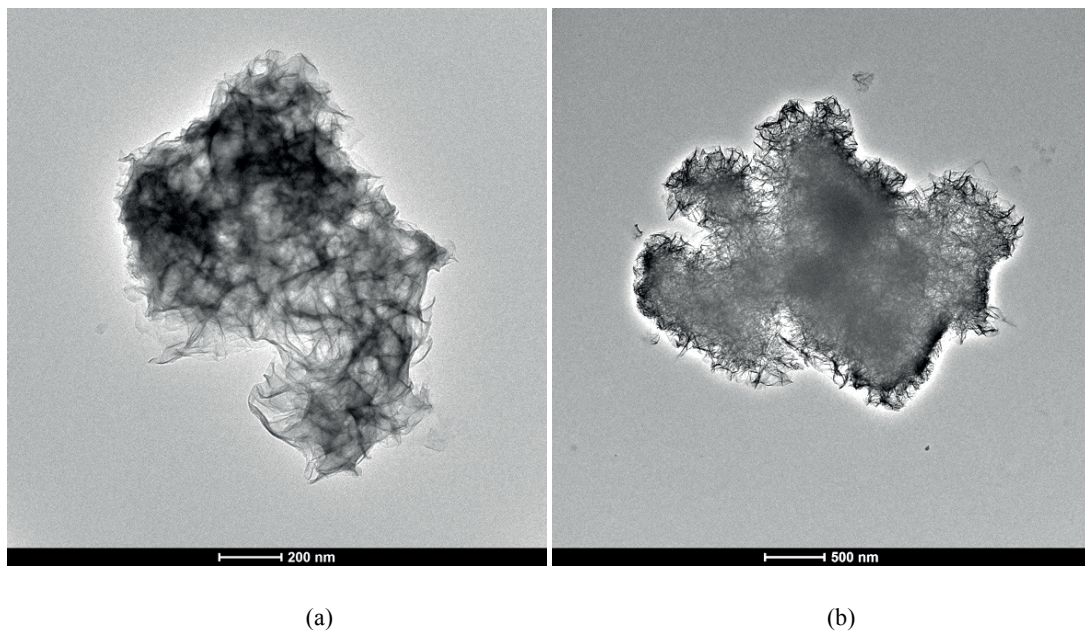
Figure 5.23 TEM images of synthetic C-S-H with presence of D-gluconate (CaGN_III) at pH 12.0±0.2.
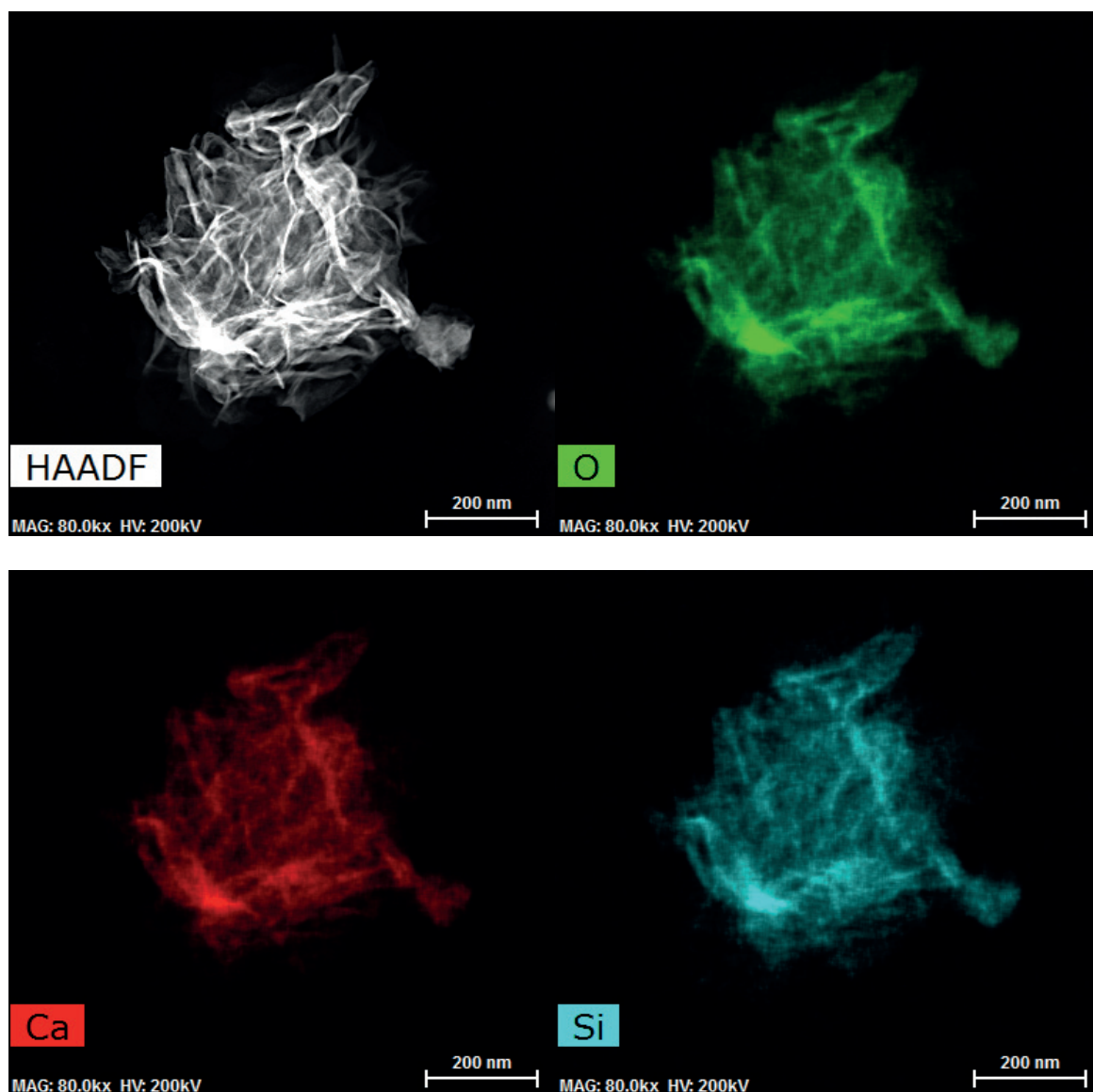
Figure 5.24 HAADF image and elemental map of pure synthetic C-S-H (C-S-H_III) at pH 12.0±0.2.
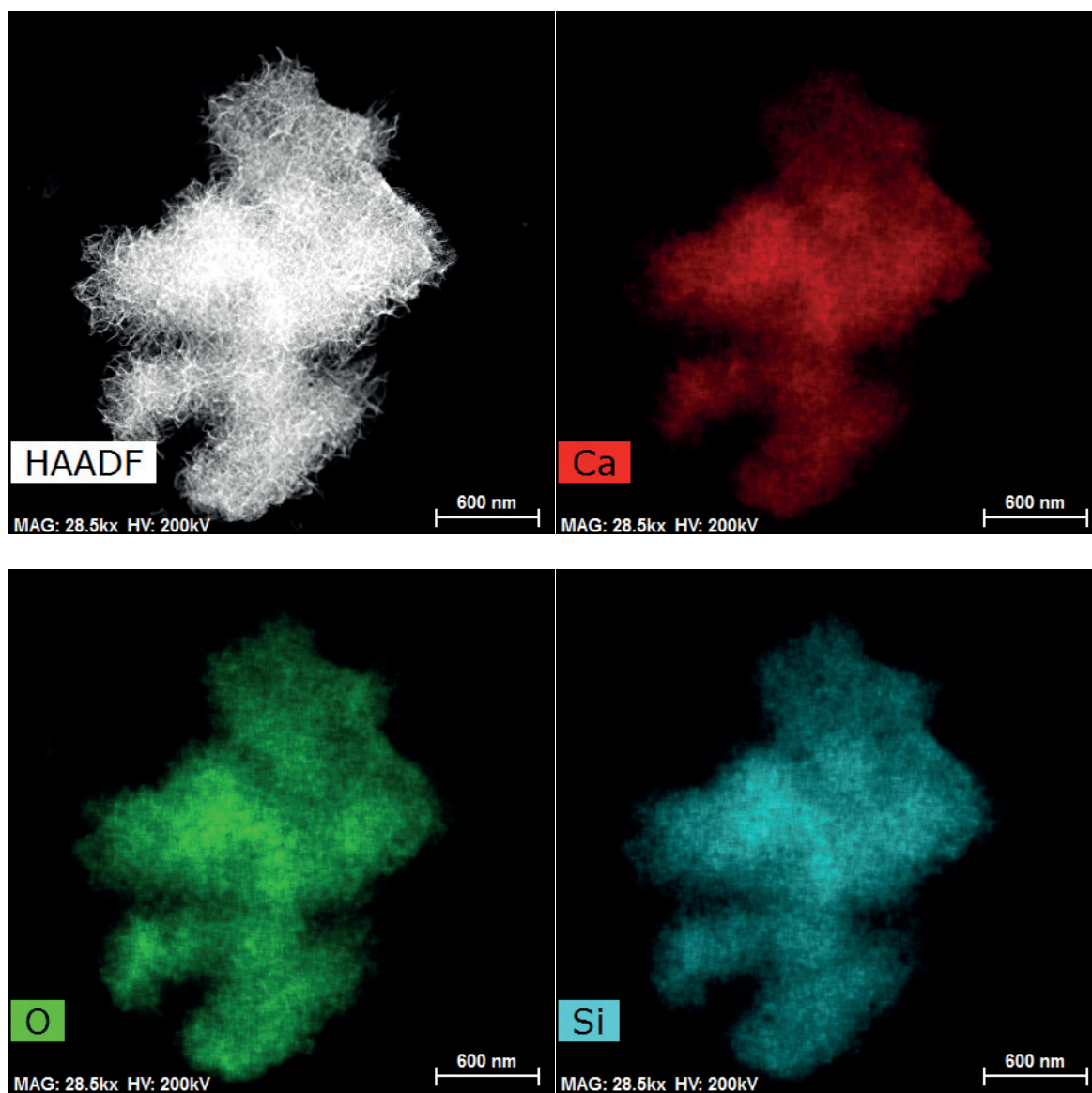
<u>Figure 5.25</u> HAADF image and elemental map of synthetic C-S-H with presence of D-gluconate (CaGN_III) at pH 12.0$\pm$0.2.

Chemical compositions

Stoichiometry of synthetic C-S-H in the presence of D-gluconate at pH 12.0±0.2 were investigated by ICP. The Ca to Si ratios (Ca/Si) are shown in Table 5.7. Presenting 1.2 mM of D-gluconate of synthetic C-S-H does not significantly change the Ca/Si ratio which was similar to the pure synthetic C-S-H (C-S-H_III). CaGN_III shows slightly decreased Ca/Si ratio at around 1.2. However, the aggregation pattern was seen in SiGN_III and CaGN_III (Fig.5.22 and 5.23, respectively). It could be due to the adsorption of D-gluconate on synthetic C-S-H surface [81] affecting the pattern [82] but not Ca/Si.

Sample	Ca/Si
C-S-H_III	1.3 ± 0.1
CaGN_III	1.2 ± 0.1
SiGN_III	1.3 ± 0.1

Table 5.7 Ca/Si ratios from ICP measurements of synthetic C-S-H with different premixed solution of 1.2 mM D-gluconate.

Kinetics data

Figure 5.26 shows free calcium concentration as a function of calcium added in the synthetic C-S-H system at pH 11±0.2. The synthetic C-S-H with and without D-gluconate shows highly calcium consumption compared to the amount of added calcium (dotted line – calculated from the flow rate) due to precipitation of C-S-H and formation of complexes. However, the free calcium evolution in the system of each sample was different. At this pH around 11.0±0.2, the free calcium with presence of D-gluconate (SiGN_II and CaGN_II) was consumed more than without the presence of D-gluconate (C-S-H_II.) SiGN_II shows the lowest calcium concentration. In this case, D-gluconate was premixed in the silicate solution. It meant total concentration of D-gluconate presented in the mixture prior to reaction with calcium. When calcium was constantly dropped into the reactor, D-gluconate and silicate ions compete to complex with calcium. In the case of CaGN, D-gluconate already complexed with calcium because D-gluconate was premixed with calcium solution prior to add into silicate solution. When the premixed solution of calcium was constantly added in the silicate solution, the rest of free calcium may react with silicate to form C-S-H.
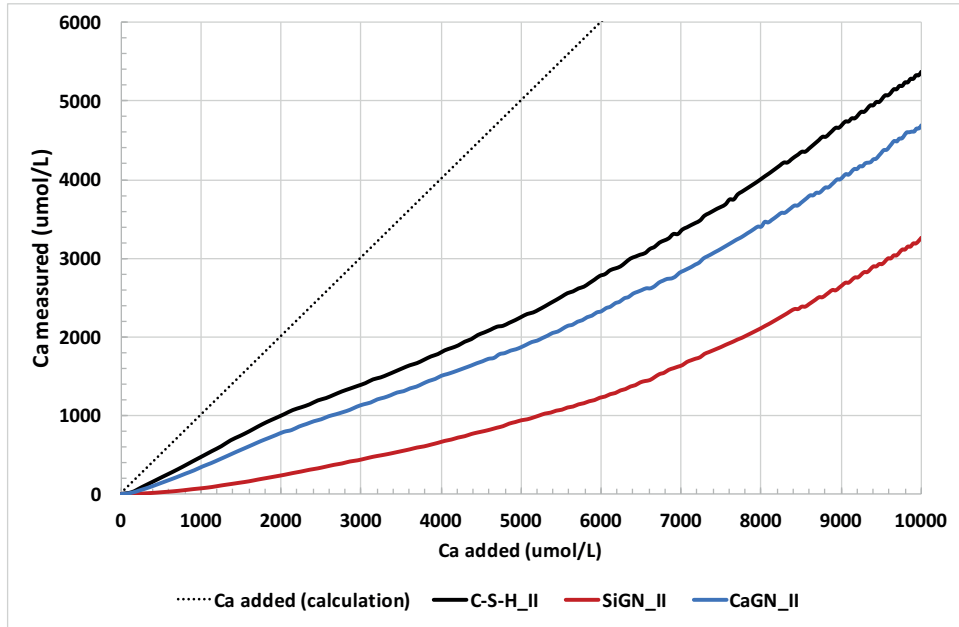
Figure 5.26 Early C-S-H precipitation curve of C-S-H_II, CaGN_II and SiGN_II at pH 11.0±0.2.
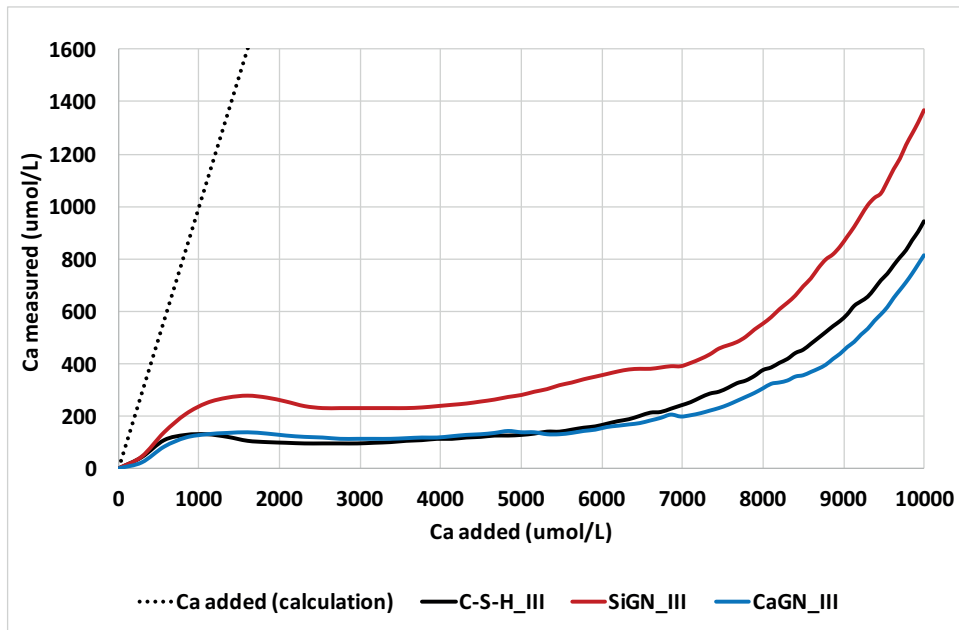
Figure 5.27 Early C-S-H precipitation curve of C-S-H_III, CaGN_III and SiGN_III at pH 12.0±0.2.

Figure 5.27 presents the free calcium evolution as a function of calcium added in the synthetic C-S-H system with and without presence of D-gluconate at pH 12.0. Again, the dotted line is amount of calcium that was added to the system. Changing pH from 11.0 and 12.0, the free calcium ion of pH 11.0 (Fig.5.26) is higher than pH 12.0 (Fig.5.27) this is probably because of increasing $CaOH^+$ con-

centrations at pH 12.0. A big difference between pH 11.0 and 12.0 is seen for the premixed solution of silicate with D-gluconate. SiGN_III shows a slower kinetics of calcium consumption and hence C-S-H formation. The free calcium ions in the system of pure synthetic C-S-H (C-S-H_III) were similar to CaGN_III, which had D-gluconate in premixed calcium solution. When added calcium is at 6,800 µmol/L, the calcium consumption of CaGN_III was a bit higher than C-S-H_III. This could be due to a faster growth of C-S-H in CaGN_III. It seems the pH effect on ion speciation of chemicals in the system will also effect the kinetics of C-S-H formation. Full analysis of the speciation, including the complexation with D-gluconate using the PBE approach will allow us to gain further insight into this kinetics data and the role on the nucleation (primary and secondary) and growth events during the precipitation of these two different C-S-H morphologies. The work is currently underway in collaboration with Mr. Mohammad Reza Andalibi (PSI) who has developed the PBE approach for C-S-H.

5.3.4 Conclusions

Single morphologies, globule and sheet, of synthetic C-S-H with and without presence of D-gluconate have been prepared by using the dropwise precipitation method. Kinetics data and morphology have been investigated. Both pH 11.0±0.2 and 12.0±0.2 give a single morphology with different morphology. At pH 11.0±0.2, synthetic C-S-H with and without D-gluconate show a nanoglobule morphology, whereas at pH 12.0±0.2 they show a nanofoil morphology. With presence of D-gluconate, there is square aggregation pattern at the higher pH of 12.0±0.2. The elemental maps of nanoglobules and nanofoils present uniform distributions of Ca, Si and O which corresponds to a single-phase C-S-H composition. With the presence of 1.2 mM of D-gluconate no significant change of the Ca/Si ratio compared to pure synthetic C-S-H. This kinetics data is currently being evaluated by population balance modeling in order to describe nucleation and growth of precipitated synthetic C-S-H formation in more detail and to try and discern the exact role of D-gluconate complexation and modifications in supersaturation on the growth of synthetic C-S-H. Such insight will be invaluable for a better understanding of the role of admixtures in the more complex Portland cement systems.

Chapter 6 Synthesis and characterization of synthetic C-S-H with presence of heterogeneous substrates

This chapter investigates the effects of heterogeneous surfaces on the nucleation and growth of synthetic C-S-H. Firstly, quartz and calcite were introduced in calcium and silicate solutions for 24 hours, respectively. Then quartz and calcite were introduced to the silicate solution and their effect on the nucleation and growth on addition of the calcium solution was investigated. Further, the kinetics of nucleation and growth of synthetic C-S-H was monitored via the dropwise precipitation method within-situ pH, conductivity and calcium selective electrodes. Precipitated samples were also characterized by XRD, TGA, TEM and STEM-EDX.

6.1 Introduction

Concrete has a significant carbon footprint due to the high quantity used and the release of CO_2 during the formation of clinker. To reduce its carbon footprint, supplementary cementitious materials (SCMs) have been generally used in concrete to replace clinker contents (~5-20% replacement) [8,9]. Quartz and calcite are common materials which have been used to replace clinker content for concrete or mixed cement. Quartz is a material composed of silicon and oxygen atoms (SiO_2). Its chemical reaction is very slow in terms of dissolution rate [101,102]. The calcite or limestone is a material which chemical formula is $CaCO_3$. Calcite is also thought to be relatively inert in Portland cement pore solution which has a relatively high calcium activity of around 20 mM [103].

Calcium silicate hydrate (C-S-H) is the most important and main hydrate phases in Portland cement. In Portland cement, C-S-H precipitates with others phases such as portlandite, ettringite and calcium carbonate [3]. The chemical composition of C-S-H has variable stoichiometry (Ca/Si from 1.0-2.0) and is composed of tetrahedral silicate chains flanked on both sides with calcium oxide layers. Its is a poorly crystalline and non-stoichiometric material. So, it is difficult to analyze C-S-H by using XRD. Therefore, many researchers have been studied synthetic C-S-H in order to try to un-

derstand interaction of ions or fillers on pure C-S-H [13,18,79–81,104]. The dropwise precipitation method has been used to prepare homogeneous precipitated synthetic C-S-H by Kumar et al. [20] and this is attractive method to study the kinetics of nucleation and growth [21]. The molar ratio between calcium and silicon (Ca/Si) of synthetic C-S-H up to 2.0 can be produced with the dropwise precipitation method with well-controlled mixing conditions. To approach real Portland cement systems, heterogeneous particles, quartz and calcite, will be introduced in this synthetic C-S-H system. This will help us to better understand mechanisms of heterogeneous substrate on the nucleation and growth of synthetic C-S-H.

Many researchers have studied the effect of quartz and calcite on cement hydration which are often used as fillers [9,48,51,104–107]. The quartz and calcite fillers or particles can act as heterogeneous nucleation sites. These can accelerate cement hydration by shortening the induction period as well as modifying the effective water to cement ratio. Kadri et al. [108] showed the effect of fillers at very early stages which accelerate the cement hydration. The inert (quartz) and active (alumina and calcite) fillers act as heterogeneous surfaces of hydration products. Kadri et al. [108] did not see any significant acceleration of the hydration with quartz. However, some research has presented the effect of quartz that can increase rate of the cement hydration. Berodier et al. [48] observed the presence of nuclei on the quartz surface which confirmed quartz can act as a heterogeneous substrate for calcium silicate hydrate (C-S-H). Kumar et al. [51] suggested that quartz and limestone can accelerate the cement hydration. The acceleration rate with replacement of limestone was higher than with replacement of quartz because of ion-exchange reaction with C-S-H. Since limestone partially dissociated releasing Ca^{2+} and CO_3^{2-} into the system, the sorption of carbonate ions on C-S-H in turn to release OH^- increasing C_3S hydration kinetics by pH elevation [109,110]. So, there are some conflicting results but in general in cement mixtures quartz and calcite are expected to accelerate hydration. In this paper, we will investigate their effect on the nucleation and growth of synthetic C-S-H opening the way for further insights into the heterogeneous nucleation process assumed to dominate in cementitious systems.

6.2   Materials and methods

6.2.1 Observation of quartz and calcite in solutions of calcium and silicate, respectively

Quartz (1%w/v) was dispersed in 0.2 M, 100 mL of a calcium nitrate ($Ca(NO_3)_2.4H_2O$, *Fluka Chemicals,* CAS:13477-34-4) solution. The pH was adjusted by adding sodium hydroxide (NaOH, *Acros organic*, CAS:1310-73-2) until it reached 13.5. The suspension was mixed using a magnetic stirrer at 1,100 rpm under an N_2 atmosphere at 25°C, for 24 hours. After 24 hours, the sample was collected by filtration and then washed with a mixture of deionized water:ethanol (50:50), 100 mL and pure ethanol, 100 mL. The sample was kept in an airtight plastic bottle. For calcite, 1%w/v of calcite was dispersed in 0.1 M, 100 mL of silicate (Na_2SiO_3, S*igma-Aldric*h, CAS:6834-92-0) solution and as for the quartz mixed using a magnetic stirrer at 1,100 rpm under an N_2 atmosphere at 25°C, for 24 hours. The experimental condition is shown in Table 6.1.

Sample	$Ca(NO_3)_2.4H_2O$	Na_2SiO_3	Quartz (wt %)	Calcite (wt %)	pH
Quartz in Ca solution	0.2 M	-	1.0	-	13.5
Calcite in Si solution	-	0.1 M	-	1.0	13.5

Table 6.1 Experimental conditions of heterogeneous particles in the starting solutions used for the synthesis of synthetic C-S-H by the dropwise precipitation method [13].

Thermodynamic modelling using GEMS

Thermodynamic modelling has been performed using the Gibbs free energy minimisation program GEMS [25,26]. This model can compute the chemical speciation of the pore solution and hydrate phase assemblage during cement hydration at the equilibrium stage. GEMS was used to calculate and predict possible phases under our experimental conditions with presence of quartz and calcite. *Cem 18* was used as the database for GEMS calculation.

6.2.2 Kinetics data of synthetic C-S-H precipitation with quartz and calcite

The dropwise precipitation method has been used to study the kinetics of C-S-H synthesis in the presence of heterogeneous particles (same protocol as in Chapter 3, Section 3.2, and schematic in Chapter 3, Figure 3.1). Heterogeneous particles (quartz or calcite) were introduced in 0.01 M, 150 mL of the silicate (Na_2SiO_3, S*igma-Aldric*h, CAS:6834-92-0) solution and mixed in the stirred reactor under N_2 atmosphere for 30 min before adding the calcium solution. The 0.02 M, 150 mL of calcium nitrate ($Ca(NO_3)_2.4H_2O$, *Fluka Chemicals,* CAS:13477-34-4) solution was dropped into suspension of the silicate solution with a constant flow rate of 2.0 mL/min. pH was controlled at 12.0 ± 0.2 because of the limitation of Ca ISE electrode that we used to collect the data. At high pH (13.5), it is difficult to follow accurately the kinetics due to high complexation of $CaOH^+$ and low Ca^{2+}. The more dilute solution compared to the standard synthetic route [13] were used to allow the heterogeneous surface to compete with homogeneous nucleation and give kinetics data that could then be used in a population balance model [14]. The total reaction time is 3 hours with a mixing speed of 1,100 rpm. The temperature was controlled at $22.5\pm0.5°C$. Conductivity, pH and calcium selective electrodes were used in-situ to monitor the changes in the reactor.

Characterization methods

X-Ray Diffraction (XRD) - Data of synthetic C-S-H were collected using $CuK\alpha$ XRD (PANanalytical) analyses of wavelength λ=1,54 Å with a fixed divergence slit. The size of the slit is ½. Samples were placed in the sample holder and the patterns were collected between 5 and 70 degree 2θ. Scan step size is 0.0167113 degrees 2θ. The XRD pattern was recorded by X'PERT Data Collector software.

Transmission electron microscopy (TEM) The morphology of the synthetic C-S-H was investigated by using TEM, Thermo Scientific™ Talos F200X scanning transmission electron microscope (STEM) with TEM mode. It was operated at an acceleration voltage of 200 kV. TEM images were collected and then exported by using TEM Imaging and Analysis (TIA) software. The samples were prepared by dispersing the precipitated C-S-H in isopropanol and treated in an ultrasonic bath for 15 minutes. The dispersed samples were dropped on to the charged grid (carbon films on 300 mesh grids copper, *Agar Scientific Ltd.*) and allowed to dry for few minutes.

Scanning transmission electron microscope-energy dispersive x-ray (STEM-EDX) - High-angle annular dark-field (HAADF) STEM measurement combined with EDX were used to investigate the elemental distribution. The elemental map of the samples was operated by Talos F200X scanning transmission electron microscope (STEM) with STEM-EDX mode. It was operated at an acceleration voltage of 200 kV. After STEM alignment, the elemental map was performed by using *Bruker Esprit 1.9* software. The samples were prepared with the same procedure as for TEM.

6.3   Results and discussion

6.3.1 Observation of quartz and calcite in solutions of calcium and silicate, respectively

Quartz in calcium solution –TEM images of quartz before (Fig.6.1) and after (Fig.6.2) contact with the calcium solution. Quartz particles before reaction show irregular shapes with smooth surfaces (Fig.6.1 (a) and (b)). After reaction with calcium nitrate solution, Figure 6.2 (a) shows a large particle of quartz with has smooth surface and various small particles of precipitation products. Figure 6.2 (b) shows the small square particles surrounded by nanofoils – the typical morphology of synthetic C-S-H under these solution conditions.

(a)   (b)
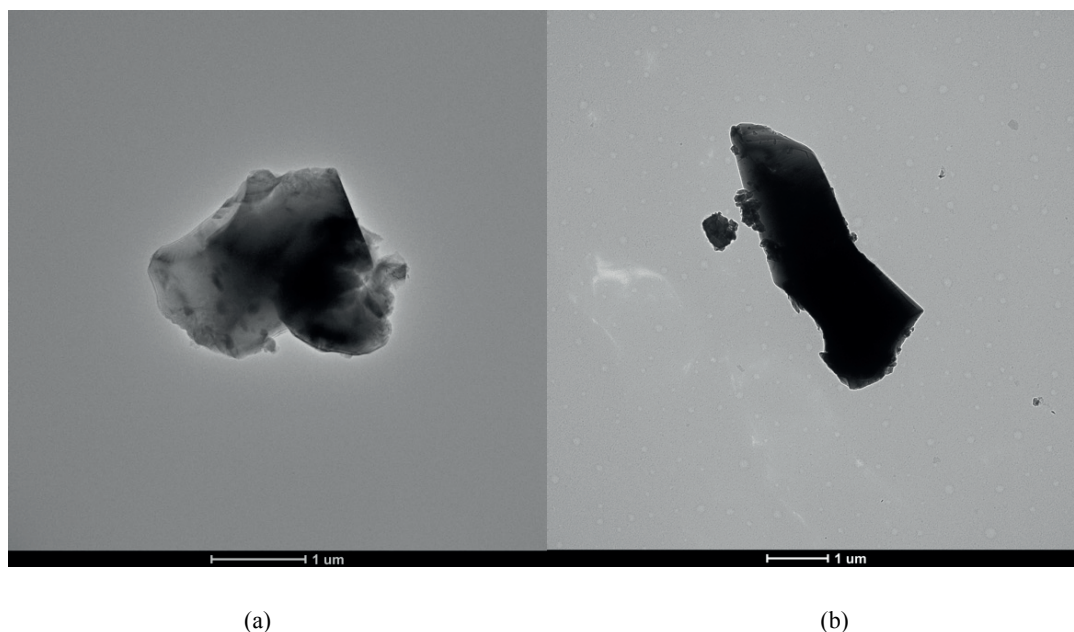
Figure 6.1 TEM images of pure quartz as supplied before reaction.

(a) (b)
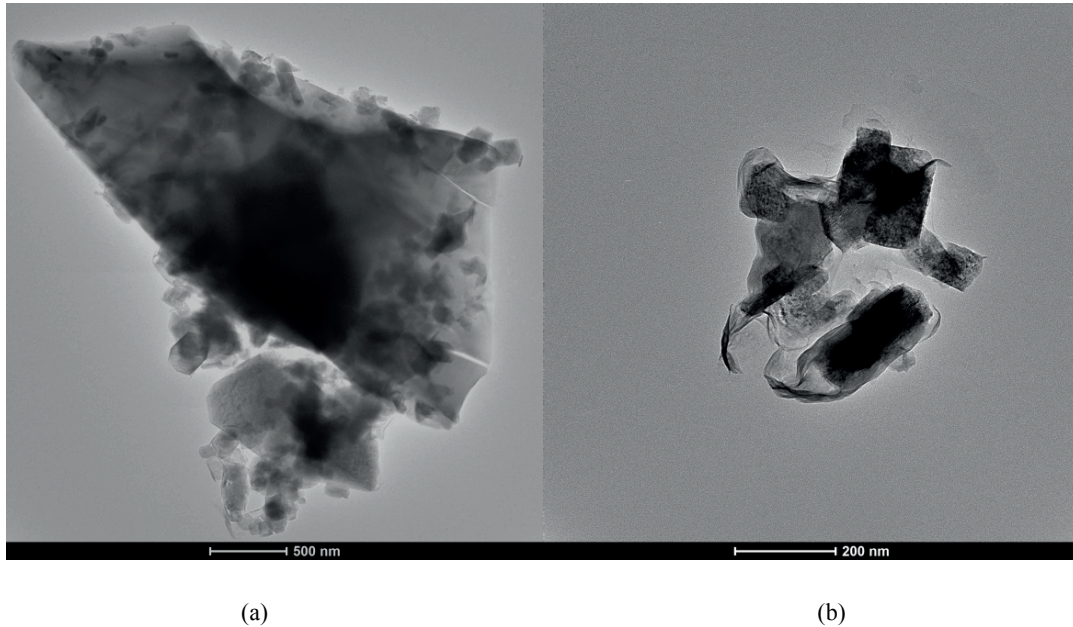
Figure 6.2 TEM images of quartz after 24 hrs in a calcium nitrate solution at pH 13.5.

STEM-EDX was used to determine elemental map of the particles as shown in Figure 6.3 and 6.4. Figure 6.3 shows HAADF image and elemental map of big and small particles. The large particle showed strong and uniform signal of Si and O on the elemental maps relating to chemical composition of quartz. In contrast, the small particles showed signal of Ca and O probably corresponding to $Ca(OH)_2$. As mentioned previously the nanofoils in Figure 6.2, Figure 6.4 shows elemental distribution of the small particles including nanofoils. The square shapes of small particles showed strong signal of Ca and O which could be $CaOH_2$. The nanofoils which is close to Ca-rich particle surfaces has the distribution of Ca, Si and O which corresponds to C-S-H composition.
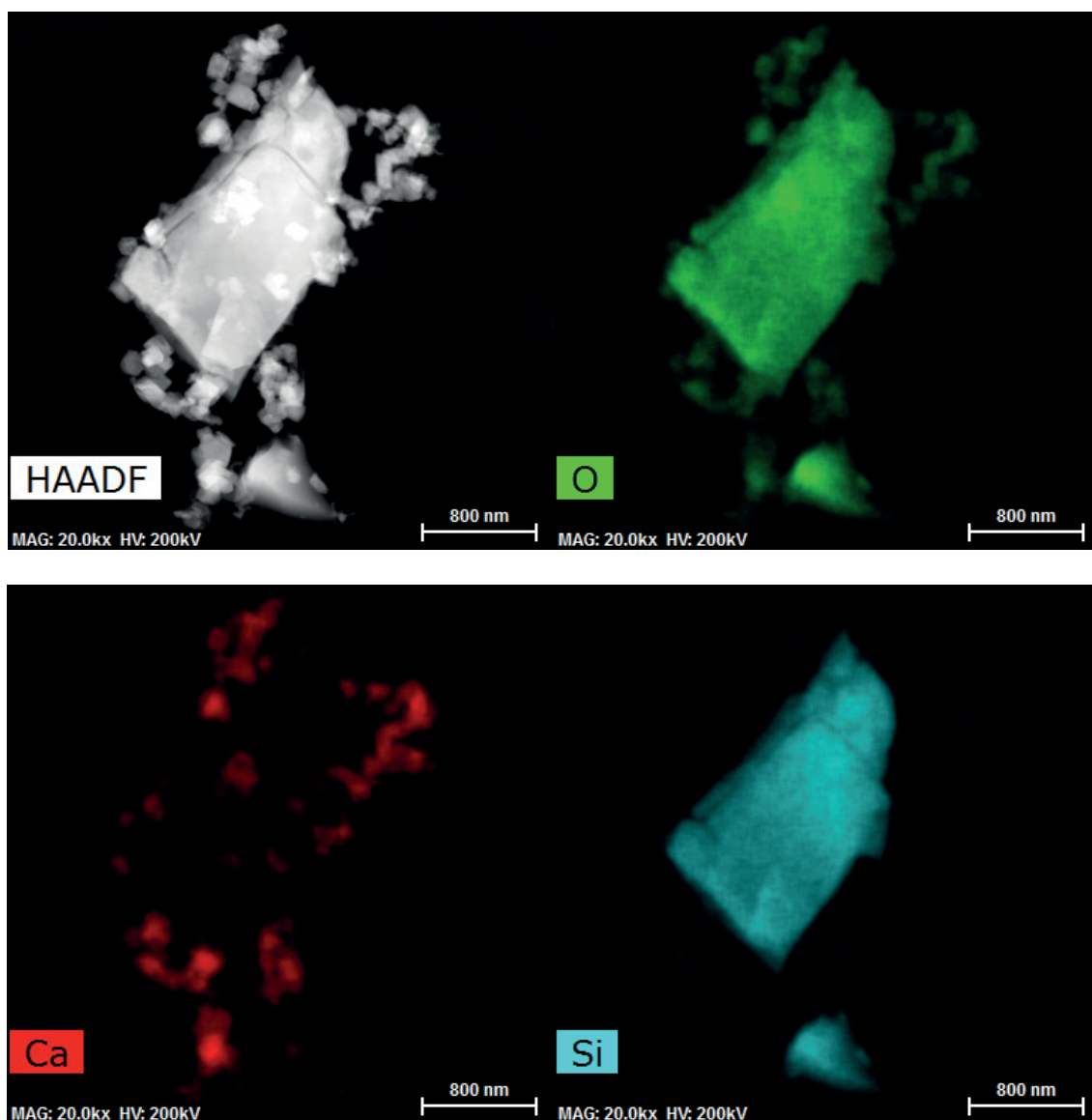
Figure 6.3 Elemental maps of Ca, Si and O of quartz in calcium solution at pH 13.5 (1).
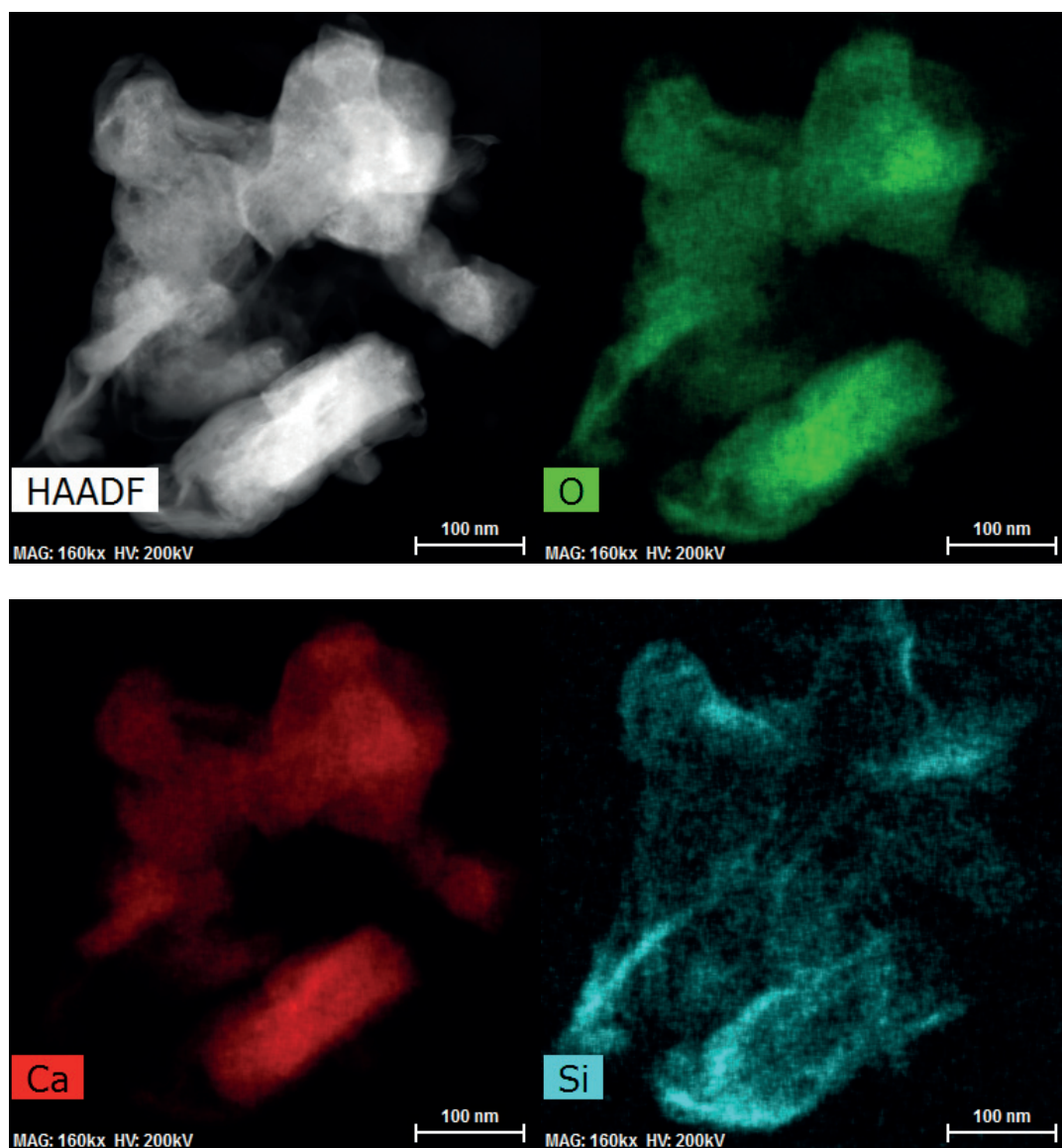
Figure 6.4 Elemental maps of Ca, Si and O of quartz in calcium solution at pH 13.5 (2).

Calcite in silicate solution – calcite particles before addition to the silicate solution is shown in Figure 6.5 (a) and (b). The particles have irregular shapes with generally smooth surfaces. TEM images at different time of calcite contact after mixing in the silicate solution are shown in Figure 6.6. The surface roughness of calcite is a function of time (3 and 8 hours) with the longer reaction times showing higher degrees of surface roughness. This is probably due to dissolution of calcite in the silicate solution. At 16 hours, nanofoil growth (~80 nm) on the calcite surface is observed and the growth of these C-S-H like foils is increased at 24 hours (~250 nm). The elemental map of the samples at 24 hours was investigated by STEM-EDX. Figure 6.6 shows the homogeneous distribution of Ca, Si and O of these nanofoils which covers the particle indicating they correspond to C-S-H. The particle in the middle has strong signal of Ca and O which relates to the underlying calcite particle.

(a)   (b)
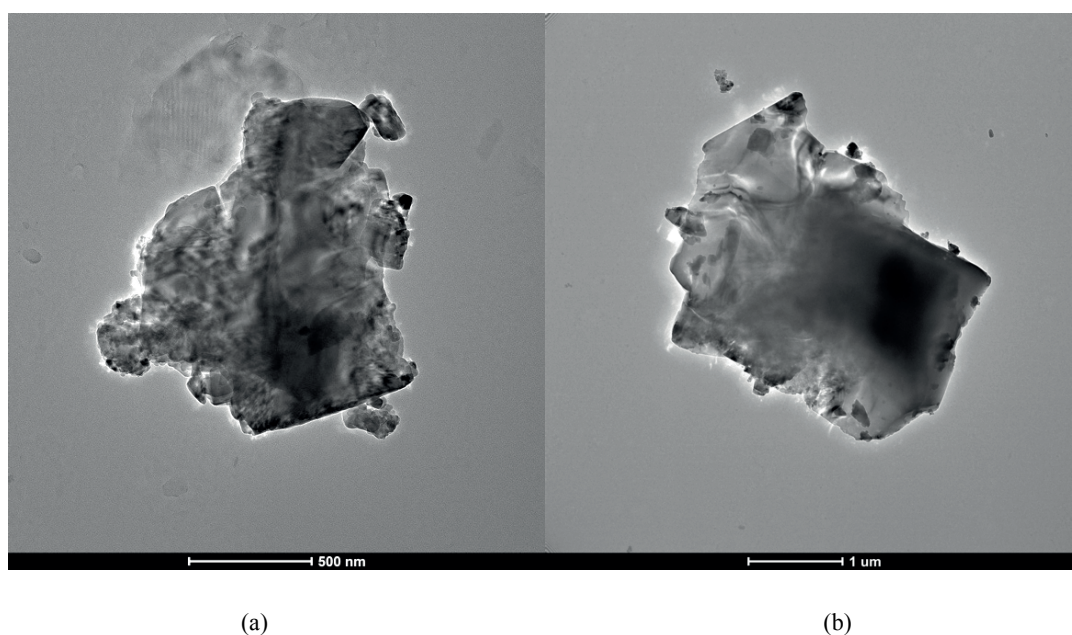
Figure 6.5 TEM images of pure calcite as supplied before immersion into a silicate solution.
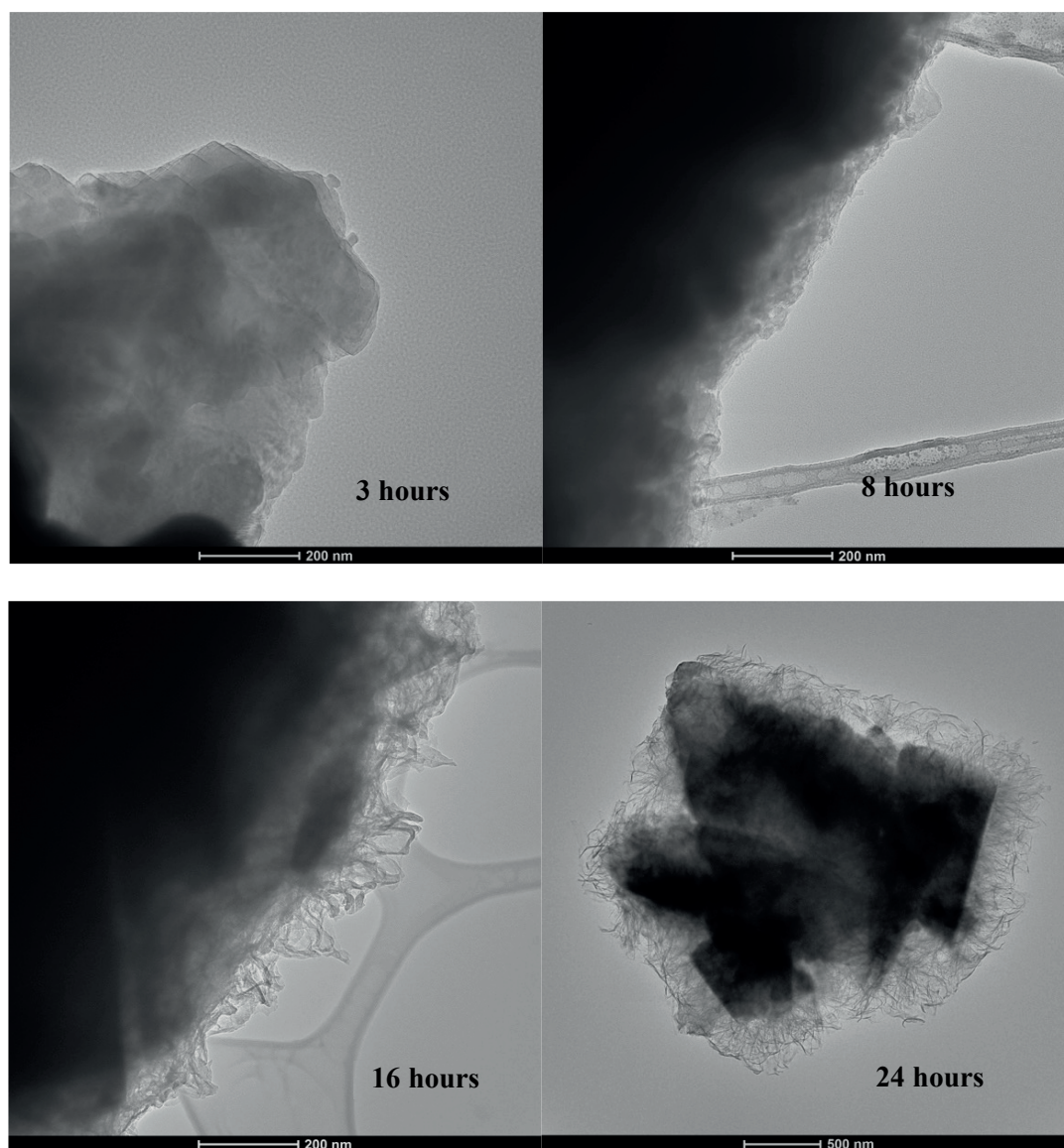
Figure 6.6 TEM images of calcite in silicate solution at pH 13.5 as a function of time.
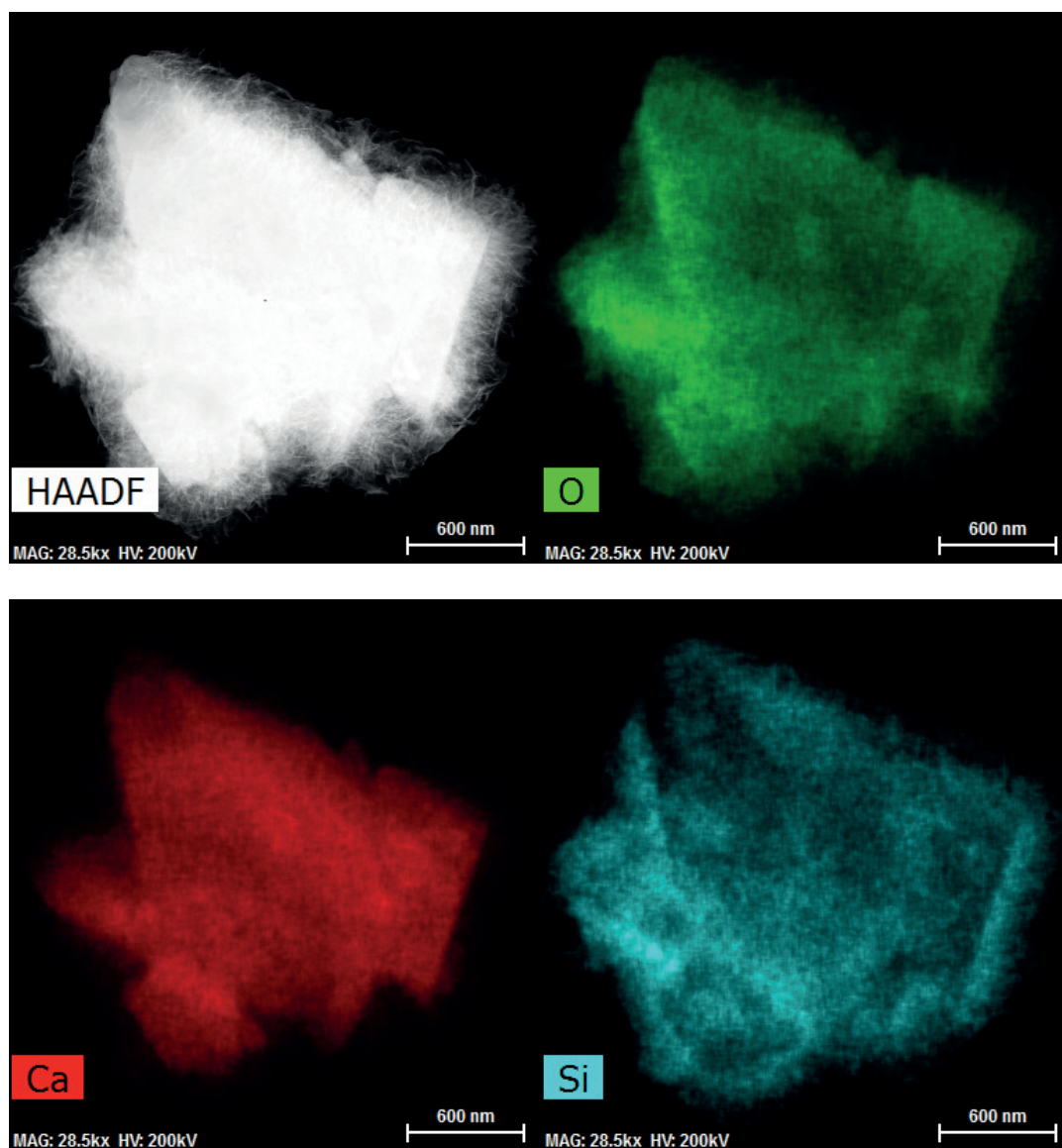
Figure 6.7 Elemental maps of Ca, Si and O of calcite in silicate solution at pH 13.5, 24 hrs.

Thermodynanic modelling, GEMS

GEMS is a thermodynamic modelling software which calculates chemical speciation and possible solid phases at the equilibrium stage for a given chemical composition. From our experimental conditions, GEMS computed the ionic speciation at equilibrium stage (Fig.6.8 and 6.9) and the possible solid phases which are shown in Table 6.2. Figure 6.8 shows ionic speciation at the equilibrium stage of quartz in calcium solution at pH 13.5. The most abundant of the ionic species in the system is SiO_3^{2-} and $HSiO_3^{-}$. Whereas for the ionic speciation of calcite in silicate solution at equilibrium stage is shown in Figure 6.9, the most abundant species are $Na(CO_3)^{-}$, CO_3^{2-}, SiO_3^{2-} and $HSiO_3^{-}$.

For the solid phases, C-S-H is the major phase for both of quartz and calcite in calcium and silicate solutions, respectively. For the calcite in the silicate solution, calcite as a final product in the system is also expected, i.e. under these experimental conditions we would not expect the full dissolution of calcite if the reactions were allowed to reach equilibrium. Compared with the experimental results, quartz in the calcium solution shows a small amount of C-S-H with a lot of residual quartz and a secondary phase rich in calcium.
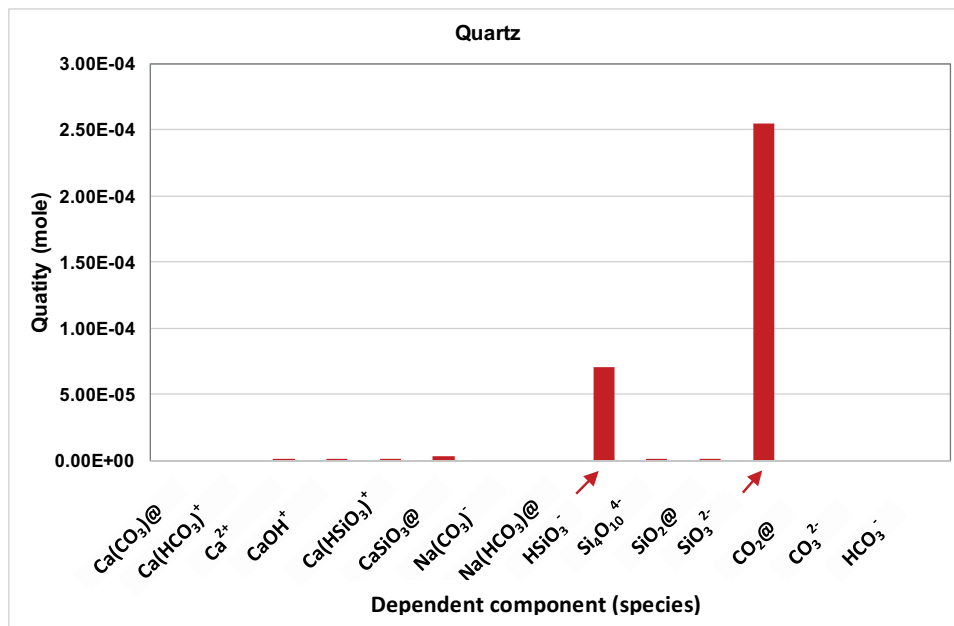
Figure 6.8 Dependent component (species) of quartz in calcium solution, pH 13.5.
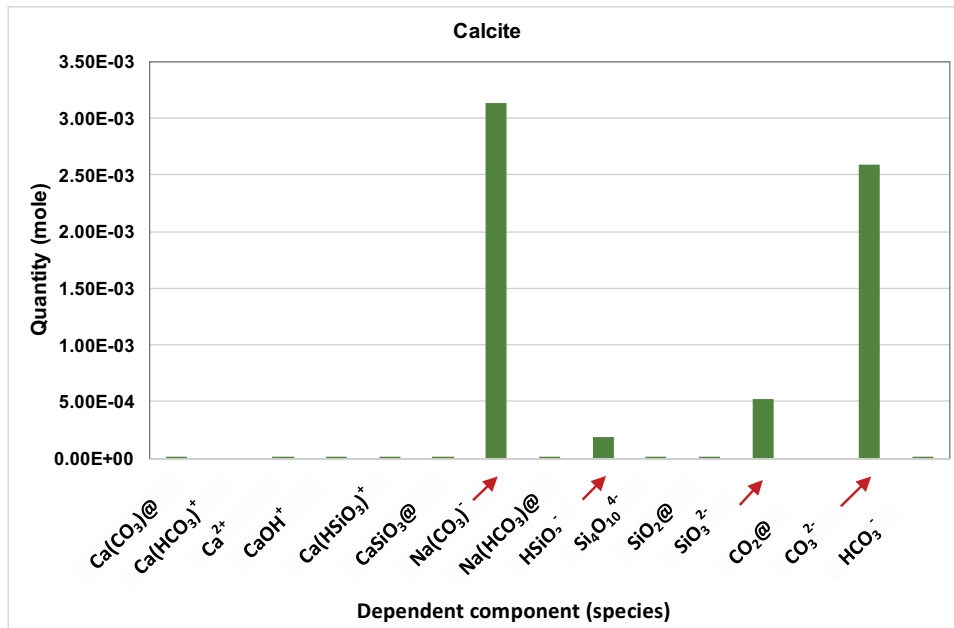
Figure 6.9 Dependent component (species) of calcite in silicate solution, pH 13.5.

Sample	Quartz (mol)	Calcite (mol)	C-S-H (mol)
Quartz in calcium solution	-	-	33.58 x 10^{-5}
Calcite in silicate solution	-	4.25 x 10^{-5}	18.92 x 10^{-5}

Table 6.2 Possible phases of quartz and calcite in solutions predicted by GEMS.

Discussion of quartz and calcite in solutions

Quartz in calcium solution – At high pH, quartz has strongly negative charge ($\sim$ -50 mV) due to dissociation of silanol group [101,104,111]. Calcium ion can balance this negative charge and then possibly formed the precipitated synthetic C–S–H on quartz surface. In our experiment, quartz particles were added in calcium solution at pH 13.5 for 24 hours. In this case, quartz, which has a very low dissolution rate [51,112,113], was the only silicate source in the system to form precipitated synthetic C-S-H. Moreover, GEMS calculated the ionic speciation at equilibrium stage in this condition which showed abundant species of SiO_3^{2-} and $HSiO_3^-$ (Fig.6.8) and the possible solid phase was only C-S-H phase as shown in Table 6.2. However, small quantity of precipitated C-S-H which was observed by TEM and STEM-EDX as shown in Figure 6.2 (b) and 6.4, respectively. This could be the reaction time in our condition was far from equilibrium stage. Figure 6.2 (a), after 24 hours,

shows quartz with smooth surface and small square particles with nanofoils. Uniform distribution of Ca, Si and O was shown in nanofoils which related to precipitated C-S-H composition as shown in Figure 6.4. The square particles could be precipitated $Ca(OH)_2$ as the system is not exposed to air.

Calcite in silicate solution – Calcite is a mineral which is more reactive and less negatively charged ($\sim$ -20 mV) at high pH than quartz [104]. When adding calcite in silicate solution at pH 13.5 for 24 hours, the precipitated C-S-H that nucleates and grow at calcite surfaces were monitored by TEM and STEM-EDX (Fig.6.6 and 6.7). In this experiment, calcite was the only calcium source in the reaction. As a proposed reaction mechanism, firstly, calcite was dissolved as shown by the rough surface at 3 and 8 hours (Fig.6.6). This dissolution of calcite giving Ca^{2+} and CO_3^{2-} [51,104,111,114–116] in the silicate solution. Once the released calcium ions reached supersaturation, the precipitated C-S-H formed on the calcite surface. Nanofoils of precipitated C-S-H was shown at 16 and 24 hours (Fig.6.6). The elemental map of the sample at 24 hours (Fig.6.7) showed uniformly distribution of Ca, Si and O of nanofoils at the calcite surface corresponding to C-S-H composition. The amount of residual calcite compared to the amount of C-S-H also suggests that 24 hrs is not sufficient to reach the equilibrium proportions of the solid phases (Table 6.2)

6.3.2 Kinetics data of precipitated synthetic C-S-H with the presence of quartz and calcite

Characterization of synthetic of C-S-H in the presence of quartz and calcite from kinetics experiment

Figure 6.10 shows XRD pattern of synthetic C-S-H. With presence of heterogeneous particles, XRD pattern of quartz and 1% quartz in synthetic C-S-H is shown in Figure 6.11 and XRD pattern of calcite and 1% calcite in synthetic C-S-H is shown in Figure 6.12. Although, C-S-H is a poorly crystalline material the XRD pattern of the pure synthetic C-S-H (Fig.6.10) shows characteristic peaks around 16-25°, 29.2°, 33°, 50°, 55° and 67° (2θ) (no secondary phases observed).
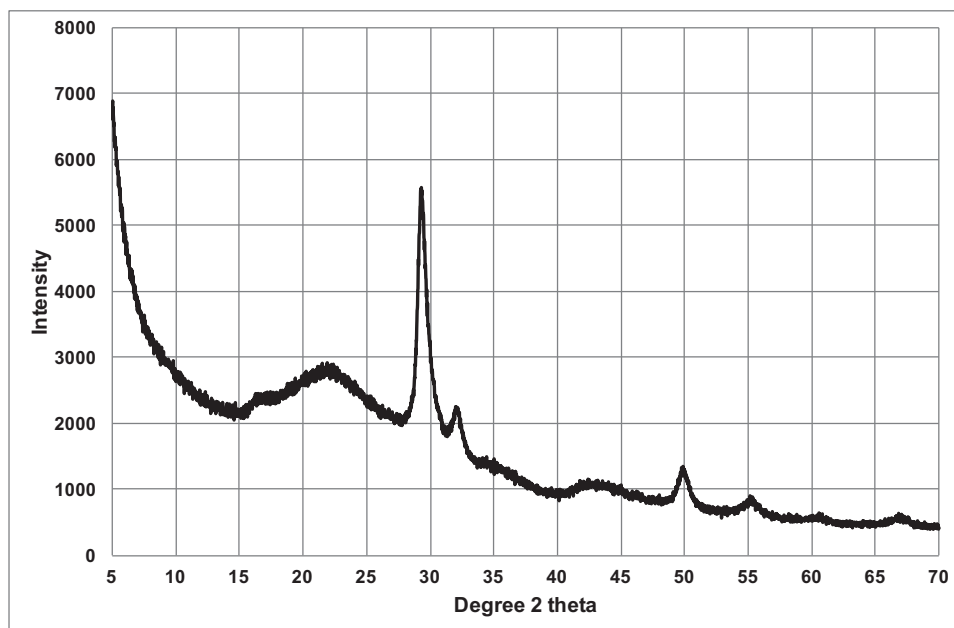
Figure 6.10 XRD pattern of synthetic C-S-H, pH 12.0 $\pm$ 0.2.

Figure 6.11 shows XRD patterns of pure quartz and 1% quartz in synthetic C-S-H which shows same signal at 21.8°, 26.6°, 36.5°, 39.5°, 40.3°, 42.4°, 45.8°, 50.1°, 54.9°, 55.3°, 59.9°, 64.0°, 67.7°, 68.1° and 68.2° [117]. The XRD patterns of pure calcite and 1% calcite in synthetic C-S-H which shows same signal at 23.1°, 29.4°, 31.5°, 36.0°, 39.5°, 43.2°, 47.2°, 47.6°, 48.6°, 56.7°, 57.5°, 60.8°, 61.1°, 61.5°, 63.2°, 64.8°, 65.7° and 69.3° as shown in Figure 6.12 [118]. However, the signal of synthetic C-S-H is difficult to observe and validate because of the low signal of C-S-H with the heterogeneous particles (quartz and calcite).
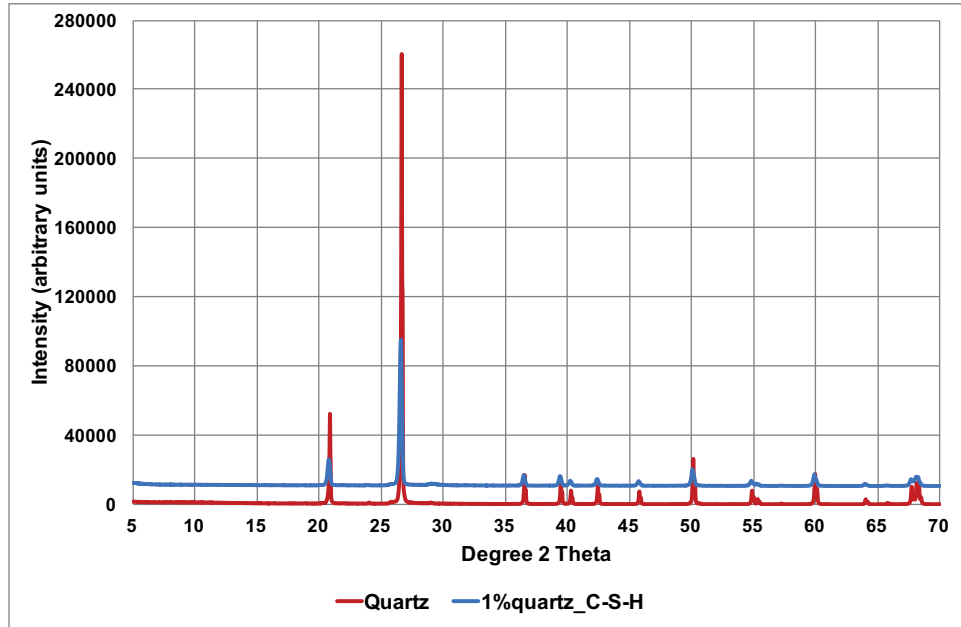
Figure 6.11 XRD pattern of quartz and synthetic C-S-H with presence of 1% quartz, pH 12.0±0.2.
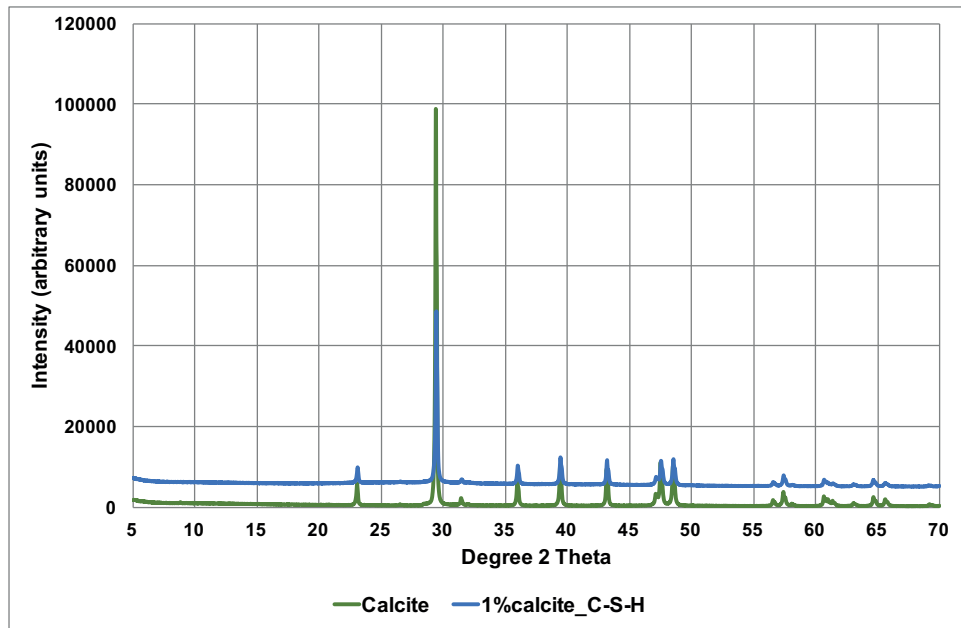
Figure 6.12 XRD pattern of calcite and synthetic C-S-H with presence of 1% calcite, pH 12.0±0.2.

Morphology analysis

Morphology of pure synthetic C-S-H precipitated at pH 12.0±0.2 is shown in Figure 6.13. TEM images of the synthetic C-S-H show the expected nanofoil morphology. The morphology of heterogeneous particles in synthetic C-S-H is shown in Figure 6.14. Figure 6.14 (a) and (b) shows typical nanofoil morphology of synthetic C-S-H covering the quartz particles. While synthetic C-S-H with presence of 1% calcite shows the rough surfaces of the calcite particles sometimes without synthetic C-S-H (Fig.6.15 (b)) and sometimes with nanofoils of synthetic C-S-H covering the particles (Fig.6.15 (a)). The rough particle surfaces could be due to either the dissolution of calcite particles or precipitation of calcite from calcium and carbonate in the reaction. Additionally, the elemental distribution of Ca, Si and O has been investigated by STEM-EDX as shown in Figure 6.16. The rough surface shows high signal of Ca and O and low signal of Si on the elemental mapping. It could be C-S-H nuclei on the calcite surface.
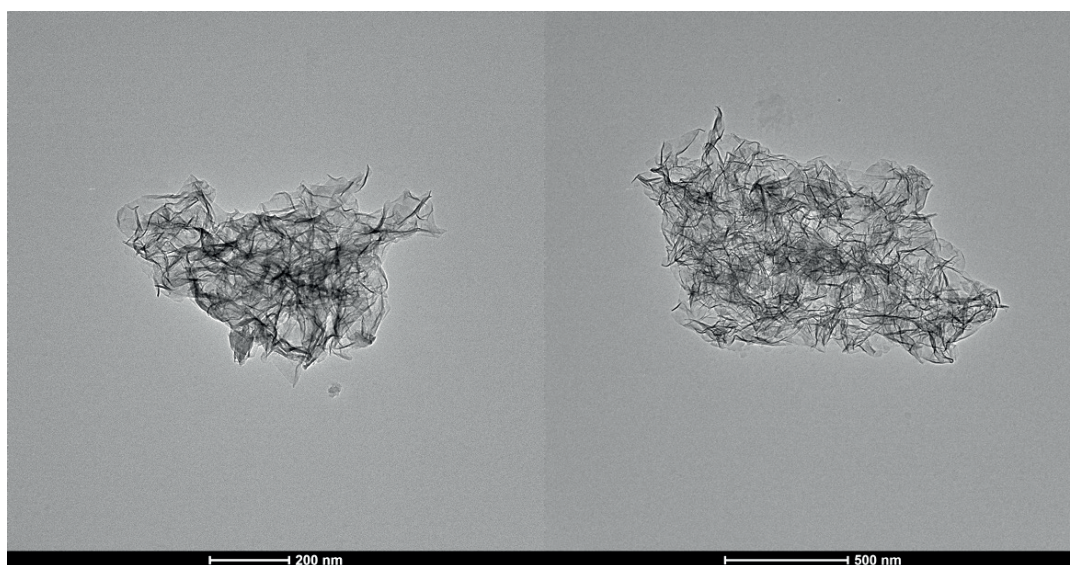
Figure 6.13 TEM images of synthetic C-S-H, pH 12.0±0.2.

(a)	(b)
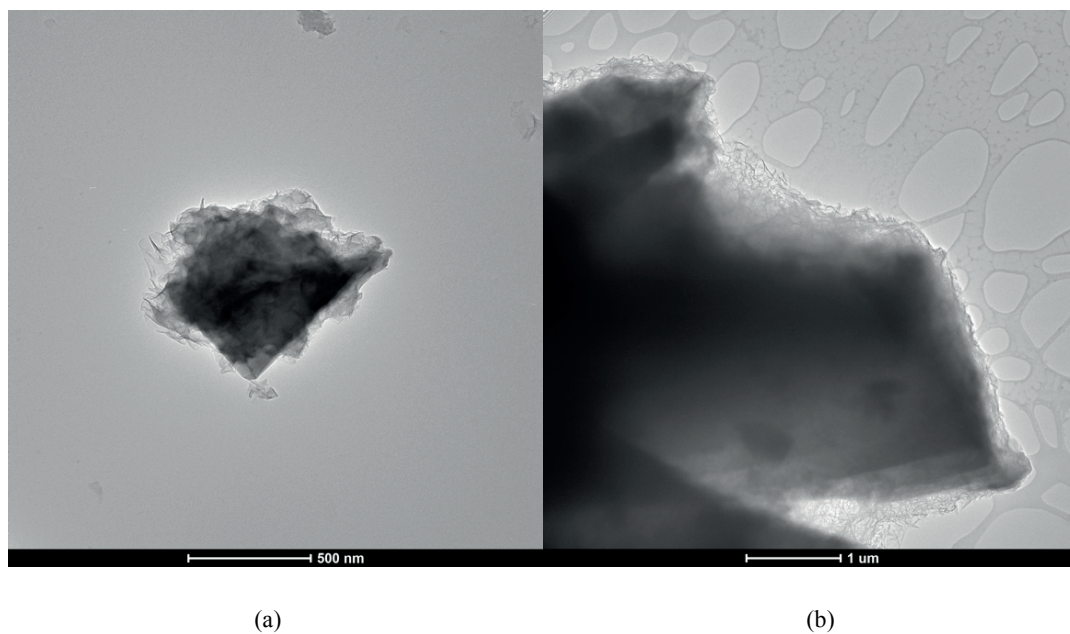
Figure 6.14 TEM images of synthetic C-S-H with presence of 1% quartz, pH 12.0±0.2.

(a)	(b)
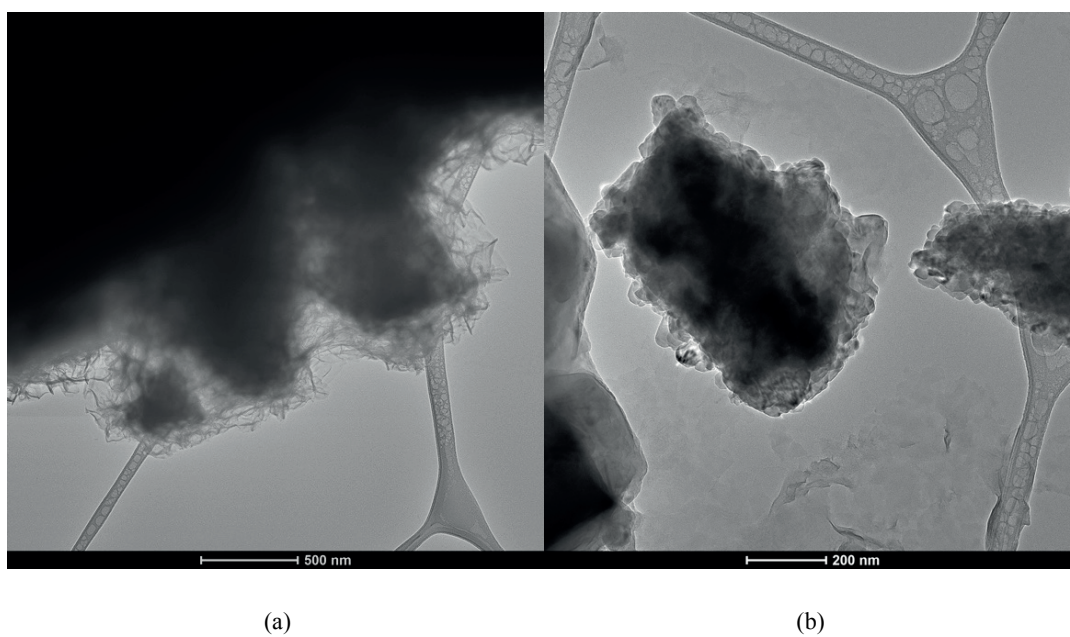
Figure 6.15 TEM images of synthetic C-S-H with presence of 1% calcite, pH 12.0±0.2.
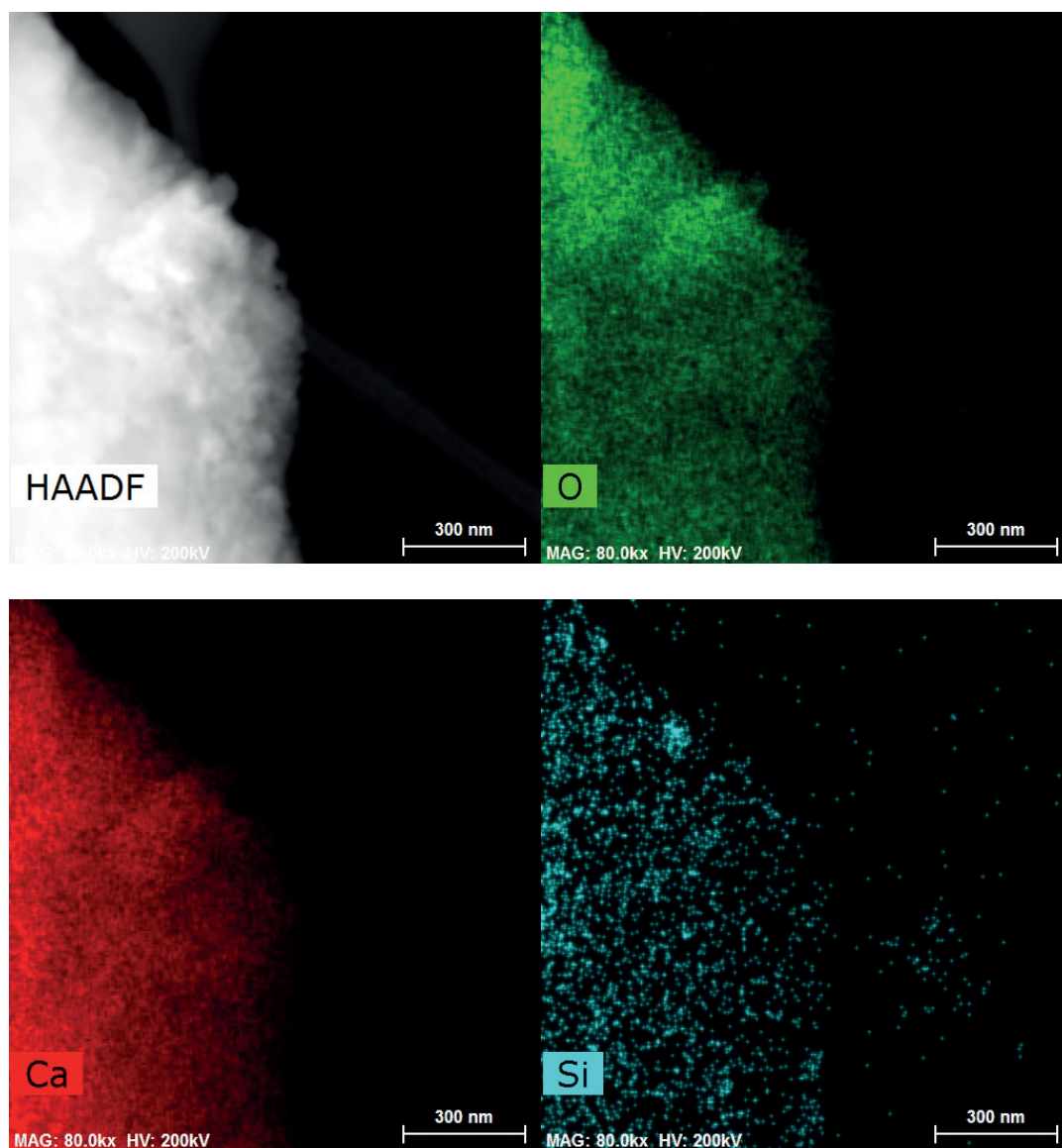
Figure 6.16 Elemental maps of Ca, Si and O of rough surface of calcite in synthetic C-S-H, pH 12.0±0.2.

Kinetics data

Effect of quartz and calcite on the kinetics of synthetic C-S-H precipitation was investigated by using the dropwise precipitation method and the Ca^{2+} activity as a function of calcium concentration is shown in Figure 6.17 and 6.18. The dotted line in Figure 6.17 and 6.18 is the amount of added calcium (calculated from the flow rate of the calcium solution, the total time to add all the calcium was 150 minutes). All samples show a lower amount of free calcium ions than the amount of added calcium because calcium was consumed in reactions (Fig.6.18). Figure 6.17 shows the evolution of Ca^{2+} activity as a function of calcium concentration at the early stages of precipitation. With the presence of 1% calcite the quantity of Ca^{2+} at the beginning was around 2.5 µmol/L (added calcium 0 µmol/L) compared to pure synthetic C-S-H and with presence of 1% quartz. This because calcite partially dissolved giving the dissociated Ca^{2+} and CO_3^{2-} ions in the solution before precipitation. Whereas 1% quartz showed no Ca^{2+} until added calcium reached 170 µmol/L. It could be due to the adsorption of calcium in order to compensate the negative charge at the quartz surface.

All samples show the slopes increased until it reached a critical point at around 800 µmol/L of added calcium, where a change in slope was observed. At this point, turbidity in reactor was observed for pure C-S-H which relates to a nucleation event. However, it was difficult to observe the change of turbidity with presence of 1% quartz and 1% calcite because of the presence of these particles in the reactor. With the presence of 1% quartz, the free calcium concentration (after added calcium 250 µmol/L) was higher than the pure C-S-H and with presence of 1% calcite. It could be due to a slower reaction rate of synthetic C-S-H with presence of 1% quartz and the calcium ions were consumed to a lesser degree than the pure C-S-H and with presence of 1% calcite. It could be due to the lower energy barrier of C-S-H nucleation on calcite surface than quartz [48,106]. The details behind these phenomena remain unclear and needs a fuller kinetics analysis using the population balance equation approach to understand the mechanistic details [21].

At the critical point (800 µmol/L) of added calcium, the amount of free calcium concentration with presence of 1% calcite (78.5 µmol/L) was a bit lower amount than pure synthetic C-S-H (99.0 µmol/L). After the nucleation event, the calcium consumption rate is close to the calcium addition rate as shown by the near horizontal portion of the Ca^{2+} data. At 5,000.0 µmol/L of added calcium (or 28 min of reaction time), the free calcium concentration of synthetic C-S-H with presence of 1% calcite was lower than pure synthetic C-S-H. This implies that the growth rate of C-S-H on heterogeneous particles (1%wt calcite) was faster than homogeneous synthetic C-S-H. This may be related to a higher surface for secondary nucleation which was seen to be the dominating mechanism in

pure C-S-H kinetics analysis by the population balance equation method [21]. Further detailed analysis using the population balance approach will allow us to confirm these qualitative hypotheses.
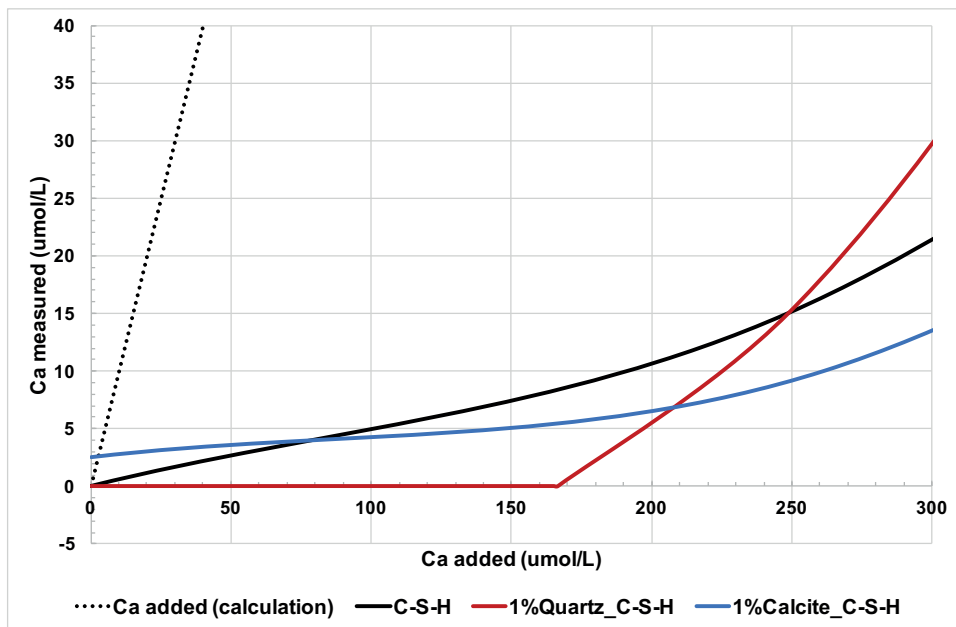
Figure 6.17 Kinetics data of at early stage of the precipitation of synthetic C-S-H with presence of quartz and calcite at pH 12.0±0.2 and the pure system.
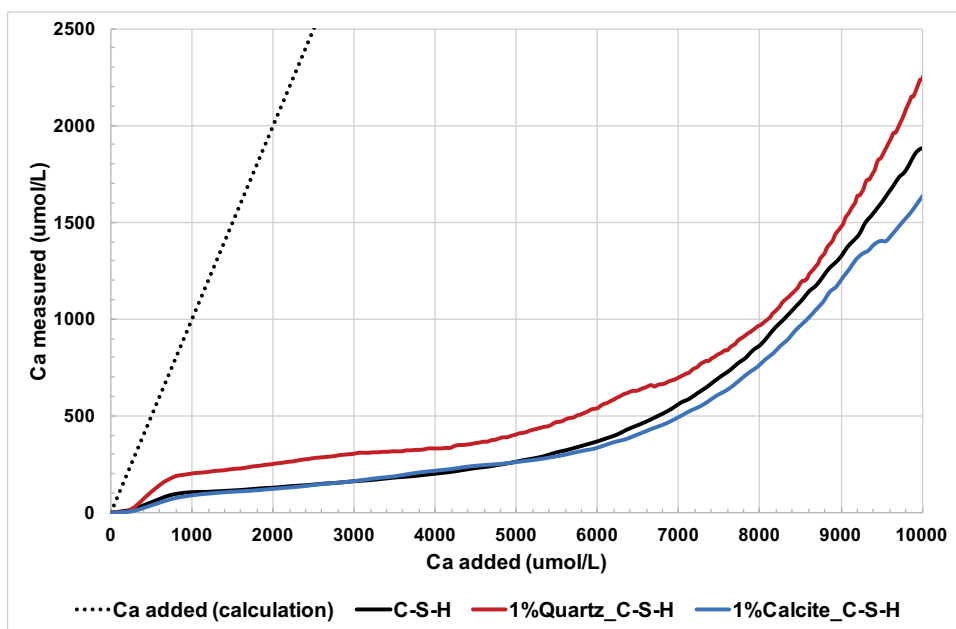
Figure 6.18 Kinetics data of synthetic precipitation C-S-H with presence of quartz and calcite at pH 12.0±0.2 and the pure system.

6.4   Conclusions

Quartz and calcite can act as heterogeneous substrates for the precipitation of synthetic C-S-H. Adding quartz into a calcium solution at high pH, a small quantity of precipitated C-S-H was observed close to calcium rich particles. From thermodynamic modelling only C-S-H as a solid phase is expected at equilibrium. This relates to the slow dissolution rate of quartz and the 24 hrs studied here is not sufficient for the system to reach equilibrium. Whereas calcite is more reactive than quartz and precipitated C-S-H was observed to nucleate and growth directly on the calcite surfaces without adding extra calcium to the reaction. Thermodynamic modelling showed that C-S-H and calcite can co-exist as solid phases under the experimental conditions studied.

Kinetics data of synthetic C-S-H precipitation with presence of quartz and calcite have been investigated. In these experiments, the heterogeneous particles such as quartz and calcite were introduced in the synthetic C-S-H system at pH 12.0 ± 0.2. Free calcium ions were measured as a function of calcium added in the system. With presence of 1% quartz, the free calcium concentration was higher than pure synthetic C-S-H and synthetic C-S-H with presence of 1% calcite. This could be due to the slow reaction of quartz particles and preferential of C-S-H nucleation on calcite surfaces. However, nanofoils of precipitated C-S-H on quartz particles were observed. The XRD pattern did not give a clear indication of synthetic C-S-H because of strong signal of quartz, but a small broad feature at around 29° 2 theta was observed.

With presence of 1% calcite, although there were extra calcium ions from dissolution of calcite, the free calcium ions were consumed at a higher rate than the pure synthetic C-S-H and 1% quartz in synthetic C-S-H precipitation. This could imply that the growth rate of precipitated C-S-H with presence of 1% calcite are faster than pure synthetic C-S-H and with presence of 1% quartz. TEM images shows nanofoils of synthetic C-S-H covering calcite particles and the rough surface of calcite without nanofoils. The particle with rough surface was characterised by STEM-EDX. The elemental map shows strong signal of Ca and O which could be due to $CaCO_3$ and low signal of Si by adsorption of Si on particle surface. It is possible these particles with a rough surface to be either the dissolution of calcite that we added or a newly precipitated $CaCO_3$. However, the XRD pattern of synthetic C-S-H with presence of 1% calcite was not clearly seen because of strong signal of calcite.

We have seen that both quartz and calcite can act as heterogenous substrate for the growth of C-S-H – also there are changes in the kinetics of growth when compared to the pure C-S-H system. Further detailed analysis of the speciation and nucleation and growth events using recently developed population balance methods will allow us to assess the mechanistic details behind these observed and reproducible kinetics effects. These observations can then be used for quantitative assessment of nucleation and growth in real cementitious systems.

Chapter 7   Summary of the thesis

7.1   Final summary

The overall goal of this thesis was to provide fundamental insights into the effects of pore solution ions and cement or concrete admixtures on the nucleation and growth of calcium silicate hydrate (C-S-H) in a precipitated synthetic system. To reach the goal, the thesis was organized in three parts which investigated how these different parameters can affect nucleation and growth of synthetic C-S-H. The dropwise precipitation method [20] was used to prepare homogeneous precipitated synthetic C-S-H in the thesis.

In the first part (Chapter 4), the effect of iron (III) or Fe^{3+} on precipitated synthetic C-S-H was investigated. The iron is commonly found in pore solution of Portland cement because it is in the C_4AF phase of clinker. Not only the C_4AF phase, but also calcined clays, which are popular supplementary cementitious materials, also has significant iron content. So, partial replacement of clinker with calcined clay, the iron content in pore solution also increases [17,19,61]. In our work, the effect of Fe^{3+} on precipitated synthetic C-S-H by the dropwise method was reported. Overall among the two parameters treated – pH and concentration, we clearly see the strong effect of pH conditions over the concentration changes of Fe^{3+} ions in the precipitating C-S-H system. At high pH conditions, as is the case in real cement hydration, the formation of ferrihydride and hydrogarnet containing iron are seen depending on the precise experimental method. At low pH conditions (2.5), no hydrogarnet or ferrihydrite formations occurs. The concentration of Fe^{3+} ions influences the types of phases formed. Low pH conditions promote more integration of Fe into the C-S-H structure or as a nanosized amorphous phase rather than formation of separate crystalline phases. EPR and ^{29}Si NMR relaxation data strongly indicate that the Fe^{3+} substituted Si^{4+} in the C-S-H structure. However, atomistic simulation will help us to identify where Fe^{3+} is located in the C-S-H structure.

The Chapter 5 was organised into three parts that investigated the effect of D-gluconate on the nucleation and growth of precipitated synthetic C-S-H by using the dropwise precipitation method. The D-gluconate was studied because it is a small organic molecule which has functional groups

representing typical admixtures such as polycarboxylate superplasticizers (PCEs) [13,14,119] that are extensively used worldwide as a concrete admixture.

From our work in Section 5.1, the concentration of D-gluconate was varied between 3, 6 and 12 mM by premixing in a silicate solution. The variation in the concentration of D-gluconate added showed the expected nanofoil morphology but with an increase in square shaped aggregation formation. The precipitated C-S-H formed in its presence is similar to synthetic C-S-H without the presence of D-gluconate indicating that its major role is on the surface interactions during aggregation rather than the nucleation and growth of type of C-S-H formed at these chemical or pH conditions. The higher quantity of organized agglomerates with an increase in D-gluconate concentration also indicates the lowering in number of plausible new sites for C-S-H nucleation and hence promoting a possible retardation effect.

In Section 5.2, the effect of D-gluconate was determined in more detail with regard to the retardation effect in Portland cement, i.e via experiments on complexation with calcium, precipitation of C-S-H in different premixed solutions and the collection of in-situ data. From calorimetry analysis, indicative from the change in slope of the curve, D-gluconate has strong interaction with the alite/belite [14,46,86] that are calcium-rich phases. Hence not only it interacts with newly formed C-S-H surface but also on the dissolving solid, giving the calcium ions in the pore solution. The retardation effect is expected to be strong with more calcium content in the dissolving solid. Complexation between D-gluconate and calcium under our experimental conditions was determined at different concentrations of D-gluconate. Increasing D-gluconate concentration gave more complexation with calcium at pH 11.0 ± 0.1. Our results fitted the data of Kutus et al. [120] best which will be used for future thermodynamic modelling (in collaboration with Prof. Barbara Lothenbach from EMPA, Dubendorf). The aggregation pattern in the dropwise precipitation method was clearly observed with premixed D-gluconate in the silicate solution (SiGN) which was shown to have a bipyramidal cage-like structure in 3-dimensional TEM tomography. It could be due to complexation [45,120] and adsorption of D-gluconate during reaction prior to precipitation which modifies its interaction on nucleation and growth of precipitated C-S-H. Compared to the concentration using in dropwise precipitation method, dilution (10 times) of calcium and silicate solutions was used in the kinetics experiments with the same D-gluconate concentration (12 mM). The premixed of D-gluconate (either in calcium or silicate) of initial solutions showed different kinetics. Premixing of D-gluconate in silicate solution presented the lowest amount of free calcium at the beginning due to the competition between D-gluconate and silicate to complex with calcium. After at ~2,300 µmol/L of added calcium, the amount of free calcium was higher than pure C-S-H. It could be the adsorp-

tion of D-gluconate onto the C-S-H surface modifies the rate of C-S-H formation. With the presence of D-gluconate in the calcium solution, it showed the highest of measured free calcium ion concentration because of complexation between D-gluconate and calcium prior to being dropped into the sodium silicate solution by slowing down the nucleation process. We observed that different pH (12.3 and 13.5) controlled different silicate speciation in the system affecting morphology of precipitated synthetic C-S-H. With presence of D-gluconate at pH 12.3 showed mixed morphology of nanoglobules and nanofibrils, whereas at pH 13.5 shows only nanofoils. However, the experimental condition with uniform morphology of synthetic C-S-H in the presence of D-gluconate have to be optimized in order to evaluate kinetics data.

In Section 5.3, the experimental conditions which gave us uniform single morphology of synthetic C-S-H with presence of D-gluconate were found. The kinetics data were collected at different pH (11.0 and 12.0). We observed the uniform morphology of synthetic C-S-H at pH 11.0 and 12.0 by decreasing D-gluconate concentration from 12.0 (section 5.2) to 1.2 mM (Section 5.3). This unique kinetics data can now be evaluated by using population balance modeling in order to describe primary, secondary nucleation and molecular growth of precipitated synthetic C-S-H formation with presence of D-gluconate. The work is currently underway in collaboration with Mr. Mohammad Reza Andalibi (PSI) who has developed the PBE approach for C-S-H.

In the third part (Chapter 6), quartz and calcite were used to investigate the effect of heterogeneous substrates on nucleation and growth of synthetic C-S-H. These have been commonly used to replace clinker content for concrete or mixed cement to reduce carbon footprint. Quartz is SiO_2 which has very low dissolution rate compared to calcite ($CaCO_3$). Calcite partially dissolved in a silicate solution providing Ca^{2+} and CO_3^{2-} which then formed C-S-H on its surface. From kinetics results, both quartz and calcite were able to act as heterogeneous substrates for the precipitated synthetic C-S-H. However, these particles changed the kinetics of C-S-H formation compared to pure synthetic C-S-H. The slower reaction of quartz meant that it showed less calcium consumption in the collected kinetics data compared to pure C-S-H and with presence of calcite. It could be due to the preferred nucleation of C-S-H on calcite surface. The kinetics analysis of heterogeneous substrates in synthetic C-S-H will allow us to describe in detail the effects of speciation, nucleation and growth of precipitated synthetic C-S-H by using population balance modeling. The knowledge from basic system will help us approach conditions in Portland cements in order to better understand the roles of heterogeneous particles as SCMs on cement hydration in early age strength and durability effecting the C-S-H formation.

7.2   Perspectives

The replacement of clinker by supplementary cementitious materials (SCMs) is a promising strategy to reduce the carbon footprint of cementitious materials. This, however, can modify the hydration and reaction kinetics including the setting and strength of cement and concrete. Chemical admixtures are also widely used to modify properties of cement and concrete and as the amount of SCMs in blended cements is increased then also the amounts and number of admixtures also increase. Minor elements such as Zn^{2+}, Ba^{2+}, Mg^{2+} are potential contaminants in raw materials which can also have an effect on cement hydration. Interestingly, the dropwise precipitation method will allow us to identify individual parameters effecting on nucleation and growth of precipitated synthetic C-S-H once the unique kinetics data collected in this thesis has been used in the population balance model developed for C-S-H within our group. Therefore, we can then design the experimental conditions e.g. different elements, concentrations, pH within the synthetic C-S-H system to allow us to modify C-S-H structures.

Calcium alumina silicate hydrate (C-A-S-H) is hydrated product in Portland cement based materials which increases significantly with highly replacement clinker by SCMs. [6,66,121]. The fundamental knowledge from synthesis C-S-H in the presence of Fe^{3+} will be able to apply in order to prepare homogeneous precipitated C-A-S-H phase by using dropwise precipitation method. Then, the individual parameters such as pore solution ions or admixtures will be investigated on nucleation and growth of C-A-S-H.

The introduction of heterogeneous particles has shown interesting effects and structures similar to those seen in cementitious systems. Diagram of C-S-H on heterogeneous particles is shown in Figure 7.1. These could be used to produce controlled microstructures with C-S-H of specific Ca/Si ratios and thus the influence of the Ca/Si ratio on other properties such as transport, uptake of alkalis and sorption of foreign ions can be studied. Also, chemical admixtures in the synthetic system have shown a modification of the agglomeration patterns of synthetic C-S-H. This suggests that if such admixtures adsorb onto C-S-H surfaces during the growth in cementitious system they could influence the interaction between the growing C-S-H and thus modify the microstructural strength. So, a combination of heterogeneous substrates (where we produce C-S-H on the surface with a similar geometry to cement) with admixtures such as D-gluconate may allow us to produce well characterized samples by pressing or casting our powders to compact densities similar to hydrated cement which can then be analyzed for their mechanical and transport properties. This will help us to better understand the role of both minor elements and organic admixtures in order to approach real Portland cement system.

From fundamental understanding of the C-S-H, it would be interesting to apply fundamental knowledge to other applications which is not limited in cement application. For example, it could be used in waste water treatment containing heavy metal ions because of the adsorption or integration of the heavy metal ions into C-S-H structure. Furthermore, the 3-dimensional of bi-pyramidal cage-like structure could be interesting to apply in drug-delivery agent by encapsulation a drug and re-lease at a specific target.
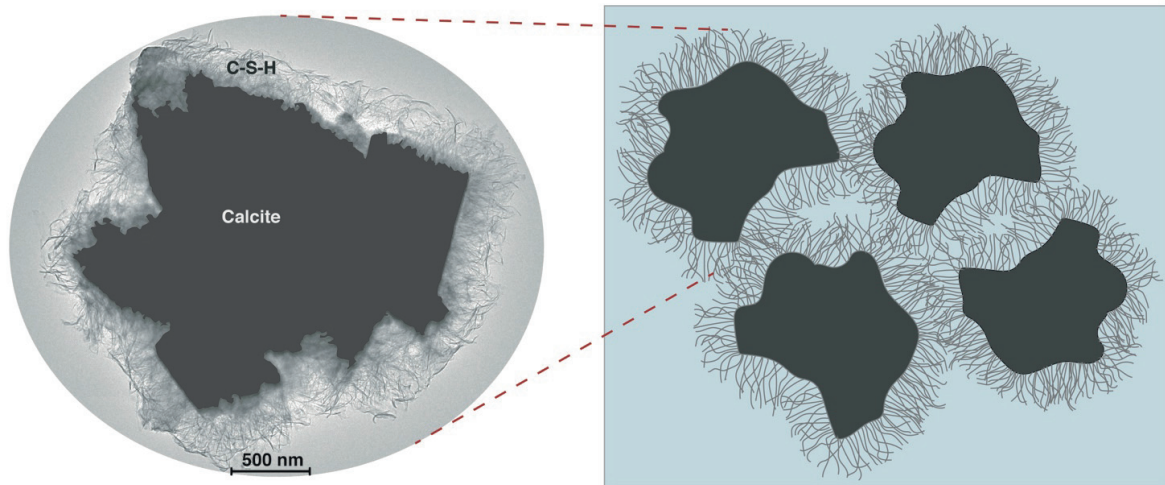
Figure 7.1 Diagram of C-S-H on heterogeneous particles.

Chapter 8   Appendix

8.1   Preliminary results of complexation between calcium and D-gluconate using thermodynamic model GEMS

This section presents the Appendix of Chapter 5, Section 5.2. The Appendix 8.1 shows preliminary results of complexation between calcium and D-gluconate by GEMS [25] (in collaboration with Prof. Barbara Lothenbach from EMPA, Dubendorf). Calcium nitrate solution was constantly added into D-gluconate solution which was varied at 20, 100 and 200 mM. Our experimental conditions fit to the data of Kutus et al. best [88]. The results are shown in Figure 8.1, 8.2 and 8.3.
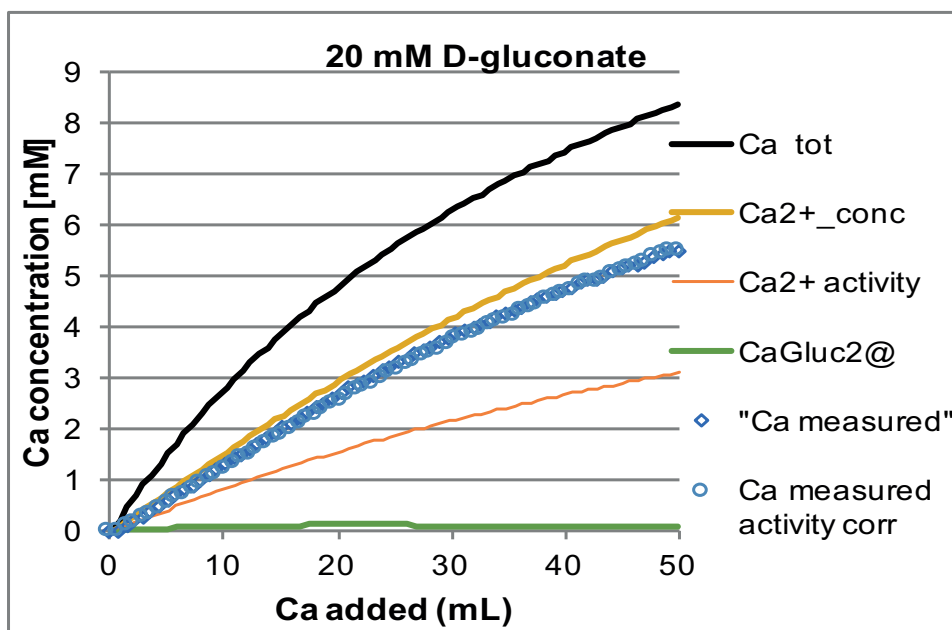
Figure 8.1 Comparison of the calcium concentration experimental (Ca measured) and GEMS calculation at 20 mM D-gluconate as a function of the volume of added calcium.
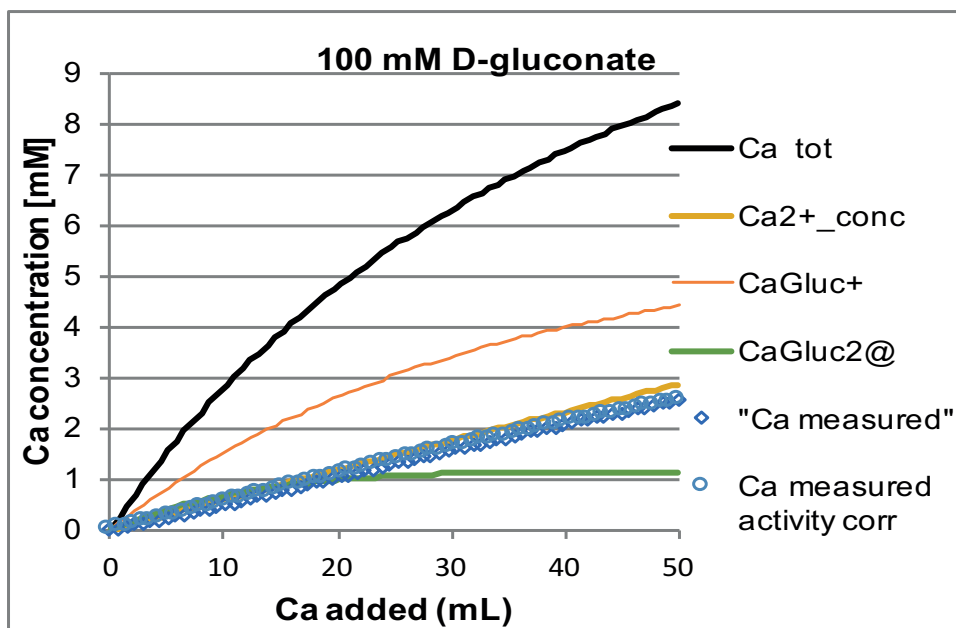
Figure 8.2 Comparison of the calcium concentration experimental (Ca measured) and GEMS calculation at 100 mM D-gluconate as a function of the volume of added calcium.
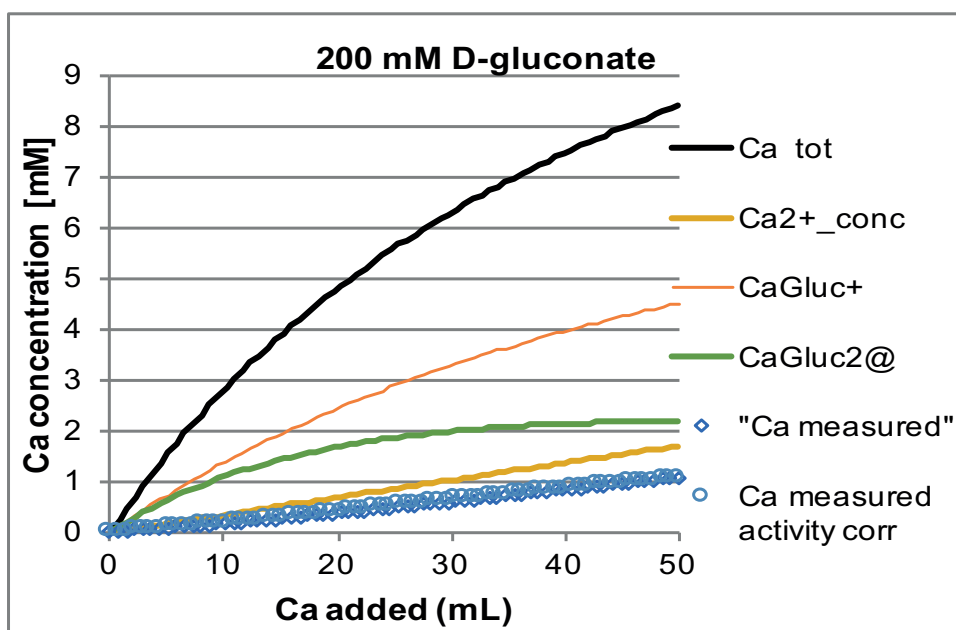
Figure 8.3 Comparison of the calcium concentration experimental (Ca measured) and GEMS calculation at 200 mM D-gluconate as a function of the volume of added calcium.

8.2 Initial observations: Effect of the presence of divalent ions (Zn^{2+}, Mg^{2+} and Ba^{2+}) on the morphology of precipitating calcium silicate hydrate

8.2.1 Introduction

Low concentrations of minor elements such as Na, Al, Mg, Fe, Zn and Cr can be in reactive cement phases which can have an impact on cement hydration and also can be incorporated into calcium silicate hydrate (C-S-H) [3,15,18,122–125]. Many researcheers have studied the effect of minor elements on C_3S dissolution and also their presenece in C-S-H structure [15,18,67,119,123–126]. Bazzoni et al. [15] observed the effect of Mg^{2+} and Zn^{2+} ions on the crystal structure and hydration of C_3S. The reactivity of C_3S is increased by the presence of Zn, while Mg gives a different polymorph with a similar reactivity. Stumm et al. [18] reported that zinc incorporates into C-S-H with Ca/Si = 2/3 and deteriorates the three-dimensionality of the C-S-H structure. Ziegler et al. [126] proposed the incorporation of Zn in the interlayer of C-S-H (I), Ca/Si = 1, with the diffusion of Zn into the C-S-H(I) particles. The results from XAFS analysis [67] showed the presence of ZnO_4 tetrahedra present in the interlayer of C-S-H (I). The adsorption of metal ions such as Sr (II), Ba (II) and U (VI) on C-S-H has been studied [119,125,127]. Tits et al. [127] reported the adsorption of Sr on synthetic C-S-H at different Ca/Si ratios and co-precipitation of Sr resulting in a different precipitation rate of C-S-H. The co-precipitation of Sr does not affect the adsorption of Sr on synthetic C-S-H. However, only a few studies of C-S-H morphology in the presence of minor elements have been published [15,125]. In this work, preliminary observation on morphology of synthetic C-S-H in the presence of doping ions will be investigated by using TEM and STEM-EDX.

Synthetic C-S-H with Ca/Si ratios from 1.0-2.0 has been produced using the route proposed by Kumar et al. [20] without the formation of any second phase. This dropwise precipitation method is an attractive method to prepare homogeneous synthetic C-S-H with Ca/Si 2.0 by controlling pH (~13.5). The typical morphology of synthetic C-S-H is nanofoils as shown in Figure 8.4. This method allows us to identify effects of individual parameters on precipitated synthetic C-S-H. The effect of divalent ions (Zn^{2+}, Mg^{2+} and Ba^{2+}) on precipitated C-S-H will be the focus in this hapter section. The dropwise method will be used to prepare synthetic C-S-H doping divalent ions (Zn^{2+}, Mg^{2+} and Ba^{2+}). The main hypothesis is to investigate what to see if they can compete and replace Ca^{2+} in the C-S-H growth mechanism in the presence of Ca^{2+} (as it would be in cement hydration) and thus modify kinetics and/or C-S-H morphology. This was carried out with two silicate concen-

trations first with an excess of silicate in solution (similar to the synthetic synthesis route of Kumar et al. [128] and secondly with a lower silicate concentration (approaching cement hydration conditions).
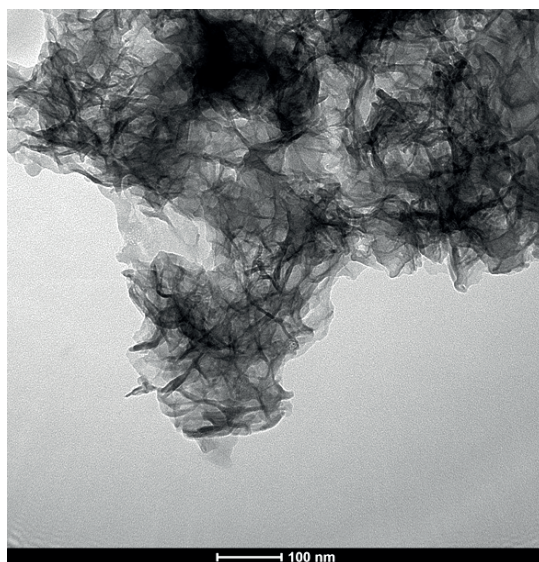
Figure 8.4 Typical morphology of synthetic C-S-H with Ca/Si 2.0.

8.2.2 Materials and Methods

Synthesis of C-S-H in the presence of divalent ions

The synthetic C-S-H in the presence divalent ions (Zn^{2+}, Mg^{2+} and Ba^{2+}) was prepared via the dropwise method. Before precipitation, the pH electrode (InLab®Expert Pro-ISM-IP67, *Mettler Toledo*) connected with benchtop pH meter (SevenExcellence pH Meter, *Mettlet Toledo*) was calibrated with standard solutions as shown in Chapter 3, Table 3.1. 100 mL of sodium silicate (Na_2SiO_3, S*igma-Aldric*h, CAS:6834-92-0) was present in the vessel (Part B, in Figure 8.5), with either high (100 mM) or low (175×10^{-3} mM) concentrations. 50 mL of calcium nitrate ($Ca(NO_3)_2.4H_2O$, *Fluka Chemicals,* CAS:13477-34-4) 0.2 M was mixed together with 0.2 M, 50 mL of the divalent ion (Zn^{2+}, Mg^{2+} and Ba^{2+}) solutions. The experimental conditions are shown in Table 8.1. The mixture of calcium and divalent ions (Zn^{2+}, Mg^{2+} and Ba^{2+}) was introduced into the vessel in a drop wise manner at a fixed rate (2.17 ml/min). The pH of the solutions was adjusted by using sodium hydroxide (NaOH, *Acros organic*, CAS:1310-73-2) in Part B. The total reaction time was 3 hrs. All solutions were prepared by using ultra-pure water previously boiled to remove the CO_2. After precipita-

tion, the samples were washed with ultra-pure water mixed with ethanol (50:50 vol%) and followed by pure ethanol to remove unwanted ionic species in the precipitate. Then, samples were collected by vacuum filtration with 0.2 μm, 50 mm diameter of membrane filter, mixed Cellulose Ester ME24/21 STL (Whatman^{TM}, GE health care). Then the sample was stored in polystyrene containers and then put in plastic zip lock bag before characterization.
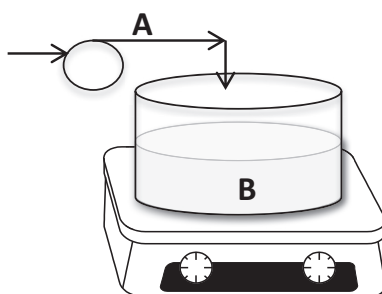
Figure 8.5 Diagram of dropwise method of synthetic C-S-H. A is calcium solution part and B is silicate solution part. The reactor vessel is made out of PMMA and has both a diameter and height of 11cm. Maximum reaction volume is 1L.

Characterization methods

Transmission electron microscopy (TEM) The morphology of the synthetic C-S-H was investigated by using TEM, *Thermo Scientific™* Talos F200X scanning transmission electron microscope (STEM) with TEM mode. It was operated at an acceleration voltage of 200 kV. TEM images were collected and then exported by using TEM Imaging and Analysis (TIA) software. The samples were prepared by dispersing the precipitated C-S-H in isopropanol and treated in an ultrasonic bath for 15 minutes. The dispersed samples were dropped on to the charged grid (carbon films on 300 mesh grids copper, *Agar Scientific Ltd.*) and allowed to dry for few minutes.

Scanning transmission electron microscope-energy dispersive x-ray (STEM-EDX) - High-angle annular dark-field (HAADF) STEM measurement combined with EDX were used to investigate the elemental distribution. The elemental map of the samples was operated by Talos F200X scanning transmission electron microscope (STEM) with STEM-EDX mode. It was operated at an acceleration voltage of 200 kV. After STEM alignment, the elemental map was performed by using *Bruker Esprit 1.9* software. The samples were prepared as the same procedure of TEM.

Sample	*A*				*B*	*pH*
	Ca(NO$_3$)$_2$.4H$_2$O (mM)	Zn(NO$_3$)$_2$.6H$_2$O (mM)	Mg(NO$_3$)$_2$.6H$_2$O (mM)	Ba(NO$_3$)$_2$.6H$_2$O (mM)	Na$_2$SiO$_3$ (mM)	
Zn_I	200	200	-	-	100	13.5
Zn_II	200	200	-	-	175 x 10^{-3}	13.5
Mg_I	200	-	200	-	100	13.5
Mg_II	200	-	200	-	175 x 10^{-3}	13.5
Ba_I	200	-	-	200	100	13.5
Ba_II	200	-	-	200	175 x 10^{-3}	13.5

<u>Table 8.1</u> Experimental conditions of synthetic C-S-H with doping divalent ions (Zn^{2+}, Mg^{2+} and Ba^{2+}).

8.2.3 Results

8.2.3.1 Divalent ions in the presence of 100 mM silicate solutions

Figure 8.6 shows morphology of synthetic C-S-H doping with Zn^{2+}, Mg^{2+} and Ba^{2+}. The Zn^{2+} (Zn_I) sample shows primary particles with a realtively regular nanoglobule morphology, with sizes between 10 and 40nm. These nanoglubules are heavily aggregated with seemingly strong necks between the primary particles. Samples in the presence of Mg^{2+} (Mg_I) shows a nanofoils morphology with characteristic lengths of < 50 nm – much finer than the C-S-H precipitated without the presence of Mg^{2+} (see Figure 8.4). These are seen to be very heavily aggregated. The sample with presence of Ba^{2+} (Ba_I) shows nanoglobule morphology with primary particle sizes between 30 and 100 nm significantly bigger than the Zn^{2+} nanoparticles, but again seem to be heavily aggregated with clear necks between particles.

STEM-EDX was used to investigate an elemental mapping of these samples and HAADF-STEM images present their morphology. The elemental mapping shows a homogeneous distribution of elements ma for the samples Zn_I, Mg_I and Ba_I as shown in Figures 8.7, 8.8 and 8.9, respectively.
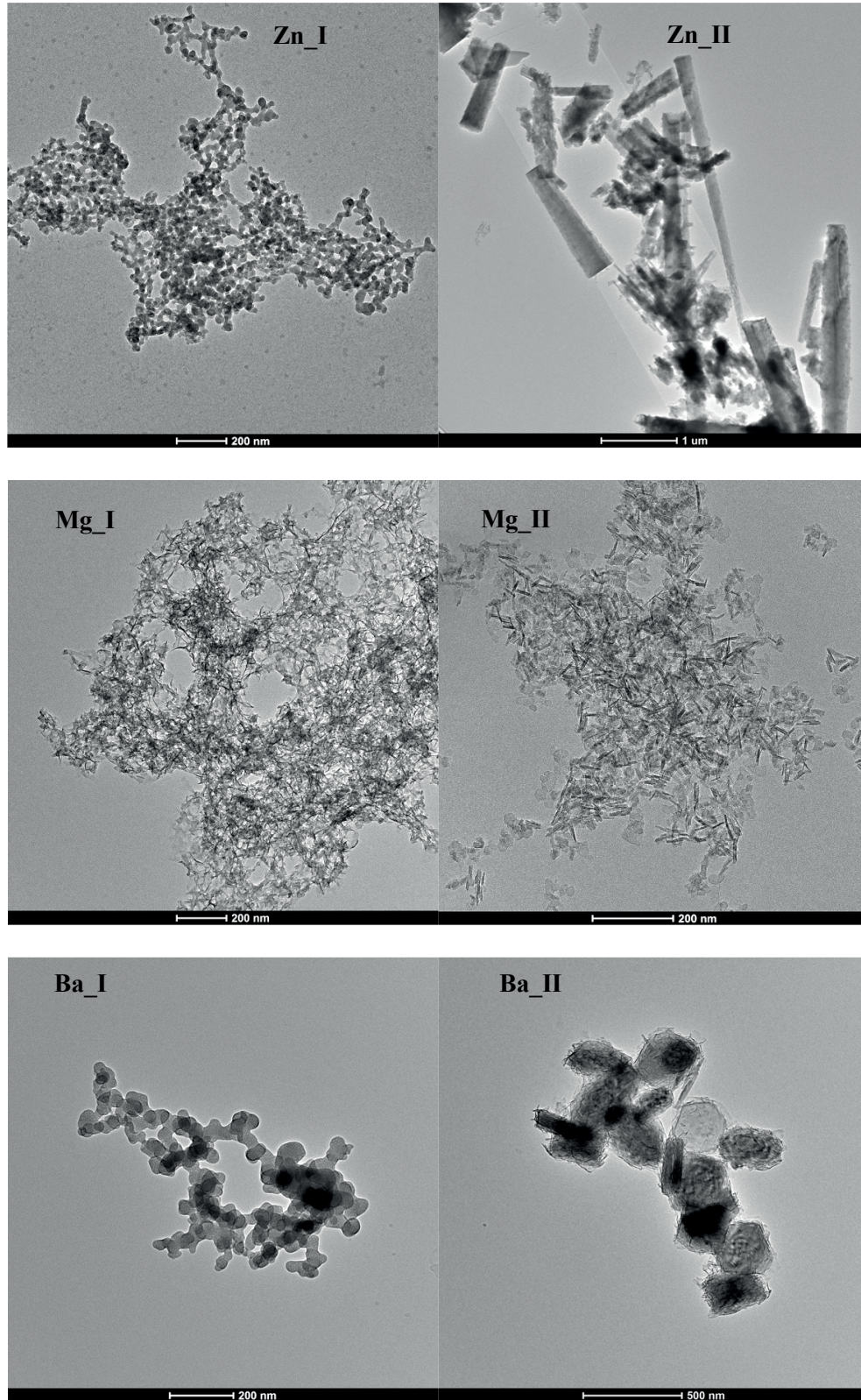
Figure 8.6 TEM images of synthetic C-S-H doping with Zn^{2+}, Mg^{2+} and Ba^{2+} at different silicate concentrations.
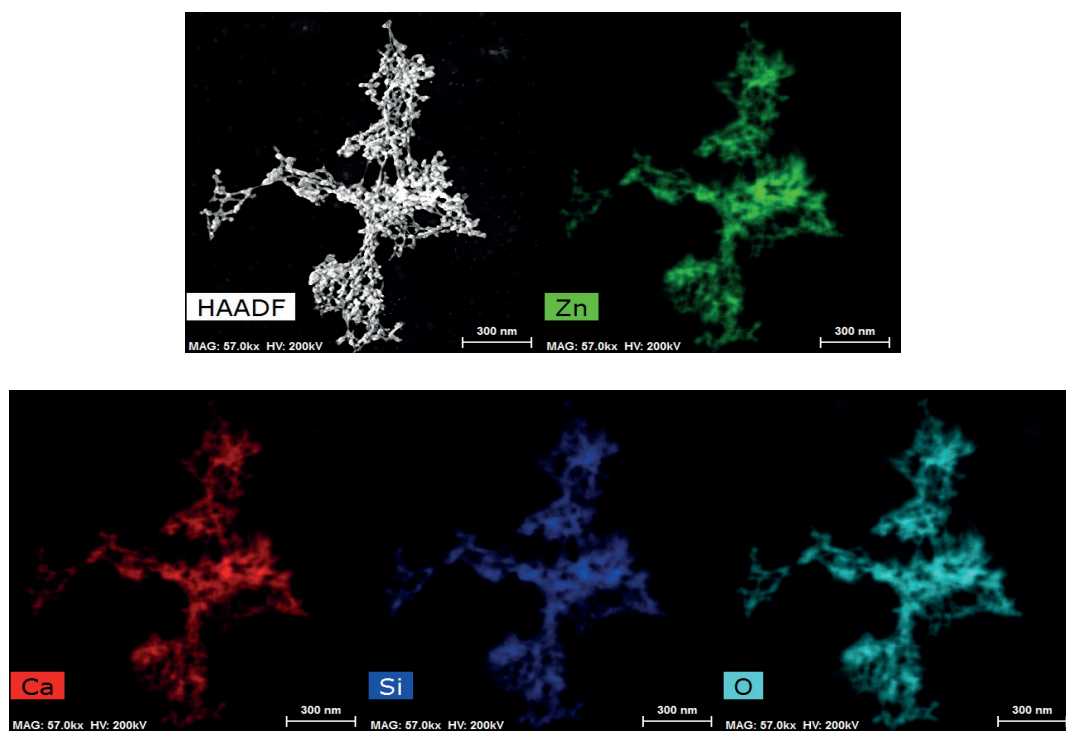
Figure 8.7 Elemental map of Ca, Si, O and Zn on synthetic C-S-H doping with Zn^{2+} (Zn_I) at 100 mM of silicate solution.
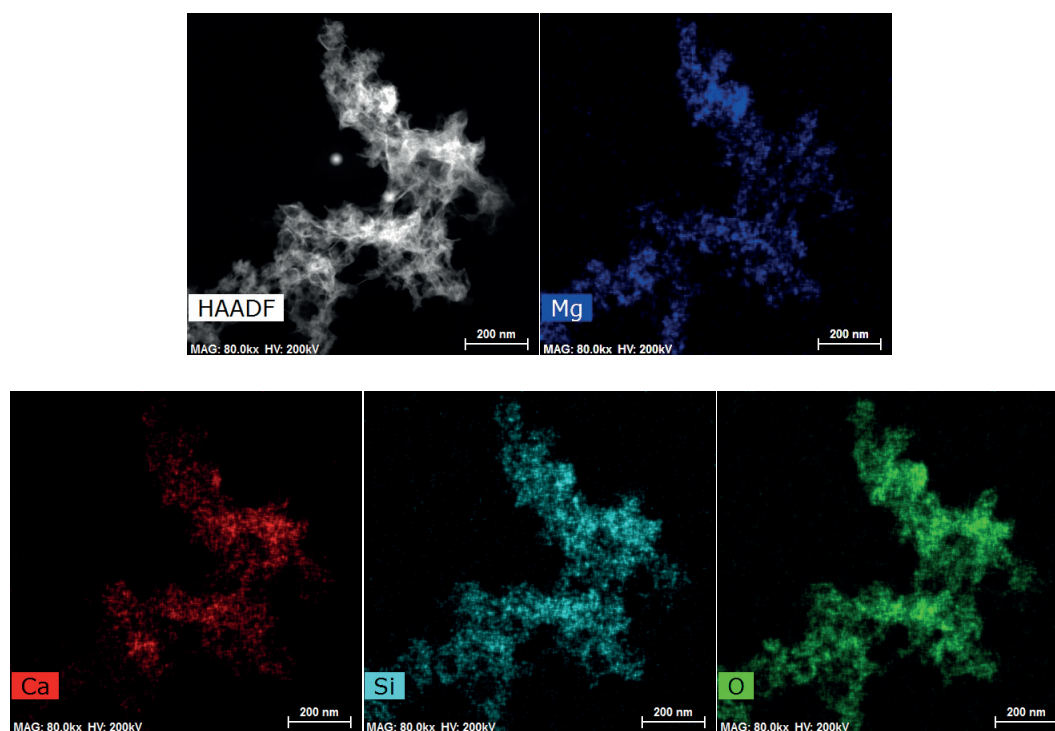
Figure 8.8 Elemental map of Ca, Si, O and Mg on synthetic C-S-H doping with Mg^{2+} (Mg_I) at 100 mM of silicate solution.
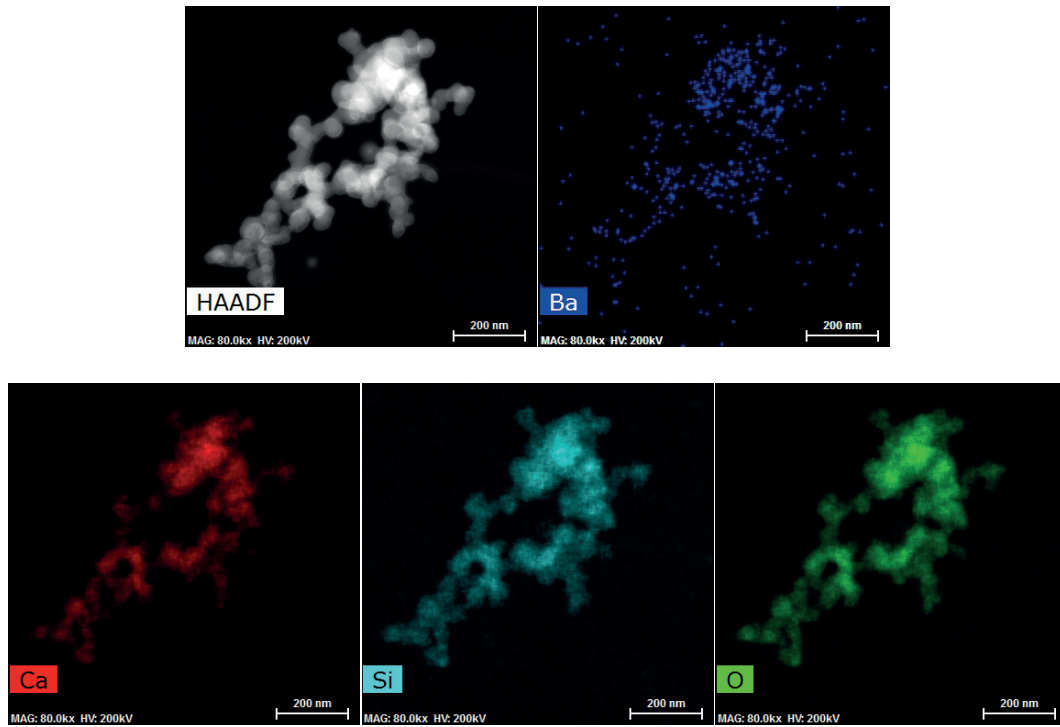
Figure 8.9 Elemental map of Ca, Si, O and Ba on synthetic C-S-H doping with Ba^{2+} (Ba_I) at 100 mM of silicate solution.

8.2.3.2 Divalent ions in the presence of 175 x 10^{-3} mM silicate solutions

At 175 x 10^{-3} mM of silicate solution, Figure 8.6 on the right-hand side shows the different morphology of samples with doping divalent ions (Zn^{2+}, Mg^{2+} and Ba^{2+}) at this lower silicate concentration. Decreasing the silicate concentration gives different mixed morphology for all of samples. With presence of Zn^{2+} (Zn_II), the morphology changes from nanoglobules to rods. Figure 8.10 (a) shows the homogeneous distribution of Zn, Ca, Si and O on these rods. Figure 8.10 (b) shows a platelet of presumably zinc silicate with a very low signal of Ca, this is a secondary phase seen much less frequently**.**

In the presence of Mg^{2+} (Mg_II) samples show a mixed morphology of nanofoils similar to the high concentration sample (Fig.8.6). but with a clear second phase of nanoneedles, Figure 8.11 (a) presents the elemental mapping of Mg, Ca, Si and O which is distributed homogeneously throughout the sample. A clear secondary phase of $Ca(OH)_2$ is observed which shows occasional hexagonal platelets with strong signals of Ca and O as shown in Figure 8.11 (b).

Doping with Ba^{2+} (Ba_II) shows mixed morphology of hexagonal platelets with nanofoils mixed with irregular rod like particles at this 175 x 10^{-3} mM of silicate solution concentration (Fig.8.6). Elemental mapping confirms that the nanofoils observed on the edge of the hexagonal and square platelets has the homogenous distribution of Ca, Si and O for a synthetic C-S-H but the strong signal of Ca and O only appear on the platelets (Fig.8.12 (a)). The platelets are probably precipitated $Ca(OH)_2$ and acts as seeding for C-S-H growth. Big irregular rods also observed in (Fig.8.12 (b)) which present only Ba and O on the elemental mapping. It could be precipitated $Ba(OH)_2$ as third phase in the system.
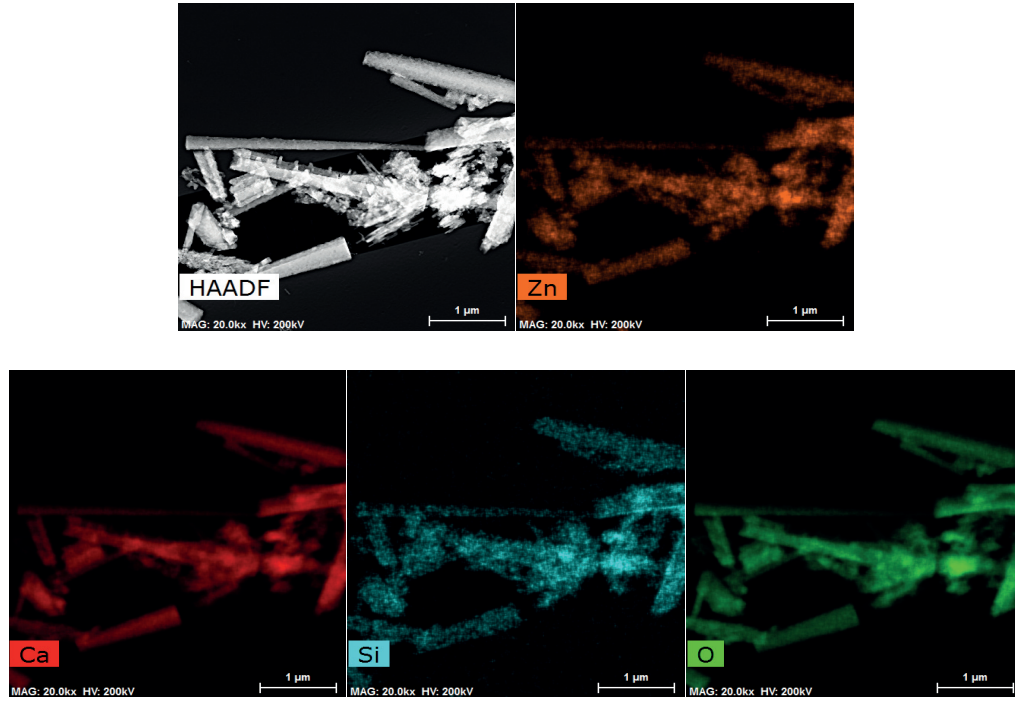
(a)
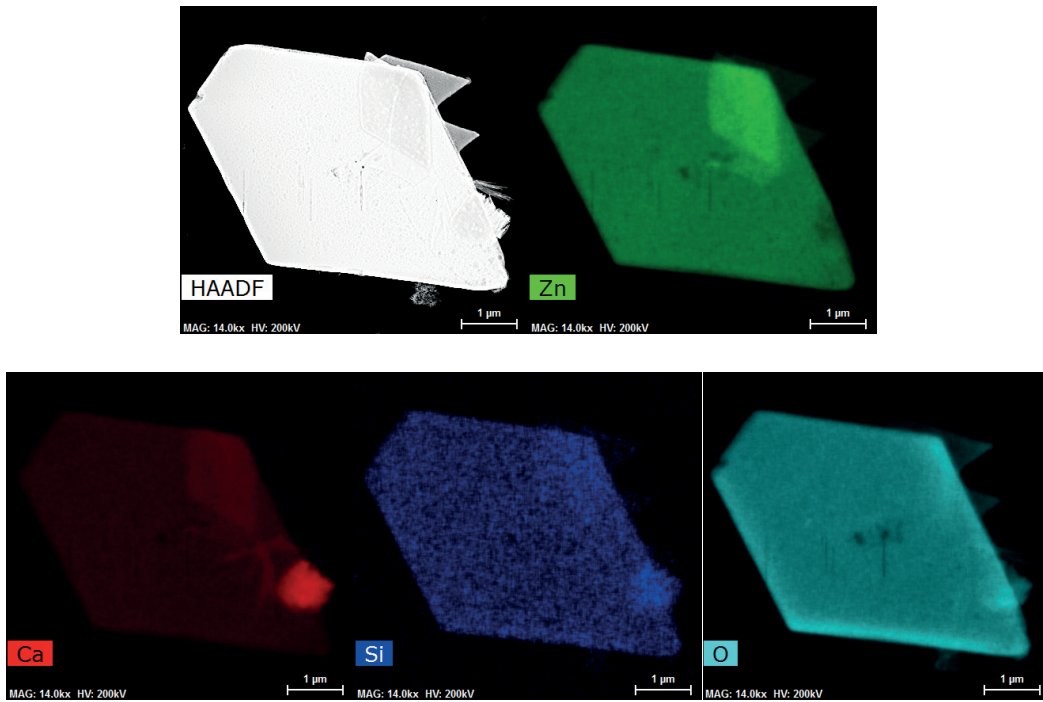
(b)

<u>Figure 8.10</u> Elemental map of Ca, Si, O and Zn on synthetic C-S-H doping with Zn^{2+} (Zn_II) at 175 x 10^{-3} mM of silicate solution.

(a)

(b)
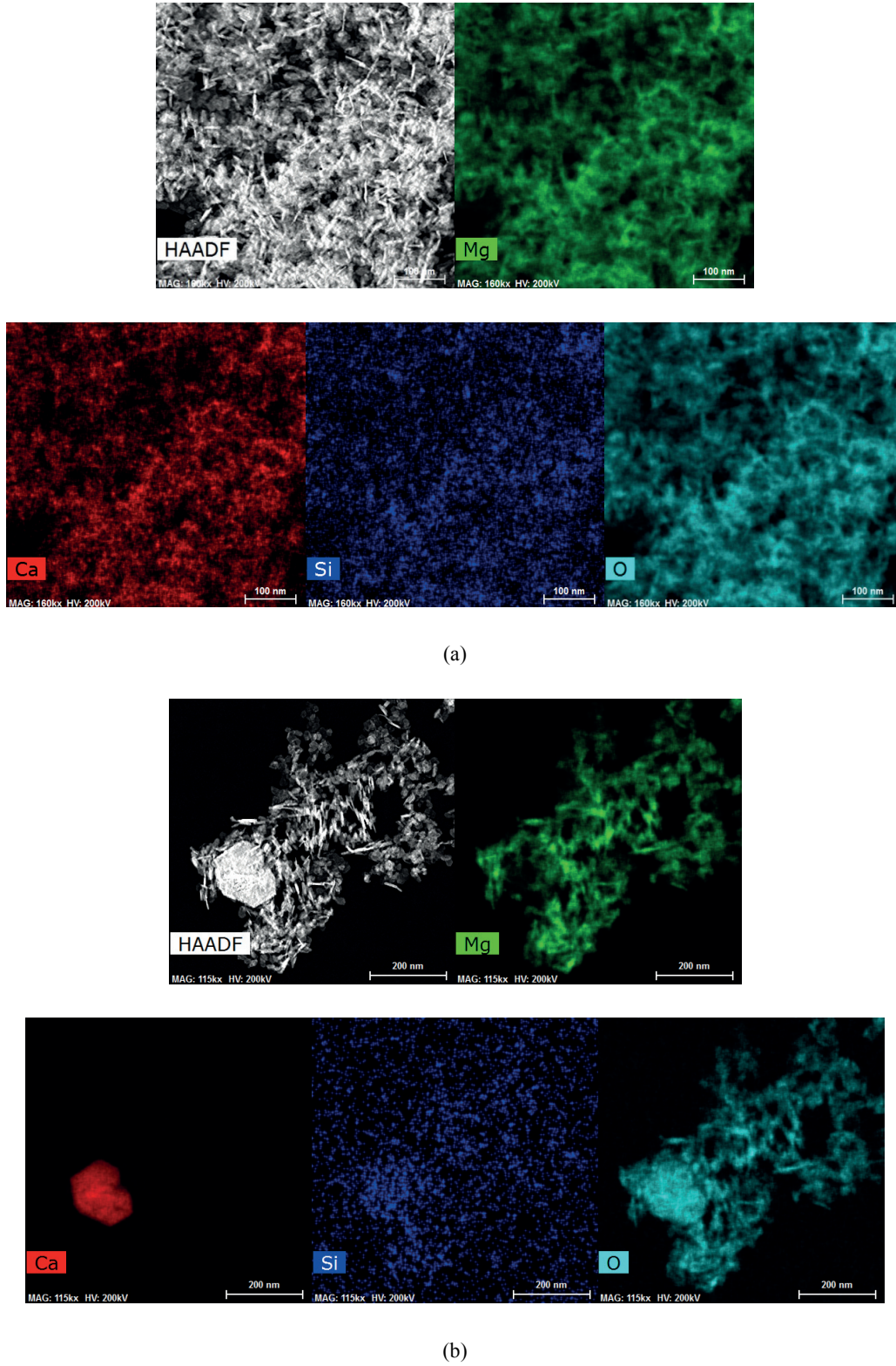
<u>Figure 8.11</u> Elemental map of Ca, Si, O and Mg on synthetic C-S-H doping with Mg^{2+} (Mg_II) at 175×10^{-3} mM of silicate solution.

(a)

(b)
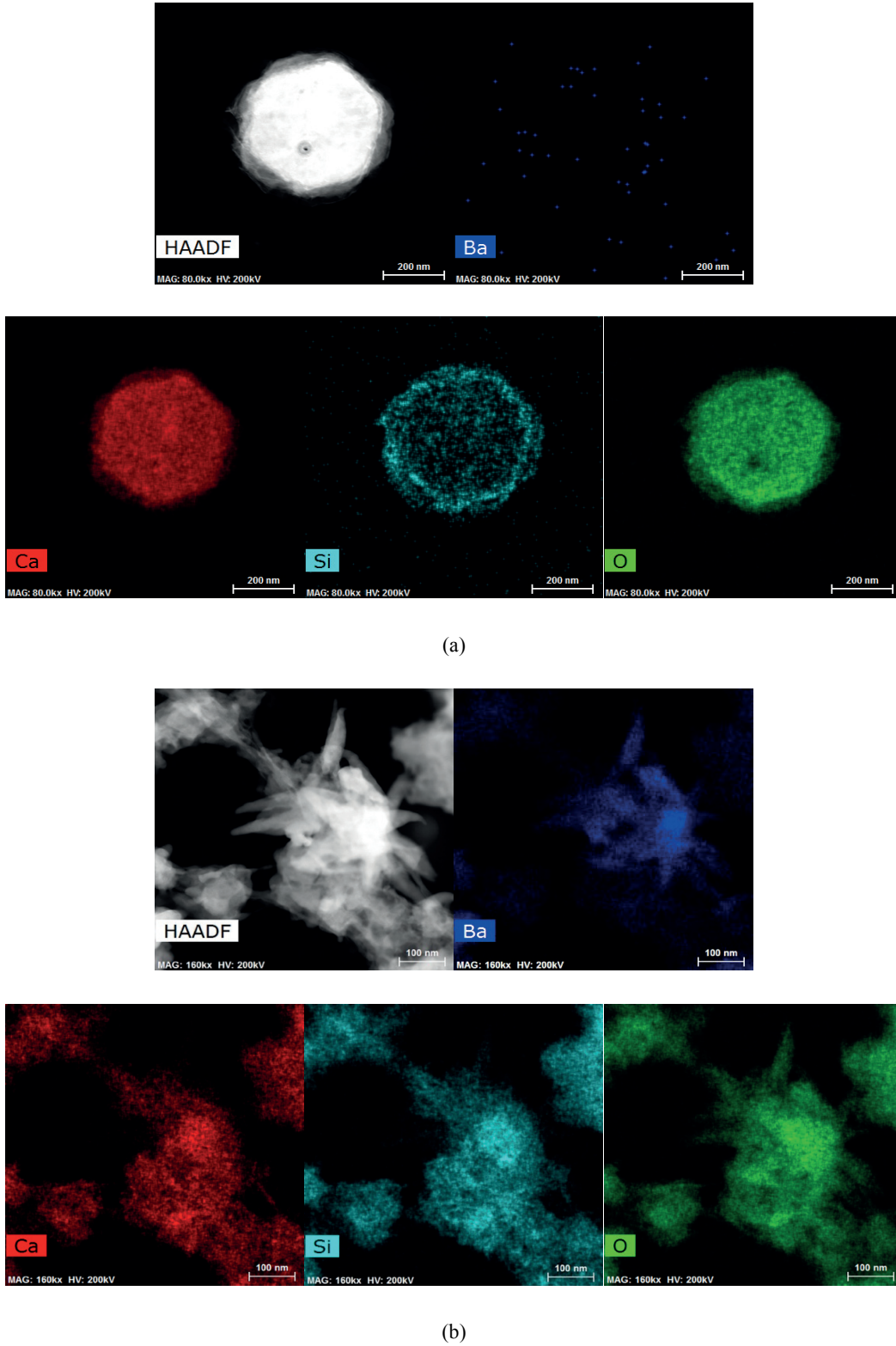
<u>Figure 8.12</u> Elemental map of Ca, Si, O and Ba on synthetic C-S-H doping with Ba^{2+} (Ba_II) at 175×10^{-3} mM of silicate solution.

8.2.4 Discussion

Typical synthetic C-S-H morphology at high pH is nanofoil [20]. The effect of divalent ions (Zn^{2+}, Mg^{2+} and Ba^{2+}) on synthetic calcium silicate hydrate (C-S-H) was observed on morphology comparing with the different silicate concentrations. At high silicate concentration (100 mM), one morphology was observed in calcium with each doping divalent ions (Zn_I, Mg_I and Ba_I). It was clearly seen the homogeneous distribution of elements on the mapping of samples by STEM-EDX. The different doping divalent ions present the different morphology and size of the samples as shown in Figure 8.6 on the left. Samples with presence of Zn^{2+} (Zn_I) and Ba^{2+} (Ba_I) showed nanoglobule morphology with the different sizes, whereas sample with presence of Mg^{2+} (Mg_I) presented nanofoils. Further characterization by XRD and TGA and thermodynamic modelling for these mixtures is needed to better interpret the results but it seems that all three ions can be incorporated into a C-X-S-H type phase.

When decreasing the silicate concentration (175×10^{-3} mM), the morphology of the samples changed significantly as shown in Figure 8.6. In this case, there was an excess of calcium and the other divalent ions (Zn^{2+}, Mg^{2+} and Ba^{2+}) in the reaction and the silicate supply was limited. Other secondary phases were observed with different morphologies and their varied compositions identifiedby STEM-EDX. With presence of Zn (Zn_II), Figure 8.7 (a) shows HAADF image of tapered needle or rod-like morphology with presence the homogeneous distribution of Zn, Ca, Si and O in the elemental mapping- perhaps a C-X-S-H phase. A secondary phase was observed with a platelet morphology as shown in Figure 8.7 (b). The elemental maps showed strong signal of Zn, Si and O but low signal of Ca suggesting a zinc silicate phase.

With presence of Mg (Mg_II), the morphology was more towards nanoneedles and hexagonal platelet, which was second phase as shown in Figure 8.8. The second phase could be precipitated $Ca(OH)_2$ as suggested by the strong signal of Ca and O by STEM-EDX (Fig.8.8 (b)). Figure 8.9 showed the morphology of synthetic C-S-H with Ba (Ba_II). There is mixed morphology of nanofoils covering hexagonal platelet surface and rods. The distribution of elements shows signal of Ca, Si and O of nanofoils relating to C-S-H composition. The hexagonal platelet showed strong signal of Ca and O which corresponds to $Ca(OH)_2$. There were also rods as shown in Figure 8.9 (b) which could be $Ba(OH)_2$.

8.2.5 Conclusions

This work showed preliminary observations on the morphology and composition of precipitated C-S-H doping different divalent ions (Zn^{2+}, Mg^{2+} and Ba^{2+}) by using dropwise precipitation method. The different of silicate concentrations (100 mM and 175×10^{-3} mM) showed the different morphologies. STEM-EDX was used to investigate the elemental distribution. At the higher silicate concentrations (standard synthetic C-S-H precipitation conditions) effect on the C-S-H morphology were observed and the EDX results showed homogeneous compositions suggesting the possibility of C-X-S-H (X= Zn, Ba, Mg) formation. With excess of Ca and the divalent ions (Zn^{2+}, Mg^{2+} and Ba^{2+}), the mixed morphology was observed. Secondary phases were shown in the samples with of the low silicate concentrations (175×10^{-3} mM). However, we need more characterization to investigate structure of precipitated products such as XRD, TGA and some thermodynamic modelling (with mother solution and precipitate compositional analysis by ICP) to see what standard phases could be produced or if we are really forming C-X-S-H phases with high levels of X substitution.

References

[1]   World Statistical Review 2004 - 2014, (n.d.). https://cembureau.eu/news-views/publications/world-statistical-review-2004-2014/ (accessed May 31, 2018).

[2]   A blueprint for a climate friendly cement industry | WWF, (n.d.). http://wwf.panda.org/wwf_news/?151621/A-blueprint-for-a-climate-friendly-cement-industry (accessed May 31, 2018).

[3]   H.F.W. Taylor, Cement Chemistry, Thomas Telford, 1997.

[4]   N. Subramanian, Design of Reinforced Concrete Structures, Oxford University Press, Oxford, New York, 2014.

[5]   B.B. Sabir, S. Wild, J. Bai, Metakaolin and calcined clays as pozzolans for concrete: a review, Cem. Concr. Compos. 23 (2001) 441–454. doi:10.1016/S0958-9465(00)00092-5.

[6]   K.L. Scrivener, A. Nonat, Hydration of cementitious materials, present and future, Cem. Concr. Res. 41 (2011) 651–665. doi:10.1016/j.cemconres.2011.03.026.

[7]   S.C. Taylor-Lange, E.L. Lamon, K.A. Riding, M.C.G. Juenger, Calcined kaolinite–bentonite clay blends as supplementary cementitious materials, Appl. Clay Sci. 108 (2015) 84–93. doi:10.1016/j.clay.2015.01.025.

[8]   B. Lothenbach, K. Scrivener, R.D. Hooton, Supplementary cementitious materials, Cem. Concr. Res. 41 (2011) 1244–1256. doi:10.1016/j.cemconres.2010.12.001.

[9]   M.C.G. Juenger, R. Siddique, Recent advances in understanding the role of supplementary cementitious materials in concrete, Cem. Concr. Res. 78, Part A (2015) 71–80. doi:10.1016/j.cemconres.2015.03.018.

[10]   Nanocem - Home, (n.d.). https://www.nanocem.org/ (accessed August 12, 2018).

[11]   C. Nalet, A. Nonat, Retarding effectiveness of hexitols on the hydration of the silicate phases of cement: Interaction with the aluminate and sulfate phases, Cem. Concr. Res. 90 (2016) 137–143. doi:10.1016/j.cemconres.2016.09.018.

[12]   C. Nalet, A. Nonat, Effects of hexitols on the hydration of tricalcium silicate, Cem. Concr. Res. 91 (2017) 87–96. doi:10.1016/j.cemconres.2016.11.004.

[13]   C. Nalet, A. Nonat, Ionic complexation and adsorption of small organic molecules on calcium silicate hydrate: Relation with their retarding effect on the hydration of C3S, Cem. Concr. Res. 89 (2016) 97–108. doi:10.1016/j.cemconres.2016.08.012.

[14] C. Nalet, A. Nonat, Effects of functionality and stereochemistry of small organic molecules on the hydration of tricalcium silicate, Cem. Concr. Res. 87 (2016) 97–104. doi:10.1016/j.cemconres.2016.06.002.

[15] A. Bazzoni, S. Ma, Q. Wang, X. Shen, M. Cantoni, K.L. Scrivener, The Effect of Magnesium and Zinc Ions on the Hydration Kinetics of C3S, J. Am. Ceram. Soc. 97 (2014) 3684–3693. doi:10.1111/jace.13156.

[16] A. Vollpracht, B. Lothenbach, R. Snellings, J. Haufe, The pore solution of blended cements: a review, Mater. Struct. 49 (2016) 3341–3367. doi:10.1617/s11527-015-0724-1.

[17] A. Chakchouk, B. Samet, S. Bouaziz, Difference in pozzolanic behaviour of Tunisian clays with lime and cement, Adv. Cem. Res. 24 (2012) 11–22. doi:10.1680/adcr.2012.24.1.11.

[18] A. Stumm, K. Garbev, G. Beuchle, L. Black, P. Stemmermann, R. Nüesch, Incorporation of zinc into calcium silicate hydrates, Part I: formation of C-S-H(I) with C/S=2/3 and its iso-chemical counterpart gyrolite, Cem. Concr. Res. 35 (2005) 1665–1675. doi:10.1016/j.cemconres.2004.11.007.

[19] H. Ghorbel, B. Samet, Effect of iron on pozzolanic activity of kaolin, Constr. Build. Mater. 44 (2013) 185–191. doi:10.1016/j.conbuildmat.2013.02.068.

[20] A. Kumar, B.J. Walder, A. Kunhi Mohamed, A. Hofstetter, B. Srinivasan, A.J. Rossini, K. Scrivener, L. Emsley, P. Bowen, The Atomic-Level Structure of Cementitious Calcium Silicate Hydrate, J. Phys. Chem. C. 121 (2017) 17188–17196. doi:10.1021/acs.jpcc.7b02439.

[21] M.R. Andalibi, A. Kumar, B. Srinivasan, P. Bowen, K. Scrivener, C. Ludwig, A. Testino, On the mesoscale mechanism of synthetic calcium–silicate–hydrate precipitation: a population balance modeling approach, J. Mater. Chem. A. (2017). doi:10.1039/C7TA08784E.

[22] K. Ioannidou, M. Kanduč, L. Li, D. Frenkel, J. Dobnikar, E.D. Gado, The crucial effect of early-stage gelation on the mechanical properties of cement hydrates, Nat. Commun. 7 (2016) 12106. doi:10.1038/ncomms12106.

[23] G. Geng, R.J. Myers, M.J.A. Qomi, P.J.M. Monteiro, Densification of the interlayer spacing governs the nanomechanical properties of calcium-silicate-hydrate, Sci. Rep. 7 (2017) 10986. doi:10.1038/s41598-017-11146-8.

[24] H. Manzano, S. Moeini, F. Marinelli, A.C.T. van Duin, F.-J. Ulm, R.J.-M. Pellenq, Confined Water Dissociation in Microporous Defective Silicates: Mechanism, Dipole Distribution, and Impact on Substrate Properties, J. Am. Chem. Soc. 134 (2012) 2208–2215. doi:10.1021/ja209152n.

[25] D.A. Kulik, T. Wagner, S.V. Dmytrieva, G. Kosakowski, F.F. Hingerl, K.V. Chudnenko, U.R. Berner, GEM-Selektor geochemical modeling package: revised algorithm and

GEMS3K numerical kernel for coupled simulation codes, Comput. Geosci. 17 (2013) 1–24. doi:10.1007/s10596-012-9310-6.

[26] D.A. Kulik, Improving the structural consistency of C-S-H solid solution thermodynamic models, Cem. Concr. Res. 41 (2011) 477–495. doi:10.1016/j.cemconres.2011.01.012.

[27] B. Lothenbach, Thermodynamic equilibrium calculations in cementitious systems, Mater. Struct. 43 (2010) 1413–1433. doi:10.1617/s11527-010-9592-x.

[28] Science and Technology of Concrete Admixtures - 1st Edition, (n.d.). https://www.elsevier.com/books/science-and-technology-of-concrete-admixtures/aitcin/978-0-08-100693-1 (accessed June 3, 2018).

[29] K.L. Scrivener, P. Juilland, P.J.M. Monteiro, Advances in understanding hydration of Portland cement, Cem. Concr. Res. 78 (2015) 38–56. doi:10.1016/j.cemconres.2015.05.025.

[30] P. Juilland, E. Gallucci, R. Flatt, K. Scrivener, Dissolution theory applied to the induction period in alite hydration, Cem. Concr. Res. 40 (2010) 831–844. doi:10.1016/j.cemconres.2010.01.012.

[31] F. Brunet, P. Bertani, T. Charpentier, A. Nonat, J. Virlet, Application of 29Si Homonuclear and 1H−29Si Heteronuclear NMR Correlation to Structural Studies of Calcium Silicate Hydrates, J. Phys. Chem. B. 108 (2004) 15494–15502. doi:10.1021/jp031174g.

[32] A Practical Guide to Microstructural Analysis of Cementitious Materials, CRC Press. (2017). https://www.crcpress.com/A-Practical-Guide-to-Microstructural-Analysis-of-Cementitious-Materials/Scrivener-Snellings-Lothenbach/p/book/9781138747234 (accessed October 17, 2017).

[33] A. Kunhi Mohamed, S.C. Parker, P. Bowen, S. Galmarini, An atomistic building block description of C-S-H - Towards a realistic C-S-H model, Cem. Concr. Res. 107 (2018) 221–235. doi:10.1016/j.cemconres.2018.01.007.

[34] P. Rejmak, J.S. Dolado, M.J. Stott, A. Ayuela, 29Si NMR in Cement: A Theoretical Study on Calcium Silicate Hydrates, J. Phys. Chem. C. 116 (2012) 9755–9761. doi:10.1021/jp302218j.

[35] B. Lothenbach, A. Nonat, Calcium silicate hydrates: Solid and liquid phase composition, Cem. Concr. Res. 78, Part A (2015) 57–70. doi:10.1016/j.cemconres.2015.03.019.

[36] A. Nonat, The structure and stoichiometry of C-S-H, Cem. Concr. Res. 34 (2004) 1521–1528. doi:10.1016/j.cemconres.2004.04.035.

[37] S.C. Galmarini, Atomistic Simulation of Cementitious Systems, (2013). doi:10.5075/epfl-thesis-5754.

[38] E. Pustovgar, R.P. Sangodkar, A.S. Andreev, M. Palacios, B.F. Chmelka, R.J. Flatt, J.-B. d'Espinose de Lacaillerie, Understanding silicate hydration from quantitative analyses of hydrating tricalcium silicates, Nat. Commun. 7 (2016) 10952. doi:10.1038/ncomms10952.

[39] Chemical Admixtures, (n.d.). http://www.cement.org/cement-concrete-applications/concrete-materials/chemical-admixtures (accessed August 12, 2018).

[40] Concrete Admixtures Handbook - 2nd Edition, (n.d.). https://www.elsevier.com/books/concrete-admixtures-handbook/ramachandran/978-0-8155-1373-5 (accessed June 7, 2018).

[41] M. Palacios, P. Bowen, M. Kappl, H.J. Butt, M. Stuer, C. Pecharromán, U. Aschauer, F. Puertas, Repulsion forces of superplasticizers on ground granulated blast furnace slag in alkaline media, from AFM measurements to rheological properties, Mater. Constr. 62 (2012) 489–513. doi:10.3989/mc.2012.01612.

[42] Y.F. Houst, P. Bowen, F. Perche, A. Kauppi, P. Borget, L. Galmiche, J.-F. Le Meins, F. Lafuma, R.J. Flatt, I. Schober, P.F.G. Banfill, D.S. Swift, B.O. Myrvold, B.G. Petersen, K. Reknes, Design and function of novel superplasticizers for more durable high performance concrete (superplast project), Cem. Concr. Res. 38 (2008) 1197–1209. doi:10.1016/j.cemconres.2008.04.007.

[43] W. Meng, P. Lunkad, A. Kumar, K. Khayat, Influence of Silica Fume and Polycarboxylate Ether Dispersant on Hydration Mechanisms of Cement, J. Phys. Chem. C. 120 (2016) 26814–26823. doi:10.1021/acs.jpcc.6b08121.

[44] D. Marchon, P. Juilland, E. Gallucci, L. Frunz, R.J. Flatt, Molecular and submolecular scale effects of comb-copolymers on tri-calcium silicate reactivity: Toward molecular design, J. Am. Ceram. Soc. 100 (2017) 817–841. doi:10.1111/jace.14695.

[45] A. Pallagi, É.G. Bajnóczi, S.E. Canton, T. Bolin, G. Peintler, B. Kutus, Z. Kele, I. Pálinkó, P. Sipos, Multinuclear complex formation between Ca(II) and gluconate ions in hyperalkaline solutions, Environ. Sci. Technol. 48 (2014) 6604–6611. doi:10.1021/es501067w.

[46] S. Ma, W. Li, S. Zhang, D. Ge, J. Yu, X. Shen, Influence of sodium gluconate on the performance and hydration of Portland cement, Constr. Build. Mater. 91 (2015) 138–144. doi:10.1016/j.conbuildmat.2015.05.068.

[47] B. Mota Gassó, Impact of alkali salts on the kinetics and microstructural development of cementitious systems, (2015). doi:10.5075/epfl-thesis-6763.

[48] E. Berodier, K. Scrivener, Understanding the Filler Effect on the Nucleation and Growth of C-S-H, J. Am. Ceram. Soc. 97 (2014) 3764–3773. doi:10.1111/jace.13177.

[49] W.A. Gutteridge, J.A. Dalziel, Filler cement: The effect of the secondary component on the hydration of Portland cement: Part I. A fine non-hydraulic filler, Cem. Concr. Res. 20 (1990) 778–782. doi:10.1016/0008-8846(90)90011-L.

[50] W.A. Gutteridge, J.A. Dalziel, Filler cement: The effect of the secondary component on the hydration of Portland cement: Part 2: Fine hydraulic binders, Cem. Concr. Res. 20 (1990) 853–861. doi:10.1016/0008-8846(90)90046-Z.

[51] A. Kumar, T. Oey, G. Falzone, J. Huang, M. Bauchy, M. Balonis, N. Neithalath, J. Bullard, G. Sant, The filler effect: The influence of filler content and type on the hydration rate of tricalcium silicate, J. Am. Ceram. Soc. 100 (2017) 3316–3328. doi:10.1111/jace.14859.

[52] A. Kumar, Synthetic Calcium Silicate Hydrates, STI, 2017. doi:10.5075/epfl-thesis-7658.

[53] D.N. Mastronarde, Automated electron microscope tomography using robust prediction of specimen movements, J. Struct. Biol. 152 (2005) 36–51. doi:10.1016/j.jsb.2005.07.007.

[54] J.R. Kremer, D.N. Mastronarde, J.R. McIntosh, Computer visualization of three-dimensional image data using IMOD, J. Struct. Biol. 116 (1996) 71–76. doi:10.1006/jsbi.1996.0013.

[55] D.N. Mastronarde, Dual-Axis Tomography: An Approach with Alignment Methods That Preserve Resolution, J. Struct. Biol. 120 (1997) 343–352. doi:10.1006/jsbi.1997.3919.

[56] B.Z. Dilnesa, E. Wieland, B. Lothenbach, R. Dähn, K.L. Scrivener, Fe-containing phases in hydrated cements, Cem. Concr. Res. 58 (2014) 45–55. doi:10.1016/j.cemconres.2013.12.012.

[57] B. Lothenbach, F. Winnefeld, Thermodynamic modelling of the hydration of Portland cement, Cem. Concr. Res. 36 (2006) 209–226. doi:10.1016/j.cemconres.2005.03.001.

[58] B.Z. Dilnesa, B. Lothenbach, G. Le Saout, G. Renaudin, A. Mesbah, Y. Filinchuk, A. Wichser, E. Wieland, Iron in carbonate containing AFm phases, Cem. Concr. Res. 41 (2011) 311–323. doi:10.1016/j.cemconres.2010.11.017.

[59] M. Vespa, E. Wieland, R. Dähn, B. Lothenbach, Identification of the Thermodynamically Stable Fe-Containing Phase in Aged Cement Pastes, J. Am. Ceram. Soc. 98 (2015) 2286–2294. doi:10.1111/jace.13542.

[60] F. Avet, R. Snellings, A. Alujas Diaz, M. Ben Haha, K. Scrivener, Development of a new rapid, relevant and reliable (R3) test method to evaluate the pozzolanic reactivity of calcined kaolinitic clays, Cem. Concr. Res. 85 (2016) 1–11. doi:10.1016/j.cemconres.2016.02.015.

[61] T. Danner, H. Justnes, G. Norden, T. Østnor, Feasibility of Calcined Marl as an Alternative Pozzolanic Material, in: Calcined Clays Sustain. Concr., Springer, Dordrecht, 2015: pp. 67–73. doi:10.1007/978-94-017-9939-3_9.

[62] S. Grangeon, F. Claret, C. Roosz, T. Sato, S. Gaboreau, Y. Linard, Structure of nanocrystalline calcium silicate hydrates: insights from X-ray diffraction, synchrotron X-ray absorption

and nuclear magnetic resonance, J. Appl. Crystallogr. 49 (2016) 771–783. doi:10.1107/S1600576716003885.

[63] H. Manzano, J.S. Dolado, A. Ayuela, Aluminum Incorporation to Dreierketten Silicate Chains, J. Phys. Chem. B. 113 (2009) 2832–2839. doi:10.1021/jp804867u.

[64] I. g. Richardson, J. Skibsted, L. Black, R. j. Kirkpatrick, Characterisation of cement hydrate phases by TEM, NMR and Raman spectroscopy, Adv. Cem. Res. 22 (2010) 233–248. doi:10.1680/adcr.2010.22.4.233.

[65] A.R. Brough, C.M. Dobson, I.G. Richardson, G.W. Groves, Application of Selective 29Si Isotopic Enrichment to Studies of the Structure of Calcium Silicate Hydrate (C-S-H) Gels, J. Am. Ceram. Soc. 77 (1994) 593–596. doi:10.1111/j.1151-2916.1994.tb07034.x.

[66] E. L'Hôpital, B. Lothenbach, D.A. Kulik, K. Scrivener, Influence of calcium to silica ratio on aluminium uptake in calcium silicate hydrate, Cem. Concr. Res. 85 (2016) 111–121. doi:10.1016/j.cemconres.2016.01.014.

[67] F. Ziegler, A.M. Scheidegger, C.A. Johnson, R. Dähn, E. Wieland, Sorption Mechanisms of Zinc to Calcium Silicate Hydrate: X-ray Absorption Fine Structure (XAFS) Investigation, Environ. Sci. Technol. 35 (2001) 1550–1555. doi:10.1021/es001437+.

[68] Ferrihydrite Mineral Data, (n.d.). http://webmineral.com/data/Ferrihydrite.shtml#.W3BhbpMzZTY (accessed August 12, 2018).

[69] T. Nagano, Color Variations Associated with Rapid Formation of Goethite from Proto-Ferrihydrite at pH 13 and 40°C, Clays Clay Miner. 40 (1992) 600–607. doi:10.1346/CCMN.1992.0400515.

[70] B.Z. Dilnesa, B. Lothenbach, G. Renaudin, A. Wichser, D. Kulik, Synthesis and characterization of hydrogarnet $Ca_3(Al_xFe_1 − x)_2(SiO_4)_y(OH)_4(3 − y)$, Cem. Concr. Res. 59 (2014) 96–111. doi:10.1016/j.cemconres.2014.02.001.

[71] G. Montes-Hernandez, P. Beck, F. Renard, E. Quirico, B. Lanson, R. Chiriac, N. Findling, Fast Precipitation of Acicular Goethite from Ferric Hydroxide Gel under Moderate Temperature (30 and 70 °C), Cryst. Growth Des. 11 (2011) 2264–2272. doi:10.1021/cg1016802.

[72] P.C.M. Francisco, T. Sato, T. Otake, T. Kasama, Kinetics of Fe^{3+} mineral crystallization from ferrihydrite in the presence of Si at alkaline conditions and implications for nuclear waste disposal, Am. Mineral. 101 (2016) 2057–2069. doi:10.2138/am-2016-5589.

[73] S. Das, M.J. Hendry, J. Essilfie-Dughan, Transformation of Two-Line Ferrihydrite to Goethite and Hematite as a Function of pH and Temperature, Environ. Sci. Technol. 45 (2011) 268–275. doi:10.1021/es101903y.

[74] G. Pokrovski, J. Schott, F. Farges, J. Hazemann, Iron (III)-silica interactions in aqueous solution: Insights from X-ray absorption fine structure spectroscopy, Geochim. Cosmochim. Acta. 67 (2003) 3559--3573. doi:10.1016/S0016-7037(03)00160-1.

[75] R.M. Bozorth, E.F. Tilden, A.J. Williams, Anisotropy and Magnetostriction of Some Ferrites, Phys. Rev. 99 (1955) 1788–1798. doi:10.1103/PhysRev.99.1788.

[76] T. Castner, G.S. Newell, W.C. Holton, C.P. Slichter, Note on the Paramagnetic Resonance of Iron in Glass, J. Chem. Phys. 32 (1960) 668–673. doi:10.1063/1.1730779.

[77] J. Rose, A. Bénard, S. El Mrabet, A. Masion, I. Moulin, V. Briois, L. Olivi, J.-Y. Bottero, Evolution of iron speciation during hydration of C4AF, Waste Manag. 26 (2006) 720–724. doi:10.1016/j.wasman.2006.01.021.

[78] M. Antoni, J. Rossen, F. Martirena, K. Scrivener, Cement substitution by a combination of metakaolin and limestone, Cem. Concr. Res. 42 (2012) 1579–1589. doi:10.1016/j.cemconres.2012.09.006.

[79] V. Kanchanason, J. Plank, Role of Ph on the Structure, Composition and Morphology of C-S-H–Pce Nanocomposites and Their Effect on Early Strength Development of Portland Cement, Cem. Concr. Res. 102 (2017) 90–98. doi:10.1016/j.cemconres.2017.09.002.

[80] S. Grangeon, F. Claret, Y. Linard, C. Chiaberge, X-ray diffraction: a powerful tool to probe and understand the structure of nanocrystalline calcium silicate hydrates, Acta Crystallogr. Sect. B Struct. Sci. Cryst. Eng. Mater. 69 (2013) 465–473. doi:10.1107/S2052519213021155.

[81] I. Androniuk, C. Landesman, P. Henocq, A.G. Kalinichev, Adsorption of gluconate and uranyl on C-S-H phases: Combination of wet chemistry experiments and molecular dynamics simulations for the binary systems, Phys. Chem. Earth Parts ABC. 99 (2017) 194–203. doi:10.1016/j.pce.2017.05.005.

[82] L. Nicoleau, T. Gädt, L. Chitu, G. Maier, O. Paris, Oriented aggregation of calcium silicate hydrate platelets by the use of comb-like copolymers, Soft Matter. 9 (2013) 4864–4874. doi:10.1039/C3SM00022B.

[83] J.J. Thomas, H.M. Jennings, J.J. Chen, Influence of Nucleation Seeding on the Hydration Mechanisms of Tricalcium Silicate and Cement, J. Phys. Chem. C. 113 (2009) 4327–4334. doi:10.1021/jp809811w.

[84] UNI-KOHA catalog › Details for: The acceleration of cement hydration by seeding: influence of the cement mineralogy, (n.d.). http://www.catalogo.uni.edu.pe/cgi-bin/koha/opac-detail.pl?biblionumber=256118 (accessed July 8, 2018).

[85] D. Marchon, Controlling cement hydration through the molecular structure of comb copolymer superplasticizers, Doctoral Thesis, ETH Zurich, 2016. doi:10.3929/ethz-a-010798278.

[86] S. Garrault, Y. Sallier, M. Michaux, A. Nonat, Retardation mechanisms of sodium gluconate for hydration of pure tricalcium silicate and alite in cement, in: 2009. https://hal.archives-ouvertes.fr/hal-00452420 (accessed April 21, 2017).

[87] H. Yang, B. Ma, H. Tan, Effect of competitive adsorption between sodium gluconate and naphthalene-based superplasticiser on fluidity of cement paste, Mag. Concr. Res. 65 (2013) 1212–1218. doi:10.1680/macr.13.00058.

[88] B. Kutus, D. Ozsvár, N. Varga, I. Pálinkó, P. Sipos, ML and ML2 complex formation between Ca(II) and D-glucose derivatives in aqueous solutions, Dalton Trans. 46 (2017) 1065–1074. doi:10.1039/C6DT04356A.

[89] J. Siramanont, C-S-H_D-Gluconate bi-pyramidal cage-like structure, 2017. https://lmc.epfl.ch/page-154501-en-html/.

[90] Sol-Gel Science - 1st Edition, (n.d.). https://www.elsevier.com/books/sol-gel-science/brinker/978-0-08-057103-4 (accessed July 11, 2018).

[91] H.F.W. Taylor, Proposed Structure for Calcium Silicate Hydrate Gel, J. Am. Ceram. Soc. 69 (1986) 464–467. doi:10.1111/j.1151-2916.1986.tb07446.x.

[92] I.G. Richardson, The calcium silicate hydrates, Cem. Concr. Res. 38 (2008) 137–158. doi:10.1016/j.cemconres.2007.11.005.

[93] E. Ntafalias, P.G. Koutsoukos, Spontaneous precipitation of calcium silicate hydrate in aqueous solutions, Cryst. Res. Technol. 45 (2010) 39–47. doi:10.1002/crat.200900538.

[94] M. Bauchy, M.J.A. Qomi, F.-J. Ulm, R.J.-M. Pellenq, Order and disorder in calcium–silicate–hydrate, J. Chem. Phys. 140 (2014) 214503. doi:10.1063/1.4878656.

[95] W.-S. Chiang, E. Fratini, F. Ridi, S.-H. Lim, Y.-Q. Yeh, P. Baglioni, S.-M. Choi, U.-S. Jeng, S.-H. Chen, Microstructural changes of globules in calcium–silicate–hydrate gels with and without additives determined by small-angle neutron and X-ray scattering, J. Colloid Interface Sci. 398 (2013) 67–73. doi:10.1016/j.jcis.2013.01.065.

[96] S.A. El-Korashy, Synthetic Crystalline Calcium Silicate Hydrate (I): Cation Exchange and Caesium Selectivity, Monatshefte Für Chem. Chem. Mon. 133 (2002) 333–343. doi:10.1007/s007060200012.

[97] M. Hounslow, The Population Balance as a Tool for Understanding Particle Rate Processes, KONA Powder Part. J. 16 (1998) 179–193. doi:10.14356/kona.1998021.

[98] B.B. Schroeder, D.D. Harris, S.T. Smith, D.O. Lignell, Theoretical Framework for Multiple-Polymorph Particle Precipitation in Highly Supersaturated Systems, Cryst. Growth Des. 14 (2014) 1756–1770. doi:10.1021/cg401892b.

[99] A. Testino, M.T. Buscaglia, V. Buscaglia, M. Viviani, C. Bottino, P. Nanni, Kinetics and Mechanism of Aqueous Chemical Synthesis of BaTiO3 Particles, Chem. Mater. 16 (2004) 1536–1543. doi:10.1021/cm031130k.

[100] A. Testino, V. Buscaglia, M.T. Buscaglia, M. Viviani, P. Nanni, Kinetic Modeling of Aqueous and Hydrothermal Synthesis of Barium Titanate (BaTiO3), Chem. Mater. 17 (2005) 5346–5356. doi:10.1021/cm051119f.

[101] F.K. Crundwell, On the Mechanism of the Dissolution of Quartz and Silica in Aqueous Solutions, ACS Omega. 2 (2017) 1116–1127. doi:10.1021/acsomega.7b00019.

[102] P.M. Dove, N. Han, J.J. De Yoreo, Mechanisms of classical crystal growth theory explain quartz and silicate dissolution behavior, Proc. Natl. Acad. Sci. U. S. A. 102 (2005) 15357–15362. doi:10.1073/pnas.0507777102.

[103] T. Matschei, B. Lothenbach, F.P. Glasser, The role of calcium carbonate in cement hydration, Cem. Concr. Res. 37 (2007) 551–558. doi:10.1016/j.cemconres.2006.10.013.

[104] X. Ouyang, D.A. Koleva, G. Ye, K. van Breugel, Insights into the mechanisms of nucleation and growth of C–S–H on fillers, Mater. Struct. 50 (2017) 213. doi:10.1617/s11527-017-1082-y.

[105] V. Bonavetti, H. Donza, G. Menéndez, O. Cabrera, E.F. Irassar, Limestone filler cement in low w/c concrete: A rational use of energy, Cem. Concr. Res. 33 (2003) 865–871. doi:10.1016/S0008-8846(02)01087-6.

[106] T. Oey, A. Kumar, J.W. Bullard, N. Neithalath, G. Sant, The Filler Effect: The Influence of Filler Content and Surface Area on Cementitious Reaction Rates, J. Am. Ceram. Soc. 96 (2013) 1978–1990. doi:10.1111/jace.12264.

[107] A.-M. Poppe, G. De Schutter, Cement hydration in the presence of high filler contents, Cem. Concr. Res. 35 (2005) 2290–2299. doi:10.1016/j.cemconres.2005.03.008.

[108] E.H. Kadri, S. Aggoun, G.D. Schutter, K. Ezziane, Combined effect of chemical nature and fineness of mineral powders on Portland cement hydration, Mater. Struct. 43 (2010) 665–673. doi:10.1617/s11527-009-9519-6.

[109] A. Kumar, G. Sant, C. Patapy, C. Gianocca, K.L. Scrivener, The influence of sodium and potassium hydroxide on alite hydration: Experiments and simulations, Cem. Concr. Res. 42 (2012) 1513–1523. doi:10.1016/j.cemconres.2012.07.003.

[110] T. Suzuki, H. Kasahara, Determination of the specific surface free energy of natural quartz crystals using measurement of contact angle of liquid droplets, Cryst. Res. Technol. 45 (2010) 1305–1308. doi:10.1002/crat.201000308.

[111] M.G. Lioliou, C.A. Paraskeva, P.G. Koutsoukos, A.C. Payatakes, Heterogeneous nucleation and growth of calcium carbonate on calcite and quartz, J. Colloid Interface Sci. 308 (2007) 421–428. doi:10.1016/j.jcis.2006.12.045.

[112] I. Pignatelli, A. Kumar, M. Bauchy, G. Sant, Topological Control on Silicates' Dissolution Kinetics, Langmuir. 32 (2016) 4434–4439. doi:10.1021/acs.langmuir.6b00359.

[113] A. Kumar, J. Reed, G. Sant, Vertical Scanning Interferometry: A New Method to Measure the Dissolution Dynamics of Cementitious Minerals, J. Am. Ceram. Soc. 96 (2013) 2766–2778. doi:10.1111/jace.12482.

[114] R.G. Compton, K.L. Pritchard, The Dissolution of Calcite at pH > 7: Kinetics and Mechanism, Philos. Trans. R. Soc. Lond. Ser. Math. Phys. Sci. 330 (1990) 47–70.

[115] J. Colombani, The Alkaline Dissolution Rate of Calcite, J. Phys. Chem. Lett. 7 (2016) 2376–2380. doi:10.1021/acs.jpclett.6b01055.

[116] E.L. Sjöberg, D.T. Rickard, Calcite dissolution kinetics: Surface speciation and the origin of the variable pH dependence, Chem. Geol. 42 (1984) 119–136. doi:10.1016/0009-2541(84)90009-3.

[117] S.M. Antao, I. Hassan, J. Wang, P.L. Lee, B.H. Toby, STATE-OF-THE-ART HIGH-RESOLUTION POWDER X-RAY DIFFRACTION (HRPXRD) ILLUSTRATED WITH RIETVELD STRUCTURE REFINEMENT OF QUARTZ, SODALITE, TREMOLITE, AND MEIONITE, Can. Mineral. 46 (2008) 1501–1509. doi:10.3749/canmin.46.5.1501.

[118] S.A. Markgraf, R.J. Reeder, High-temperature structure refinements of calcite and magnesite, Am. Mineral. 70 (1985) 590–600.

[119] J. Tits, G. Geipel, N. Macé, M. Eilzer, E. Wieland, Determination of uranium(VI) sorbed species in calcium silicate hydrate phases: A laser-induced luminescence spectroscopy and batch sorption study, J. Colloid Interface Sci. 359 (2011) 248–256. doi:10.1016/j.jcis.2011.03.046.

[120] B. Kutus, Á. Buckó, G. Peintler, I. Pálinkó, P. Sipos, Calcium complexation and acid–base properties of L-gulonate, a diastereomer of D-gluconate, Dalton Trans. 45 (2016) 18281–18291. doi:10.1039/C6DT03907C.

[121] E. L'Hôpital, B. Lothenbach, K. Scrivener, D.A. Kulik, Alkali uptake in calcium alumina silicate hydrate (C-A-S-H), Cem. Concr. Res. 85 (2016) 122–136. doi:10.1016/j.cemconres.2016.03.009.

[122] I.G. Richardson, G.W. Groves, The incorporation of minor and trace elements into calcium silicate hydrate (C S H) gel in hardened cement pastes, Cem. Concr. Res. 23 (1993) 131–138. doi:10.1016/0008-8846(93)90143-W.

[123] E. Bernard, B. Lothenbach, F. Le Goff, I. Pochard, A. Dauzères, Effect of magnesium on calcium silicate hydrate (C-S-H), Cem. Concr. Res. 97 (2017) 61–72. doi:10.1016/j.cemconres.2017.03.012.

[124] B. Lothenbach, D. Nied, E. L'Hôpital, G. Achiedo, A. Dauzères, Magnesium and calcium silicate hydrates, Cem. Concr. Res. 77 (2015) 60–68. doi:10.1016/j.cemconres.2015.06.007.

[125] T. Missana, M. García-Gutiérrez, M. Mingarro, U. Alonso, Analysis of barium retention mechanisms on calcium silicate hydrate phases, Cem. Concr. Res. 93 (2017) 8–16. doi:10.1016/j.cemconres.2016.12.004.

[126] F. Ziegler, R. Gieré, C.A. Johnson, Sorption Mechanisms of Zinc to Calcium Silicate Hydrate: Sorption and Microscopic Investigations, Environ. Sci. Technol. 35 (2001) 4556–4561. doi:10.1021/es001768m.

[127] J. Tits, E. Wieland, J.-P. Dobler, D. Kunz, The uptake of strontium by calcium silicate hydrates under high pH conditions: An experimental approach to distinguish adsorption from Co-precipitation processes, in: 2004: pp. 689–694.

[128] A. Kumar, Synthetic Calcium Silicate Hydrates, (2017). doi:10.5075/epfl-thesis-7658, urn:nbn:ch:bel-epfl-thesis7658-8.

Curriculum Vitae

PERSONAL INFORMATION

Name   Jirawan Siramanont

Date of birth   25.08.1981

Nationality   Thai

jirawans@scg.com or jirawans164@gmail.com

EMPLOYMENT HISTORY

Aug 2012 - Present	Researcher, Mortar and Concrete Research Group, Siam Research and Innovation Co., Ltd., Thailand
Apr 2008 - Jul 2012	Researcher, Durability and Mechanisms Group, Siam Research and Innovation Co., Ltd., Thailand
	Selected as the company's representative to join SCG Cement Empowerment Team, which is one of the five organizational cultural changes
Jul 2006 - Apr 2008	Chemist, Chemical Laboratory, Siam Research and Innovation Co., Ltd., Thailand

EDUCATION

Oct 2014 - Oct 2018	PhD in Materials Science and Engineering (EPFL, Switzerland)
Jun 2003 – Mar 2006	Master Degree in Petrochemical and Polymer Science (Chulalongkorn University, Thailand)
Jun 1999 – Mar 2003	Bachelor Degree in Chemistry (Chulalongkorn University, Thailand)

PROFESSIONAL EXPERIENCES

Aug 2011	STA-QMS Training (Netzsch Scientific Instrument, Germany)
Nov 2008	Simultaneous Thermal Analysis, STA 409 PC Training (Netzsch Scientific Instrument, China)
Jun 2004 – Mar 2006	Master Thesis (Topic: Reinforcement of natural rubber by silica generated from sol-gel process of silanes in latex)

PERSONAL SKILLS

Languages	Thai (native), English (fluent), French (basic)
Technical skills	Transmission electron microscopy (TEM), Thermogravimetric analysis (TGA), X-ray diffraction (XRD), Zeta potential, Fourier transform infrared spectroscopy (FTIR), Centrifugation, Freeze dry
IT skills	MS office

PUBLICATIONS

- J. Siramanont and P. Bowen, Effect of D-gluconate on nucleation and growth of synthetic Calcium Silicate Hydrate (C-S-H), ACI proceeding published in 12th International Conference on Superplasticizers and Other Chemical Additives in Concrete, (2018).

- J. Siramanont, V. Tangpasuthadol, A. Intasiri, N. Na-Ranong, S. Kiatkamjornwong, Sol-gel process of alkyltriethoxysilane in latex for alkylated silica formation in natural rubber, Polym. Eng. Sci. 49 (2009) 1099–1106.

- J. Siramanont, W Vichit-Vadakan, W. Siriwatwechakul, The impact of SAP structure on the effectiveness of internal curing, International RILEM Conference on Use of Superabsorbent Polymers and Other New Additives in Concrete (2010) 243-252.

- W. Siriwatwechakul, J. Siramanont, W Vichit-Vadakan, Ion filtration effect of superabsorbent polymers for internal curing, Recent Advances in Concrete technology and Sustainability Issues, Proceedings of 12th International Conference (2012).

- W. Siriwatwechakul, J. Siramanont, W Vichit-Vadakan, Superabsorbent Polymer Structures, International RILEM Conference on Use of Superabsorbent Polymers and Other New Additives in Concrete (2010) 253-262.

- W. Siriwatwechakul, J. Siramanont, W Vichit-Vadakan, Behavior of Superabsorbent Polymers in Calcium- and Sodium-Rich Solutions, J. Mater. Civ. Eng. 24 (2012) 976–980.

E XTRACURRICULAR ACTIVITIES

2017 - present	10 km running (6 times in Switzerland and 4 times in Thailand)
2014 - 2016	Active member of Association of Thai Students in Switzerland (ATSS)
2016	Committee of Association of Thai Students in Switzerland (ATSS)